Scholars' Mine

Doctoral Dissertations   Student Theses and Dissertations

Summer 2017

Balanced Truncation Model Reduction of Nonlinear Cable-Mass PDE System

Madhuka Hareena Lochana Weerasinghe

Follow this and additional works at: https://scholarsmine.mst.edu/doctoral_dissertations

Part of the Mathematics Commons

Department: Mathematics and Statistics

BALANCED TRUNCATION MODEL REDUCTION OF NONLINEAR

CABLE-MASS PDE SYSTEM

by

MADHUKA HAREENA LOCHANA WEERASINGHE

A DISSERTATION

Presented to the Graduate Faculty of the

MISSOURI UNIVERSITY OF SCIENCE AND TECHNOLOGY

In Partial Fulfillment of the Requirements for the Degree

DOCTOR OF PHILOSOPHY

in

MATHEMATICS

2017

Approved by

Dr. John R. Singler, Advisor
Dr. Yanzhi Zhang
Dr. Xiaoming He
Dr. Nan Jiang
Dr. Belinda A. Batten

ABSTRACT

We consider model order reduction of a cable-mass system modeled by a one dimensional wave equation with interior damping and dynamic boundary conditions. The system is driven by a time dependent forcing input to a linear mass-spring system at the left boundary of the cable. A mass-spring model at the right end of the cable includes a nonlinear stiffening force. The goal of the model reduction is to produce a low order model that produces an accurate approximation to the displacement and velocity of the mass in the nonlinear mass-spring system at the right boundary. We believe the nonlinear cable-mass model considered here has not been explored elsewhere; therefore, we prove the well-posedness and exponential stability of the unforced linear and nonlinear models under certain conditions on the damping parameters, and then consider a balanced truncation method to generate the reduced order model (ROM) of the nonlinear input-output system. Little is understood about model reduction of nonlinear input-output systems. Therefore, we present detailed numerical experiments concerning the performance of the nonlinear ROM; we find that the ROM is accurate for many different combinations of model parameters. We also prove the well-posedness and exponential stability of other cable-mass problems with unbounded input and output operators, and numerically investigate the behavior of the ROMs for these systems.

ACKNOWLEDGMENTS

It is with profound gratitude I recall the guidance, encouragement and advice offered to me by my adviser Dr. John R. Singler in no small measure, thus providing me with a conducive atmosphere enabling me to engage with the research. Compiling this dissertation would have been beyond my capability if it was not for the generous motivation I received from him.

Also, I wish to convey my heartfelt thanks to those committee members namely-Dr.Yanzhi Zhang, Dr.Xiaoming He, Dr.Nan Jiang and Dr.Belinda A.Batten whose valuable contribution certainly made a great impact to pursue my research in mathematics with determination and enthusiasm.

Let me also, gratefully remember my beloved parents- Gunasena and Swarna, affectionate sibling-Ranga and his family and all my dear friends and finally my loving spouse Pasan and sweet little son, Daham.

TABLE OF CONTENTS

LIST OF ILLUSTRATIONS

LIST OF TABLES

1. INTRODUCTION

Model order reduction (MOR) is currently a very active field of research in many disciplines with many potential applications including numerical simulation, optimization, uncertainty quantification, feedback control and data assimilation (see, e.g., [1, 2, 3, 4, 5, 6, 7]). Many types of MOR for linear problems are well established but remain challenging for nonlinear PDE systems with inputs and outputs.

One main objective of this work is to understand the numerical performance of a type of balanced truncation model order reduction approach for a specific nonlinear PDE system with inputs and outputs and also with unbounded input/output operators. Balanced truncation for linear input-output systems was first introduced by Moore in 1981 [8], and is now a very popular model reduction approach [9, 10]. The theory of balanced truncation model reduction for nonlinear input-output systems was introduced later by Scherpen [11], but this method is not computationally feasible for large-scale systems. We consider another type of nonlinear balanced truncation model reduction that is closely related to balanced truncation for linear systems; specifically, the modes obtained from linear balanced truncation are used to reduce the nonlinear system via a Petrov-Galerkin projection. This approach is computationally tractable and therefore has potential for various applications; however, there is no existing theoretical foundation for this MOR approach. Further, we can find methods of model reduction for nonlinear systems by modifing the balanced truncation method [12, 13, 14, 15, 16, 17].

In the absence of required theory, numerical studies are necessitated to test the performance of this MOR approach. We are aware of only one detailed numerical study: in [18], the authors numerically show that this nonlinear balanced truncation MOR approach is very effective for a 1D complex Ginzburg-Landau equation.

In this work, we consider the same model reduction approach for three different nonlinear input-output cable-mass systems that are represented by a one dimensional damped wave equation with dynamic boundary conditions. One model, which is introduced in Section 2, was originally considered as heuristic model for a wave tank with an energy converter [19]. In this model, the input is a force to a mass-spring system in the left boundary. In Section 3, we consider a different boundary condition in the left end: the input is the force applied to the left end of the cable.

In Section 4, we consider the model from Section 2, but with different output: the force of the cable on the right mass. The importance of doing Sections 3 and 4 is the input and output operators are unbounded in each system, respectively. So we need to study the performance of balanced truncation model reduction numerically. We note that verifying the balanced truncation theory for PDE systems with inputs and/or outputs on the boundary of the special domain can often be very challenging [20, 21, 22] since the input/output operators $\mathcal{B}$ and/or $\mathcal{C}$ are no longer bounded. The theory of balanced truncation for infinite dimensional systems with unbounded input and output operators can be found from [20, 21]. Further, in the literature some authors present numerical investigations for MOR of nonlinear systems using different techniques (see, e.g., [23, 24, 25, 26, 27, 28, 29, 30, 31, 32, 33, 34, 35]).

In Section 5, we also consider a cable-mass system where the cable is fixed at the left end. An analysis of this PDE system was originally performed in [36], and nonlinear exponential stability was shown for small enough initial data. The main purpose of doing Section 5 is to substantiate with theoretical proof the exponential stability of the original cable-mass nonlinear system in [36] for any initial condition.

We believe the nonlinear cable-mass model considered here has not been explored elsewhere; therefore, we prove the well-posedness and exponential stability of the unforced linear and nonlinear models in Sections 2, 3, and 5. The well-posedness

and exponential stability of many types of wave equation models with dynamic boundary conditions have been explored in the literature; see, e.g., [36, 37, 38, 39, 40] and the references therein. The primary difference in the models considered here with most of the models considered else where is that dynamic boundary conditions hold on all boundaries or non-dynamic boundary conditions are specified that are slightly unusual. The paper [37] also considered a 1D wave equation with dynamic boundary conditions on all boundaries; however, the physical system considered in that work leads to different boundary conditions than the one we considered.

MOR for wave equations has been discussed in the literature (see, e.g., [29, 41, 42, 43, 44, 45, 46]); however, many existing works do not consider input-output model reduction as we do here. The work [42] also considers input-output types of model reduction for a different cable-mass model; however, that work explores the effectiveness of the model reduction for a feedback control application. Feedback control of PDE models with input in dynamic boundary conditions has also been explored in other work (see, e.g., [47, 48, 49, 50]); however we do not believe model reduction has been explored in depth for such systems.

2. NONLINEAR CABLE-MASS PROBLEM WITH BOUNDED INPUT AND OUTPUT OPERATORS

2.1. THE MODEL

We consider a flexible cable with mass-spring systems attached to each end. Figure 2.1 illustrate the cable-mass system of interest. Each mass-spring system is connected to a rigid horizontal support. The dotted line represents the equilibrium position of the system. Let

- $w_0(t)$ denote the position below equilibrium of the left mass at location $x = 0$ and time t,

- $w(t, x)$ denote the position of the cable at location x and time t, and

- $w_l(t)$ denote the position above equilibrium of the right mass at location $x = l$ and time t.

The left mass is located at position $x = 0$, and the right mass is located at $x = l$. We assume the system is driven by an external force acting on the left mass-spring system, and that there are no other external forces.

We model the motion of the flexible cable with a damped 1D wave equation on $0 < x < l$. We include both Kelvin-Voigt and viscous damping in the model. We
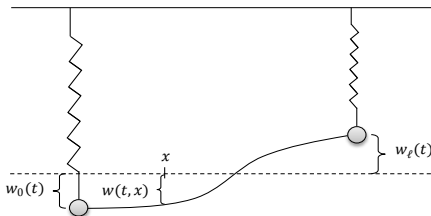
Figure 2.1. The cable-mass system

model the mass-spring system with damped second order oscillators. The left mass-spring system includes a time dependent external force input $u(t)$, and the right mass-spring system includes a nonlinear stiffening force. This gives a wave equation with dynamic boundary conditions:

$$w_{tt}(t,x) + \alpha w_t(t,x) = \gamma w_{txx}(t,x) + \beta^2 w_{xx}(t,x), \tag{2.1}$$

$$m_0 \ddot{w}_0(t) + \alpha_0 \dot{w}_0(t) + k_0 w_0(t) = (\gamma w_{tx}(t,0) + \beta^2 w_x(t,0)) + u(t), \tag{2.2}$$

$$m_l \ddot{w}_l(t) + \alpha_l \dot{w}_l(t) + k_l w_l(t) = (-\gamma w_{tx}(t,l) - \beta^2 w_x(t,l)) - k_3 \left[w_l(t) \right]^3. \tag{2.3}$$

Each term in the parenthesis in the dynamic boundary conditions is the force of the cable acting on the mass. Here, γ is the Kelvin-Voigt damping parameter, α, α_0, α_l are viscous damping parameters, m_0 and m_l are the masses, and k_0, k_l, and k_3 are the stiffness parameters. In the model the damping parameters are nonnegative, and the wave equation parameter β as well as the mass and stiffness parameters are all positive. Finally, the position of the cable at each boundary must equal the position of each mass; therefore, we have *displacement compatibility condition*

$$w(t,0) = w_0(t), \quad w(t,l) = w_l(t). \tag{2.4}$$

For the model reduction problem, we assume we have two system outputs: the position and the velocity of the right mass, i.e.,

$$y_1(t) = w_l(t), \quad y_2(t) = \dot{w}_l(t).$$

2.2. THE ENERGY FUNCTION

Next, we give a preliminary investigation of the change in energy of the unforced system, i.e., the system with $u(t) = 0$. This will help us to obtain the correct

inner products for an abstract formulation of the system. Later we prove the energy decays to zero exponentially fast under certain assumptions on the system parameters. We assume the solution for the above system is sufficiently smooth. We define the total kinetic energy of the cable by

$$E_{T,K} = \frac{1}{2} \int_0^l w_t^2 \, dx.$$

Differentiating with respect to time and using the wave equation (2.1) gives

$$\frac{dE_{T,K}}{dt} = \frac{1}{2} \int_0^l 2w_t w_{tt} \, dx$$

$$= \frac{1}{2} \int_0^l 2w_t(t,x)(\gamma w_{txx}(t,x) + \beta^2 w_{xx}(t,x) - \alpha w_t(t,x)) \, dx.$$

Integrate by parts to obtain

$$\frac{dE_{T,K}}{dt} = -\gamma \int_0^l (w_{tx}(t,x))^2 \, dx - \beta^2 \int_0^l w_x(t,x)w_{tx}(t,x)dx - \alpha \int_0^l (w_t(t,x))^2 \, dx$$

$$+ w_t(t,l) \left[\gamma w_{tx}(t,l) + \beta^2 w_x(t,l)\right] - w_t(t,0) \left[\gamma w_{tx}(t,0) + \beta^2 w_x(t,0)\right].$$

Using the boundary conditions of our cable-mass model (2.2), (2.3) and the displacement compatibility condition (2.4) gives

$$\frac{dE_{T,K}}{dt} = -\gamma \int_0^l (w_{tx}(t,x))^2 \, dx - \beta^2 \int_0^l w_x(t,x)w_{tx}(t,x)dx - \alpha \int_0^l (w_t(t,x))^2 \, dx$$

$$- \dot{w}_l(t) \left[m_l \ddot{w}_l(t) + \alpha_l \dot{w}_l(t) + k_l w_l(t) + k_3 \left[w_l(t)\right]^3\right]$$

$$- \dot{w}_0(t) \left[m_0 \ddot{w}_0(t) + \alpha_0 \dot{w}_0(t) + k_0 w_0(t)\right].$$

This can be written as

$$\frac{d}{dt}\left(\frac{1}{2}\int_0^l w_t^2 \, dx + \frac{m_l}{2}\left(\dot{w}_l(t)\right)^2 + \frac{m_0}{2}\left(\dot{w}_0(t)\right)^2 + \frac{\beta^2}{2}\int_0^l w_x^2 \, dx \right.$$

$$\left. +\frac{k_l}{2}\left(w_l(t)\right)^2 + \frac{k_0}{2}\left(w_0(t)\right)^2 + \frac{k_3}{4}\left(w_l(t)\right)^4 \right) =$$

$$-\gamma \int_0^l \left(w_{tx}(t,x)\right)^2 \, dx - \alpha \int_0^l \left(w_t(t,x)\right)^2 \, dx - \alpha_0 \left(\dot{w}_0(t)\right)^2 - \alpha_l \left(\dot{w}_l(t)\right)^2.$$

This suggests defining the system kinetic energy and potential energy as

$$E_K = \int_0^l \frac{1}{2}w_t^2 \, dx + \frac{m_l}{2}\left(\dot{w}_l(t)\right)^2 + \frac{m_0}{2}\left(\dot{w}_0(t)\right)^2,$$

$$E_P = \int_0^l \frac{\beta^2}{2}w_x^2 \, dx + \frac{k_l}{2}\left(w_l(t)\right)^2 + \frac{k_0}{2}\left(w_0(t)\right)^2 + \frac{k_3}{4}\left(w_l(t)\right)^4.$$

This energy expression can also be obtained by considering the kinetic energy and potential energy of each component of the system. The above energy equation gives

$$\frac{d}{dt}E = \frac{d}{dt}\left(E_K + E_P\right)$$

$$= -\left[\gamma \int_0^l \left(w_{tx}(t,x)\right)^2 \, dx + \alpha \int_0^l \left(w_t(t,x)\right)^2 \, dx + \alpha_0 \left(\dot{w}_0(t)\right)^2 + \alpha_l \left(\dot{w}_l(t)\right)^2\right],$$

and therefore $\dot{E}(t) \le 0$.

This result matches physical intuition and gives the correct energy inner products for the system. Later on, we prove the energy decays exponentially fast to zero under certain assumptions.

2.3. VARIATIONAL FORM

In this subsection, we introduce the variational form (weak form) of the system. Later, we use this form to analyze the model. We assume the solution $[w, w_0, w_l]$ is smooth and satisfies the displacement compatibility condition $w(t, 0) = w_0(t)$ and $w(t, l) = w_l(t)$. Multiply the wave equation (2.1) by a smooth test function $h = h(x)$ satisfying $h(0) = h_0$ and $h(l) = h_l$ and integrate:

$$\int_0^l w_{tt}(t, x)\, h\, dx + \alpha \int_0^l w_t(t, x)\, h\, dx - \gamma \int_0^l w_{txx}(t, x)\, h\, dx - \beta^2 \int_0^l w_{xx}(t, x)\, h\, dx = 0.$$

Now integrate by parts:

$$\int_0^l w_{tt}(t, x)\, h\, dx + \alpha \int_0^l w_t(t, x)\, h\, dx - h_l \left[\gamma w_{tx}(t, l) + \beta^2 w_x(t, l) \right]$$

$$+ h_0 \left[\gamma w_{tx}(t, 0) + \beta^2 w_x(t, 0) \right] + \gamma \int_0^l w_{tx}(t, x)\, h_x\, dx + \beta^2 \int_0^l w_x(t, x)\, h_x\, dx = 0.$$

As in the above energy argument, we use the boundary conditions to give the variational form:

$$0 = \int_0^l w_{tt}(t, x)\, h\, dx + m_l \ddot{w}_l(t) h_l + m_0 \ddot{w}_0(t) h_0$$

$$+ \beta^2 \int_0^l w_x(t, x)\, h_x\, dx + k_l w_l(t) h_l + k_0 w_0(t) h_0$$

$$+ \int_0^l \left[\alpha w_t(t, x)\, h + \gamma w_{tx}(t, x)\, h_x \right] dx + h_l \alpha_l \dot{w}_l(t) + h_0 \alpha_0 \dot{w}_0(t) + k_3 \left[w_l(t) \right]^3 . \quad (2.5)$$

Now we give details about the function spaces to make the formulation precise. Let H be the real Hilbert space $H = L^2(0, l) \times \mathbb{R}^2$ with the inner product of $z =$

$[w, w_0, w_l] \in H$ and $\psi = [p,\, p_0,\, p_l] \in H$ defined by

$$(z, \psi)_H = \int_0^l wp\,dx + m_0 w_0 p_0 + m_l w_l p_l. \tag{2.6}$$

Let $V \subset H$ be the set of elements $z = [w, w_0, w_l] \in H^1(0, l) \times \mathbb{R}^2$ satisfying the displacement compatibility condition $w(0) = w_0$ and $w(l) = w_l$. For $z \in V$ as above and $\psi = [p,\, p_0,\, p_l] \in V$ define the V inner product of z with ψ by

$$(z, \psi)_V = \int_0^l \beta^2 w_x p_x\,dx + k_0 w_0 p_0 + k_l w_l p_l. \tag{2.7}$$

We also use the notation $\sigma_1(z, \psi) = (z, \psi)_V$. The H and V inner products, (2.6) and (2.7), can be derived from the energy function; the H and V norms are directly related to the system kinetic and potential energies, respectively. Specifically,

$$E_K = \frac{1}{2}\,(z_t,\, z_t)_H = \frac{1}{2}\,\|z_t\|_H^2\,, \quad E_P = \frac{1}{2}\,(z,\, z)_V + \frac{k_3}{4} w_l^4 = \frac{1}{2}\,\|z\|_V^2 + \frac{k_3}{4} w_l^4.$$

Furthermore, both inner products appear in the variational form (2.5).

The Gelfand triple is $V \hookrightarrow H \hookrightarrow V'$ with pivot space H and the algebraic dual of V is V'. We define $\langle g, v \rangle$ for $g \in V'$, $v \in V$ by $\langle g, v \rangle = g(v)$. Also, we define the damping bilinear form $\sigma_2 : V \times V \to \mathbb{R}$ by

$$\sigma_2\,(z, \psi) = \int_0^l (\gamma w_x p_x + \alpha wp)\,dx + \alpha_0 w_0 p_0 + \alpha_l w_l p_l. \tag{2.8}$$

Note that this bilinear form occurs in the variational form (2.5) as a damping term with all first order time derivatives.

The spaces and inner products are motivated by the above variational form (2.5). Further we can rewrite the above variational form (2.5) as

$$(z_{tt}, \psi)_H + \sigma_1(z(t), \psi) + \sigma_2(z_t(t), \psi) + (f(z), \psi)_H = 0, \tag{2.9}$$

where $f(z) = [0, 0, k_3 m_l^{-1} w_l^3]$ is the nonlinear term.

2.4. ABSTRACT FORM

The partial differential equation (PDE) model for the physical cable-mass system can be written in an infinite dimensional abstract form as

$$\dot{x}(t) = \mathcal{A}x(t) + \mathcal{B}u(t) + \mathcal{F}(x(t)), \quad x(0) = x_0, \tag{2.10}$$

$$y(t) = \mathcal{C}x(t), \tag{2.11}$$

where $x(t)$ is the state of the system in the Hilbert space $\mathcal{H} = V \times H$, and $u(t)$ is the input of the system. The operator $\mathcal{A} : \mathcal{D}(\mathcal{A}) \subset \mathcal{H} \to \mathcal{H}$ contains the dynamics of the physical system. Similar to Burns & King's work [36], the PDE system suggests that the domain of the operator $\mathcal{A}$ and the operator $\mathcal{A}$ can be formally defined as

$$D(\mathcal{A}) = \left\{ x = [w, w_0, w_l, v, v_0, v_l]^T \in \mathcal{H} \; : \; w \in H^1(0, l), \; v \in H^1(0, l), \right.$$

$$\left. \left[\beta^2 \frac{d}{d\xi} w + \gamma \frac{d}{d\xi} v \right] \in H^1(0, l), \; w(0) = w_0, \; w(l) = w_l, \; v(0) = v_0, \; v(l) = v_l \right\},$$

and

$$\mathcal{A}x = \mathcal{A} \begin{bmatrix} w \\ w_0 \\ w_l \\ v \\ v_0 \\ v_l \end{bmatrix} = \begin{bmatrix} v \\ v_0 \\ v_l \\ \frac{d}{d\xi}\left[\beta^2 \frac{d}{d\xi} w + \gamma \frac{d}{d\xi} v\right] - \alpha v \\ -\delta_0\left[\frac{\beta^2}{m_0}\frac{d}{d\xi} w + \frac{\gamma}{m_0}\frac{d}{d\xi} v\right] - \frac{k_0}{m_0} w_0 - \frac{\alpha_0}{m_0} v_0 \\ -\delta_l\left[\frac{\beta^2}{m_l}\frac{d}{d\xi} w + \frac{\gamma}{m_l}\frac{d}{d\xi} v\right] - \frac{k_l}{m_l} w_l - \frac{\alpha_l}{m_l} v_l \end{bmatrix}$$

where δ_0 and δ_l denote the evaluation operator defined as $\delta_l(\phi(\cdot)) = \phi(l)$ and $\delta_0(\phi(\cdot)) = \phi(0)$ in $H^1(0,l)$. Also, we define the input/output operators and nonlinear term ($\mathcal{A}$, $\mathcal{B}$ and $\mathcal{F}$) by

$$\mathcal{B} = \begin{bmatrix} 0 & 0 & 0 & 0 & \frac{1}{m_0} & 0 \end{bmatrix}^T, \ C = \begin{bmatrix} 0 & 0 & 1 & 0 & 0 & 0 \\ 0 & 0 & 0 & 0 & 0 & 1 \end{bmatrix}$$

$$\mathcal{F}(x) = \begin{bmatrix} 0 & 0 & 0 & 0 & 0 & m_l^{-1} k_3 w_l^3 \end{bmatrix}^T.$$

In our analysis, we do not use the formal definition of the operator $\mathcal{A}$ given above. Instead, we use theory from Banks [51] to rigorously define the operator $\mathcal{A}$ using the bilinear forms σ_1 and σ_2. We use this rigorous definition for the analysis. We prove the operator $\mathcal{A}$ generates an exponentially stable C_0-semigroup in the following section.

2.5. THE LINEAR PROBLEM

We begin by analyzing the variational form for the linear problem

$$(z_{tt}, \psi)_H + \sigma_1(z(t), \psi) + \sigma_2(z_t, \psi) = 0. \tag{2.12}$$

We prove the linear problem is well-posed, and also exponentially stable under certain assumptions on the damping parameters. The exponential stability is necessary for the application of the balanced truncation model reduction technique considered later.

2.5.1. Function Spaces. We first present basic results about the function spaces that we frequently use in this work.

Lemma 2.1. *The space V with the above inner product (2.7) is a real Hilbert space, and V is dense in H.*

Proof. First, if $(z, z)_V = 0$, where $z = [w, w_0, w_l]$, then $w(x)$ is a constant function and $w_0 = w_l = 0$. The compatibility condition implies $w(x) = 0$ for all x, and so $z = 0$. It is clear that $(\cdot, \cdot)_V$ satisfies the remaining properties of an inner product.

Next, let $\{z^n\} \subset V$ be a Cauchy sequence, where $z^n = [w^n, w_0^n, w_l^n]$. Therefore, $[w_x^n, w_0^n, w_l^n]$ is a Cauchy sequence in $L^2(0, l) \times \mathbb{R}^2$, and so there exists $[q, w_0, w_l] \in L^2(0, l) \times \mathbb{R}^2$ such that

$$w_x^n \to q \text{ in } L^2(0, l), \quad w_0^n \to w_0, \quad w_l^n \to w_l.$$

Define w by $w(x) = w_0 + \int_0^x q(\eta)d\eta$. Then $w \in H^1(0, l)$, $w_x = q$, and $w(0) = w_0$. Also, we have $w(l) = w_l$ since

$$w(l) = \lim_{n \to \infty} w_0^n + \int_0^l w_x^n(\eta)d\eta = \lim_{n \to \infty} w_l^n = w_l.$$

Therefore $z = [w, w_0, w_l]$ satisfies the displacement compatibility condition and z^n converges in V to $z \in V$. This shows V is a Hilbert space. To show V is dense in H, let $z = [w, w_0, w_l] \in H$ and define

$$g(x) = w_0 + l^{-1}(w_l - w_0)x$$

Note that $g(0) = w_0$ and $g(l) = w_l$. Since $H_0^1(0, l)$ is dense in $L^2(0, l)$, there exists a sequence $q_n \in H_0^1(0, l)$ such that $q_n \to w - g$ in L^2. Define

$$z_n = [q_n + g, \, w_0, \, w_l]$$

Due to the properties of q_n and g, we have $z_n \in V$ for all n and also $z_n \to z$ in H as $n \to \infty$. This proves V is dense in H. $\qquad\square$

We use the inequalities in the following lemma to prove the well-posedness and exponential stability of the system.

Lemma 2.2. *If $z = [w, w_0, w_l] \in V$, then*

$$|w(x)|^2 \leq 2|w_0|^2 + 2l \, \|w_x\|_{L^2(0,l)}^2 , \tag{2.13}$$

$$\|w\|_{L^2(0,l)}^2 \leq 2l \left[|w_0|^2 + l \, \|w_x\|_{L^2(0,l)}^2 \right] , \tag{2.14}$$

$$w_l^2 \leq 2w_0^2 + 2l \, \|w_x\|_{L^2(0,l)}^2 , \tag{2.15}$$

$$|w(x)|^2 \leq 2|w_l|^2 + 2l \, \|w_x\|_{L^2(0,l)}^2 , \tag{2.16}$$

$$w_0^2 \leq 2w_l^2 + 2l \, \|w_x\|_{L^2(0,l)}^2 , \tag{2.17}$$

$$\|w\|_{L^2(0,l)}^2 \leq 2l \left[|w_l|^2 + l \, \|w_x\|_{L^2(0,l)}^2 \right] . \tag{2.18}$$

Proof. Since $w \in H^1(0, l)$ and $w(0) = w_0$, we have

$$w(x) = w_0 + \int_0^x w_\xi(\xi) \, d\xi.$$

Taking absolute values and using the triangle inequality gives

$$|w(x)| \leq |w_0| + \int_0^x |w_\xi(\xi)| \, d\xi.$$

Then applying Hölder's inequality $(|w_\xi(\xi)| = 1. |w_\xi(\xi)|)$ gives

$$|w(x)| \leq |w_0| + \left(\int_0^l 1^2 d\xi \right)^{\frac{1}{2}} \cdot \left(\int_0^l |w_x(x)|^2 \, dx \right)^{\frac{1}{2}}$$

$$\leq |w_0| + l^{\frac{1}{2}} \|w_x\|_{L^2(0,l)} \, .$$

Squaring this inequality and using Young's inequality gives (2.13); integrating (2.13) from $x = 0$ to $x = l$ gives (2.14); and evaluating equation (2.13) at $x = l$ yields (2.15).

Further note that beginning from $w(x) = w_l - \int_x^l w_\xi(\xi) \, d\xi$ and applying similar ideas gives (2.16), (2.17) and (2.18). □

Lemma 2.3. *V is continuously embedded in H.*

Proof. Let $z = [w, w_0, w_l] \in V$. We use the H and V inner products and the inequality (2.14) from Lemma 2.2 to obtain

$$\|z\|_H^2 = \int_0^l w^2 dx + m_0 w_0^2 + m_l w_l^2$$

$$= \|w\|_{L^2(0,l)}^2 + m_0 w_0^2 + m_l w_l^2$$

$$\leq 2l \left[|w_0|^2 + l \|w_x\|_{L^2(0,l)}^2 \right] + m_0 w_0^2 + m_l w_l^2$$

$$\leq 2l^2 \int_0^l w_x^2 \, dx + (2l + m_0) w_0^2 + m_l w_l^2$$

$$\leq \left(\frac{2l^2}{\beta^2} \right) \beta^2 \int_0^l w_x^2 \, dx + \left(\frac{2l + m_0}{k_0} \right) k_0 w_0^2 + \left(\frac{m_l}{k_l} \right) k_l w_l^2$$

$$\leq C_1 \left[k_0 w_0^2 + k_l w_l^2 + \beta^2 \int_0^l w_x^2 \, dx \right] \, .$$

where $C_1 = \max \left\{ \frac{2l + m_0}{k_0}, \frac{m_l}{k_l}, \frac{2l^2}{\beta^2} \right\}$. This gives $C_1^{-1} \|z\|_H^2 \leq \|z\|_V^2$ and therefore V is continuously embedded in H. □

2.5.2. Well-Posedness and Exponential Stability. To show the linear problem is well-posed, we rewrite the problem as $\dot{x} = \mathcal{A}x$ and show $\mathcal{A}$ generates a C_0-semigroup on $\mathcal{H} = V \times H$. We need the following basic concepts concerning bilinear forms acting on V.

Definition 2.1.

- A bilinear form $\sigma : V \times V \to \mathbb{R}$ is V-continuous if $|\sigma(\varphi, \psi)| \leq c_1 \|\varphi\|_V \|\psi\|_V$ for all φ and ψ in V.

- A bilinear form $\sigma : V \times V \to \mathbb{R}$ is V-elliptic if there exists a constant $c_2 > 0$ such that $\sigma(\varphi, \varphi) \geq c_2 \|\varphi\|_V^2$ for all φ in V.

- A bilinear form $\sigma : V \times V \to \mathbb{R}$ is H-semielliptic if there exists a constant $c_3 \geq 0$ such that $\sigma(\varphi, \varphi) \geq c_3 \|\varphi\|_H^2$ for all φ in V. Also, σ is H-elliptic if $c_3 > 0$.

Lemma 2.4. *σ_2 is V-continuous.*

Proof. Let $\Phi = [\varphi, \varphi_0, \varphi_l]$ and $\Psi = [\psi, \psi_0, \psi_l]$ and recall

$$\sigma_2(\Phi, \Psi) = \int_0^l \left[\alpha \varphi \psi + \gamma \varphi_x \psi_x \right] dx + \alpha_0 \varphi_0 \psi_0 + \alpha_l \varphi_l \psi_l.$$

Applying Hölder's inequality and using the result (2.14) proves the lemma. □

We follow the presentation in [51], Section 8.1, in order to find the linear operator $\mathcal{A}$. First, σ_2 is V-continuous. Since σ_1 and σ_2 are V-continuous we have that there exists operators $A_i \in \mathcal{L}(V, V')$ for $i = 1, 2$ such that

$$\sigma_i(\varphi, \psi) = \langle A_i \varphi, \psi \rangle \quad \text{for all} \quad \varphi, \psi \in V.$$

Define the operator $\mathcal{A} : D(\mathcal{A}) \subset \mathcal{H} \to \mathcal{H}$, where $\mathcal{H} = V \times H$, by

$$D(\mathcal{A}) = \{ x = [\varphi, \psi] \in \mathcal{H} \ : \ \psi \in V, A_1 \varphi + A_2 \psi \in H \}$$

and

$$\mathcal{A} = \begin{bmatrix} 0 & I \\ -A_1 & -A_2 \end{bmatrix}. \qquad (2.19)$$

Theorem 2.5. *The operator $\mathcal{A}$ defined above generates a C_0-semigroup on $\mathcal{H} = V \times H$.*

Proof. Due to the properties of the spaces H and V, the result follows directly from Theorem 8.2 in [51] since σ_1 is the V inner product and σ_2 is H-semielliptic. $\square$

Since $\mathcal{A}$ generates a C_0-semigroup $T(t)$ on $\mathcal{H} = V \times H$, then $T(t)x_0$ is the unique solution of $\dot{x} = \mathcal{A}x$ where $x(0) = x_0$.

For the exponential stability of the problem, we restrict our attention to the model with interior damping, i.e., the Kelvin-Voigt damping parameter γ is positive or the viscous damping parameter α is positive. In this case, the easiest way to prove exponential stability is to show σ_2 is H-elliptic or V-elliptic. Note that since V is continuously embedded in H, if σ_2 is V-elliptic then it must also be H-elliptic; additionally, if σ_2 is V-elliptic then the semigroup is also analytic.

Theorem 2.6. *If σ_2 is H-elliptic, then the operator $\mathcal{A}$ defined in (2.19) is the infinitesimal generator of an exponentially stable C_0-semigroup $T(t)$ on $\mathcal{H} = V \times H$. Furthermore, if σ_2 is V-elliptic, then $T(t)$ is exponentially stable and also analytic.*

Proof. This follows directly from Theorems 8.1 and 8.3 in [51]. $\square$

In this work, we restrict our analysis to the cases where the damping bilinear form σ_2 is H-elliptic or V-elliptic. The analysis of exponential stability for the model when this condition is not satisfied is more involved. We prove exponential stability for the linear system for three main examples of damping parameter sets. We also consider model reduction computations for two other examples in the numerical results.

Example 1: $\gamma, \alpha_l > 0$ and $\alpha_0 = \alpha = 0$. We first consider the case of Kelvin-Voigt damping $(\gamma > 0)$ and viscous damping in the right mass-spring system $(\alpha_l > 0)$. We prove σ_2 is V-elliptic. Let $z = [w, w_0, w_l] \in V$, and recall the bilinear form σ_2 and the V inner product are given by

$$\sigma_2(z, z) = \int_0^l \gamma w_x^2 \, dx + \alpha_l w_l^2,$$

$$\|z\|_V^2 = \int_0^l \beta^2 w_x^2 dx + k_0 w_0^2 + k_l w_l^2.$$

Use the inequality (2.17) to obtain

$$\|z\|_V^2 \leq (\beta^2 + 2lk_0) \int_0^l w_x^2 dx + (k_l + 2k_0) w_l^2$$

$$\leq \left(\frac{\beta^2 + 2lk_0}{\gamma} \right) \int_0^l \gamma w_x^2 dx + \left(\frac{k_l + 2k_0}{\alpha_l} \right) \alpha_l w_l^2$$

$$\leq C_2 \left(\int_0^l \gamma w_x^2 dx + \alpha_l w_l^2 \right)$$

$$\leq C_2 \sigma_2(z, z),$$

where $C_2 = \max\left\{ \frac{\beta^2 + 2lk_0}{\gamma}, \frac{k_l + 2k_0}{\alpha_l} \right\}$. This proves that σ_2 is V-elliptic. It can also be shown that σ_2 is V-elliptic in the similar case when $\gamma, \alpha_0 > 0$ and $\alpha, \alpha_l = 0$.

Example 2: $\gamma = 0$ and $\alpha, \alpha_0, \alpha_l > 0$. Next, we consider the case of viscous damping in the wave equation and both mass-spring systems $(\alpha, \alpha_0, \alpha_l > 0)$. We prove σ_2 is H-elliptic. Let $z = [w, w_0, w_l] \in V$. Recall

$$\sigma_2(z, z) = \int_0^l \alpha w^2 dx + \alpha_0 w_0^2 + \alpha_l w_l^2,$$

$$\|z\|_H^2 = \int_0^l w^2 dx + m_0 w_0^2 + m_l w_l^2.$$

Then

$$\|z\|_H^2 = \int_0^l \left(\frac{1}{\alpha}\right) \alpha w^2 dx + \left(\frac{m_0}{\alpha_0}\right) \alpha_0 w_0^2 + \left(\frac{m_l}{\alpha_l}\right) \alpha_l w_l^2$$

$$\leq C_3 \left[\int_0^l \alpha w^2 dx + \alpha_0 w_0^2 + \alpha_l w_l^2 \right]$$

$$\leq C_3 \sigma_2(z,z),$$

where $C_3 = \max\left\{\frac{1}{\alpha}, \frac{m_0}{\alpha_0}, \frac{m_l}{\alpha_l}\right\}$, This proves that σ_2 is H-elliptic.

Example 3: $\gamma, \alpha > 0$ and $\alpha_0, \alpha_l = 0$. In this last case, we consider Kelvin-Voigt damping ($\gamma > 0$) and interior viscous damping ($\alpha > 0$) but no other boundary viscous damping. We prove σ_2 is V-elliptic. We rewrite the bilinear form of σ_2 and the V inner products according to the above parameters:

$$\sigma_2(z,z) = \int_0^l \left(\gamma w_x^2 + \alpha w^2\right) dx,$$

$$\|z\|_V^2 = \int_0^l \beta^2 w_x^2 dx + k_0 w_0^2 + k_l w_l^2.$$

Recall the Sobolev inequality for the H^1 norm and L^∞ norm:

$$\|u\|_\infty \leq C \|u\|_{H^1(a,b)},$$

$$\|u\|_{H^1(a,b)}^2 = \int_a^b \left(u^2 + u_x^2\right) dx,$$

$$\|u\|_\infty = \operatorname*{ess\,sup}_{x \in (a,b)} |u(x)|.$$

Apply the L^∞ norm for w_0^2 and w_l^2, then use the Sobolev inequality to obtain

$$
\begin{aligned}
\|z\|_V^2 &\leq \int_0^l \beta^2 w_x^2 dx + k_0 \|w\|_\infty^2 + k_l \|w\|_\infty^2 \\
&= \int_0^l \beta^2 w_x^2 dx + (k_0 + k_l) \|w\|_\infty^2 \\
&\leq \int_0^l \beta^2 w_x^2 dx + (k_0 + k_l) C \|w\|_{H^1(0,l)}^2 \\
&= \int_0^l \beta^2 w_x^2 dx + (k_0 + k_l) C \int_0^l (w^2 + w_x^2)\, dx \\
&= \int_0^l ((\beta^2 + (k_0 + k_l)C) w_x^2 + (k_0 + k_l)C w^2) dx \\
&= C_4\, \sigma_2(z, z),
\end{aligned}
$$

and therefore $C_4^{-1} \|z\|_V^2 \leq \sigma_2(z, z)$, where $C_4 = \max\left\{ \frac{\beta^2 + (k_0 + k_l)C}{\gamma}, \frac{(k_0 + k_l)C}{\alpha} \right\}$, This proves that σ_2 is V-elliptic.

In Examples 1, 3 we proved that σ_2 is V-elliptic and Theorem 2.6 gives us $\mathcal{A}$ is the infinitesimal generator of an analytic exponentially stable semigroup.

In Example 2 we proved that σ_2 is H-elliptic and Theorem 2.6 gives us $\mathcal{A}$ generates an exponentially stable C_0-semigroup that is not analytic.

2.6. THE NONLINEAR PROBLEM

Next, we analyze the well-posedness and exponential stability of the full unforced nonlinear problem. First, we write the nonlinear problem as

$$
\dot{x}(t) = \mathcal{A}x(t) + \mathcal{F}(x(t)), \quad x(0) = x_0, \tag{2.20}
$$

on $\mathcal{H} = V \times H$ where the linear operator $\mathcal{A}$ is defined in Section 2.5.2 and the nonlinear term $\mathcal{F} : \mathcal{H} \to \mathcal{H}$ is defined for $x = [\varphi, \psi] \in \mathcal{H}$ with $\varphi = [w, w_0, w_l] \in V$ by

$$
\mathcal{F}(x) = \begin{bmatrix} 0 \\ F_0(\varphi) \end{bmatrix}, \quad F_0(\varphi) = \begin{bmatrix} 0 \\ 0 \\ m_l^{-1} k_3 w_l^3 \end{bmatrix}.
$$

Theorem 2.7. *The nonlinear cable-mass system has a unique mild solution on some time interval $[0, t^*)$.*

Proof. From Section 2.5.2 we know $\mathcal{A}$ generates a C_0-semigroup in $\mathcal{H} = V \times H$. We can check that the nonlinear term $\mathcal{F}$ is locally Lipschitz continuous on $\mathcal{H}$. Therefore, the result follows using semigroup theory; see, e.g., Theorem 1.4 in Section 6.1 in [52]. $\square$

Next, we prove the unforced nonlinear system is exponential stability when the damping bilinear form σ_2 is $H-$elliptic. For the proof, we use the energy argument from Section 2.2, the variational formulation in Section 2.3, and also Lemma 2.8.

Lemma 2.8. *(Theorem 8.1 in [53]). Let $E : \mathbb{R}^+ \to \mathbb{R}^+$ be a non-increasing function. If there exists a constant $T > 0$ such that $\int_s^\infty E(t) \leq TE(s)$ for all $s \geq 0$, then $E(t) \leq E(0)e^{1-t/T}$ for all $t \geq 0$.*

Theorem 2.9. *If σ_2 is $H-$elliptic and the solution $x = [z, z_t]$, with $z = [w, w_0, w_l]$, of the unforced nonlinear cable-mass problem (2.20) is sufficiently smooth, then the energy $E(t) = \frac{1}{2} \|z_t\|_H^2 + \frac{1}{2} \|z\|_V^2 + \frac{k_3}{4} [w_l(t)]^4$ of the solution with the initial data $x(0) = x_0 \in \mathcal{H}$ decays exponentially fast as $t \to \infty$.*

Remark 2.1. It may be possible to identify conditions on the damping parameters or the initial data $x_0 \in \mathcal{H}$ that provides the required smoothness of the solution for the proof of this exponentially stable result. We do not investigate this here.

Proof. First, since the solution is sufficiently smooth, the energy argument from Section 2.2 gives $E'(t) \leq 0$, where

$$E(t) = E_K(t) + E_P(t), \quad E_K = \frac{1}{2} \|z_t\|_H^2, \quad E_P = \frac{1}{2} \|z\|_V^2 + \frac{k_3}{4} [w_l]^4.$$

Therefore, $E(t)$ is non-increasing. Also, $\frac{1}{2} \|x\|_{\mathcal{H}}^2 = \frac{1}{2} \|z\|_V^2 + \frac{1}{2} \|z_t\|_H^2 \leq E(t)$. Since $E(t)$ is bounded, $\|x\|_{\mathcal{H}}^2$ cannot blow up in finite time; therefore, semigroup theory gives that the solution must exist for all $t > 0$ (Theorem 1.4 in Section 6.1 in [52]).

Next, we show that the energy function satisfies the remaining condition in Lemma 2.8 by separately considering the kinetic and potential energies. Our proof use ideas from the proof of Theorem 3.2 in Fourrier and Lasiecka's work [38]. To use the above lemma, let $s \geq 0$ and $t > s$.

Step 1 : First, we consider the kinetic energy. Recalling the energy argument from Section 2.2 immediately gives

$$E'(t) = -\sigma_2(z_t, z_t).$$

Integrate with respect to time from s to t to obtain

$$E(t) = E(s) - \int_s^t \sigma_2(z_t, z_t) d\tau.$$

Since σ_2 is H-elliptic, there is a constant $C > 0$ such that $\sigma_2(z_t, z_t) \geq (C/2) \|z_t\|_H^2 = CE_K$. Therefore, for $C_1 = C^{-1}$,

$$\int_s^t E_K(\tau) \, d\tau \leq C_1 E(s) - C_1 E(t) \leq C_1 E(s),$$

since $E(t) \geq 0$.

Step 2 : Next, we consider the potential energy. Substitute $\psi = z = [w, w_0, w_l]$ in the vatiational form (2.9) to give

$$(z_{tt}, z)_H + (z, z)_V + \sigma_2(z_t, z) + (f(z), z)_H = 0.$$

Since σ_2 is a symmetric bilinear form, we have $\sigma_2(z_t, z) = \frac{1}{2}\frac{d}{dt}\sigma_2(z, z)$. Integrate with respect to time from s to t, and then integrate by parts in time to obtain

$$(z_t(t), z(t))_H - (z_t(s), z(s))_H - \int_s^t (z_t, z_t)_H \, d\tau + \int_s^t (z, z)_V d\tau$$

$$+ \quad \frac{1}{2}(\sigma_2(z(t), z(t)) - \sigma_2(z(s), z(s)) + \int_s^t k_3(z_l(t))^4 d\tau = 0.$$

Using the definition of kinetic energy and potential energy gives

$$\frac{1}{2}\sigma_2(z(t), z(t)) + 2\int_s^t E_P(\tau)d\tau = -\int_s^t \frac{k_3}{2}\left[z_l(t)\right]^4 d\tau + 2\int_s^t E_K(\tau)d\tau$$

$$- (z_t(t), z(t))_H + (z_t(s), z(s))_H + \frac{1}{2}\sigma_2(z(s), z(s)).$$

We remove the nonnegative term $\int_s^t \frac{k_3}{2}\left[z_l(t)\right]^4 d\tau \geq 0$, and the equality becomes the inequality

$$\frac{1}{2}\sigma_2(z(t), z(t)) + 2\int_s^t E_P(\tau)d\tau \leq 2\int_s^t E_K(\tau)d\tau - (z_t(t), z(t))_H$$

$$+ (z_t(s), z(s))_H + \frac{1}{2}\sigma_2(z(s), z(s)).$$

Use $(u,v)_H \leq \|u\|_H \|v\|_H$ and the V-continuity of σ_2, i.e., $\sigma_2(\Phi, \Psi) \leq C_2 \|\Phi\|_V \|\Psi\|_V$ to obtain

$$\frac{1}{4}\sigma_2(z(t), z(t)) + \int_s^t E_P(\tau)d\tau$$

$$\leq \int_s^t E_K(\tau)d\tau + \frac{1}{2}\left[\|z_t(s)\|_H \|z(s)\|_H + \|z_t(t)\|_H \|z(t)\|_H + \frac{C_2}{2}\|z(s)\|_V^2 \right].$$

Using the result from Step 1 and Young's inequality gives

$$\frac{1}{4}\sigma_2(z(t), z(t)) + \int_s^t E_P(\tau)d\tau \leq C_1 E(s) + \frac{1}{2}\left[\frac{1}{2}\|z_t(s)\|_H^2 + \frac{1}{2}\|z(s)\|_H^2 \right.$$

$$\left. + \frac{1}{2}\|z_t(t)\|_H^2 + \frac{1}{2}\|z(t)\|_H^2 + \frac{C_2}{2}\|z(s)\|_V^2 \right].$$

Use V is continuously embedded in H, i.e., $\|z\|_H^2 \leq C_3 \|z\|_V^2$, to obtain

$$\frac{1}{4}\sigma_2(z(t), z(t)) + \int_s^t E_P(\tau)d\tau \leq C_1 E(s) + \frac{1}{2}\left[\frac{1}{2}\|z_t(s)\|_H^2 + \frac{1}{2}\|z_t(t)\|_H^2 \right.$$

$$\left. + \frac{C_3}{2}\|z(s)\|_V^2 + \frac{C_3}{2}\|z(t)\|_V^2 + \frac{C_2}{2}\|z(s)\|_V^2 \right].$$

Use the definition of kinetic energy and add positive terms $\frac{k_3}{4}[z_l(t)]^4$ and $\frac{k_3}{4}[z_l(s)]^4$ to the right hand side of the inequality to obtain

$$\frac{1}{4}\sigma_2(z(t), z(t)) + \int_s^t E_P(\tau)d\tau \leq C_1 E(s) + C_4\left[\frac{1}{2}\|z_t(t)\|_H^2 + \right.$$

$$\left. + \frac{1}{2}\|z(t)\|_V^2 + \frac{k_3}{4}[z_l(t)]^4 \right] + C_5\left[\frac{1}{2}\|z_t(s)\|_H^2 + \frac{1}{2}\|z(s)\|_V^2 + \frac{k_3}{4}[z_l(s)]^4 \right]$$

where $C_4 = \max\left\{ \frac{1}{2}, 1, C_3 \right\}$, and $C_5 = \max\left\{ \frac{1}{2}, 1, C_2 + C_3 \right\}$.

Since $t > s$ and $E'(t) \le 0$ for all $t \ge 0$, we have $E(t) \le E(s)$. Also since $\frac{1}{4}\sigma_2(z(t), z(t)) \ge 0$ we get

$$\int_s^t E_P(\tau)d\tau \le C_6 E(s),$$

where $C_6 = C_1 + C_4 + C_5$. Combining the result of Step 1, letting $t \to \infty$, and using Lemma 2.8 proves the result. $\qquad\square$

2.7. BALANCED TRUNCATION MODEL REDUCTION

Next, we return to the forced nonlinear cable-mass system (2.1) with the system input $u(t)$ in the dynamic boundary condition (2.3) and system output

$$y(t) = [w_l(t),\ \dot{w}_l(t)]^T$$

of the position and velocity of the right mass. In this section, we describe a balanced truncation model reduction approach for this nonlinear system. We begin by briefly reviewing balanced truncation model reduction for linear input-output ordinary differential equation systems and then infinite dimensional systems. We outline the finite difference method we use to approximate the nonlinear cable-mass model, and then describe the balanced truncation model reduction method for the approximating nonlinear finite dimensional system.

2.7.1. Finite Dimensional Balanced Truncation. Balanced Truncation is one of the most popular model reduction methods in control and system theory, and it is based on the idea of controllability and observability [9, 10]. To review the main ideas, consider the exponentially stable linear time invariant dynamical system

in state space form

$$\dot{x}(t) = Ax(t) + Bu(t),$$

$$y(t) = Cx(t). \tag{2.21}$$

The above physical problem with dynamics has state $x(t) \in \mathbb{R}^N$, where N is the dimension of the state space, $u(t) \in \mathbb{R}^m$ is the input, and $y(t) \in \mathbb{R}^p$ is the output. Moreover, $A \in \mathbb{R}^{N \times N}$, $B \in \mathbb{R}^{N \times m}$, and $C \in \mathbb{R}^{p \times N}$ are constant matrices, and A is stable.

To reduce the complexity of the system, we approximate the problem using a reduced number of states $r \ll N$. Balanced truncation looks for a reduced order model

$$\dot{a}(t) = A_r a(t) + B_r u(t),$$

$$y_r(t) = C_r a(t),$$

where $a(t) \in \mathbb{R}^r$ is the reduced order state, such that the error in the output $\|y(t) - y_r(t)\|$ is small when the same input $u(t)$ is applied to both systems.

To do this, let $T \in \mathbb{R}^{N \times N}$ be invertible, and make the change of variable $z = Tx$. Then we can write the original system (2.21) as

$$\dot{z}(t) = T^{-1}ATz(t) + T^{-1}Bu(t),$$

$$y(t) = CTz(t).$$

It can be checked that the transfer function $G(s) = C(sI - A)^{-1}B$ relating inputs to outputs in the original system is equal to the transfer function of the transformed system. If A is exponentially stable, then the controllability and observability Gramians, $P, Q \in \mathbb{R}^{N \times N}$ are the unique positive semidefinite solutions to the Lyapunov equations $AP + PA^T + BB^T = 0$ and $A^T Q + QA + C^T C = 0$. It can be checked that the

Gramians of the transformed system are given by $\hat{P} = TPT^T$ and $\hat{Q} = (T^{-1})^T QT^{-1}$. Furthermore, if P and Q are positive definite, there exists T such that transformed Gramians $\hat{P}$ and $\hat{Q}$ are *balanced,* i.e., they are equal and diagonal; the positive diagonal entries are called the Hankel singular values of the system, and they are ordered from greatest to least.

The states in the transformed system corresponding to "small" Hankel singular values are truncated to produce the balanced low order model. In addition, the truncation error between the transfer function $G(s)$ of the original system and transfer function $G_r(s) = C_r(sI - A_r)^{-1}B_r$ of the balanced low order model is bounded by

$$\|G(s) - G_r(s)\|_\infty \leq 2 \sum_{i>r} \sigma_i, \tag{2.22}$$

where $\{\sigma_i\}_{i=1}^N$ are the ordered Hankel singular values of the system and the norm is the $\mathcal{H}_\infty$ system norm. Therefore, if the Hankel singular values decay to zero quickly, then the balanced low order model can provide a good approximation to the input-output response of the full order system. Once the Hankel singular values are computed, the above error bound can be used as a guide to choose an appropriate value for r.

2.7.2. Infinite Dimensional Balanced Truncation. Since we consider a partial differential equation system in this work, we briefly review balanced truncation model reduction for a linear infinite dimensional system of the form

$$\dot{x}(t) = \mathcal{A}x(t) + \mathcal{B}u(t),$$
$$y(t) = \mathcal{C}x(t), \tag{2.23}$$

holding over a Hilbert space $\mathcal{H}$, where $\mathcal{A}: D(\mathcal{A}) \subset \mathcal{H} \to \mathcal{H}$ is the generator of an exponentially stable C_0-semigroup on $\mathcal{H}$, and $\mathcal{B}: \mathbb{R}^m \to \mathcal{H}$ and $\mathcal{C}: \mathcal{H} \to \mathbb{R}^P$ are both

bounded linear operators. We also verify the theory holds for the linear cable-mass system.

The theoretical background for the existence of the balanced truncation for this class of infinite dimensional linear systems can be found in [20, 54]. Specifically, there is a transformed system holding over the Hilbert space l^2 that is balanced, i.e., the controllability and observability Gramians are equal and diagonal; also, as in the finite dimensional case, the diagonal entries are called the Hankel singular values and are ordered from greatest to the least. Truncating the states in the transformed system corresponding to small Hankel singular values again yields the reduced order model. The transfer function error bound (2.22) still holds, and the right hand side of the error bound is finite and tends to zero as r increases.

We can write our linear cable-mass system in the above first order abstract form (2.23) with Hilbert space $\mathcal{H} = V \times H$, as in Section 2.5.2. The operator $\mathcal{A}$ was defined previously. The operator $\mathcal{B} : \mathbb{R} \to \mathcal{H}$ and $\mathcal{C} : \mathcal{H} \to \mathbb{R}^2$ are defined as follows. First, $\mathcal{B}u = [0, B_0 u]$, where $B_0 u = [0, m_0^{-1} u, 0]$. Then

$$
\begin{aligned}
\|\mathcal{B}u\|_{\mathcal{H}}^2 = \|\mathcal{B}u\|_V^2 + \|\mathcal{B}u\|_H^2 = \|\mathcal{B}u\|_H^2 &= \left\| \left[0, m_0^{-1}, 0 \right] u \right\|_H^2 = \left| m_0^{-1} u \right|^2 \\
&\leq m_0^{-2} \left| u \right|^2,
\end{aligned}
$$

and therefore $\mathcal{B}$ is bounded. Then let $x = [z, \chi] \in \mathcal{H}$, where z is the position and χ is the velocity. For $z = [w, w_0, w_l]$ and $\chi = [p, p_0, p_l]$, $\mathcal{C}x$ is defined by $Cx = [w_l, p_l]$.

Then

$$\begin{aligned}
\|\mathcal{C}x\|_{R^2}^2 &= \|[w_l, p_l]\|_{R^2}^2 \\
&= w_l^2 + p_l^2 \\
&= \left[\frac{1}{m_l}\right] m_l w_l^2 + \left[\frac{1}{k_l}\right] k_l p_l^2 \\
&\leq \int_0^l w^2 dx + m_0 w_0^2 + \left[\frac{1}{m_l}\right] m_l w_l^2 + \int_0^l \beta^2 p_x^2 dx + k_0 p_0^2 + \left[\frac{1}{k_l}\right] k_l p_l^2 \\
&\leq C_2 \left[\|z\|_H^2 + \|\chi\|_V^2\right] \\
&\leq C_2 \|x\|_{\mathcal{H}}^2,
\end{aligned}$$

where $C_2 = \max\left\{1, \frac{1}{m_l}, \frac{1}{k_l}\right\}$. This proves the result that $\mathcal{C}$ is bounded. Since $\mathcal{B}$, $\mathcal{C}$ are bounded, the balanced truncation theory holds for the linear cable-mass system.

2.7.3. Formulating the Finite Difference Approximation.

Finding exact solutions of the nonlinear cable-mass problem is usually impossible. Therefore, we use a basic numerical method, the finite difference method, to approximate the solution to our model problem with dynamic boundary conditions. Using this method, we convert our PDE system to an ODE system, and we apply the model reduction method to the resulting nonlinear finite dimensional system.

We place n equally spaced nodes $\{x_j\}_{j=1}^n$ in the interval $[0, l]$, where $x_j = (j-1)h$ and $h = l/(n-1)$ so that $x_1 = 0$ and $x_n = l$. In order to apply balanced truncation below, we also eliminate the second order time derivatives by introducing a velocity variable. Therefore, let d_i denote the finite difference approximation to the displacement $w(t, x_i)$, and let v_i denote the finite difference approximation to the velocity $w_t(t, x_i)$. We assume the solution is smooth so that the displacement and

velocity compatibility conditions are satisfied; we obtain

$$w_0(t) = d_1(t), \quad w_l(t) = d_n(t),$$

$$\dot{w}_0(t) = v_1(t), \quad \dot{w}_l(t) = v_n(t).$$

We use second order centered differences to form finite difference equations for the wave equation (2.1)

$$v_i' = \frac{\gamma}{h^2}[v_{i+1} - 2v_i + v_{i-1}] + \frac{\beta^2}{h^2}[d_{i+1} - 2d_i + d_{i-1}] - \alpha v_i,$$

$$d_i' = v_i \quad \text{for } i = 2, ..., n-1. \tag{2.24}$$

To discretize our system we use (2.24) to obtain

$$v_i' = \left[-\alpha - \frac{2\gamma}{h^2}\right]v_i + \left[\frac{\gamma}{h^2}\right]v_{i-1} + \left[\frac{\gamma}{h^2}\right]v_{i+1} + \left[\frac{\beta^2}{h^2}\right]d_{i+1} - \left[\frac{2\beta^2}{h^2}\right]d_i + \left[\frac{\beta^2}{h^2}\right]d_{i-1},$$

$$d_i' = v_i, \quad \text{for } i = 2, ..., n-1.$$

To discretize the dynamic boundary conditions we use second order accurate one sided finite difference approximations to the first order spatial derivatives. First,

$$w_x(t, x) \approx \frac{-3w(t, x) + 4w(t, x + h) - w(t, x + 2h)}{2h}. \tag{2.25}$$

Then we replace h by $-h$ to obtain another second order accurate one sided finite difference approximation for $w_x(t, x)$ in terms of $w(t, x)$, $w(t, x - h)$ and $w(t, x - 2h)$, i.e.,

$$w_x(t, x) \approx \frac{3w(t, x) - 4w(t, x - h) + w(t, x - 2h)}{2h}. \tag{2.26}$$

Using these approximations we discretize the term $w_x(t, 0)$ in the left boundary condition by

$$w_x(t, 0) \approx \frac{-3d_1 + 4d_2 - d_3}{2h}, \tag{2.27}$$

and we discretize the term $w_x(t, 1)$ in the right boundary condition by

$$w_x(t, 1) \approx \frac{3d_n - 4d_{n-1} + d_{n-2}}{2h}. \tag{2.28}$$

Using these one-side finite difference approximations allows us to keep the the second order accuracy without introducing "ghost" nodes outside of the spatial domain. After discretizing the dynamic boundary conditions we obtain

$$v_1' = \left[-\frac{k_0}{m_0} - \frac{3\beta^2}{2hm_0} \right] d_1 + \left[\frac{4\beta^2}{2hm_0} \right] d_2 - \left[\frac{\beta^2}{2hm_0} \right] d_3 + \left[-\frac{3\gamma}{2hm_0} - \frac{\alpha_0}{m_0} \right] v_1$$
$$+ \left[\frac{4\gamma}{2hm_0} \right] v_2 - \left[\frac{\gamma}{2hm_0} \right] v_3 + \frac{u(t)}{m_0},$$

$$d_1' = v_1,$$

and

$$v_n' = \left[-\frac{k_l}{m_l} - \frac{3\beta^2}{2hm_l} \right] d_n + \left[\frac{4\beta^2}{2hm_l} \right] d_{n-1} - \left[\frac{\beta^2}{2hm_l} \right] d_{n-2}$$
$$+ \left[-\frac{\alpha_l}{m_l} - \frac{3\gamma}{2hm_l} \right] v_n + \left[\frac{4\gamma}{2hm_l} \right] v_{n-1} - \left[\frac{\gamma}{2hm_l} \right] v_{n-2} - \left[\frac{k_3}{m_l} \right] [d_n]^3,$$

$$d_n' = v_n,$$

where d_i, v_i and $u(t)$ represent displacement, velocity, and input respectively. Then the matrix form of the above system becomes

$$\begin{bmatrix} d' \\ v' \end{bmatrix} = \begin{bmatrix} 0 & I \\ A_{11} & A_{12} \end{bmatrix} \begin{bmatrix} d \\ v \end{bmatrix} + \begin{bmatrix} 0 & 0 \\ F_{12} & 0 \end{bmatrix} \begin{bmatrix} d^3 \\ v^3 \end{bmatrix} + \begin{bmatrix} 0 \\ B_1 \end{bmatrix} u, \tag{2.29}$$

$$\begin{bmatrix} y_1 \\ y_2 \end{bmatrix} = \begin{bmatrix} 0 & \cdots & 1 & \cdots & 0 \\ 0 & \cdots & 0 & \cdots & 1 \end{bmatrix} \begin{bmatrix} d \\ v \end{bmatrix}, \tag{2.30}$$

where the matrices are defined below. First, the matrix A_{11} has nonzero (i,j) entries, where i, j represent the row and column respectively, as specified below. The nonzero first row entries of A_{11} in the $(1,1)$, $(1,2)$ and $(1,3)$ entries are $\left(-\frac{k_0}{m_0} - \frac{3\beta^2}{2hm_0}\right)$, $\left(\frac{4\beta^2}{2hm_0}\right)$, $\left(-\frac{\beta^2}{2hm_0}\right)$, respectively. The nonzero last row entries of A_{11} in the $(n, n-2)$, $(n, n-1)$ and (n,n) entries are $\left(-\frac{\beta^2}{2hm_l}\right)$, $\left(\frac{4\beta^2}{2hm_l}\right)$, $\left(-\frac{k_l}{m_l} - \frac{3\beta^2}{2hm_l}\right)$, respectively. The middle part of the matrix $i = 2, 3, \ldots, n-1$ is a tridiagonal matrix. The entries are

$$[A_{11}]_{i,j} = \begin{cases} \frac{\beta^2}{h^2}, & j = i-1, \\ -\frac{2\beta^2}{h^2}, & j = i, \\ \frac{\beta^2}{h^2}, & j = i+1. \end{cases}$$

Similarly, the nonzero first row entries of A_{12} in the $(1,1)$, $(1,2)$ and $(1,3)$ entries are $\left(-\frac{3\gamma}{2hm_0} - \frac{\alpha_0}{m_0}\right)$, $\left(\frac{4\gamma}{2hm_0}\right)$, $\left(-\frac{\gamma}{2hm_0}\right)$, respectively. The nonzero last row entries of A_{12} in the $(n, n-2)$, $(n, n-1)$ and (n,n) entries are $\left(-\frac{\gamma}{2hm_l}\right)$, $\left(\frac{4\gamma}{2hm_l}\right)$, $\left(-\frac{\alpha_l}{m_l} - \frac{3\gamma}{2hm_l}\right)$, respectively. The middle part of the matrix $i = 2, 3, \ldots, n-1$ is a tridiagonal matrix. So the entries are

$$[A_{12}]_{i,j} = \begin{cases} \frac{\gamma}{h^2}, & j = i-1, \\ -\alpha - \frac{2\gamma}{h^2}, & j = i, \\ \frac{\gamma}{h^2}, & j = i+1. \end{cases}$$

Also,

$$F_{12} = \begin{bmatrix} 0 & \cdots & 0 \\ \vdots & \ddots & \vdots \\ 0 & \cdots & -m_l^{-1}k_3 \end{bmatrix}, \quad C = \begin{bmatrix} 0 & \cdots & 1 & \cdots & 0 \\ 0 & \cdots & 0 & \cdots & 1 \end{bmatrix}, \quad B_1 = \begin{bmatrix} 0 \\ \vdots \\ m_0^{-1} \\ \vdots \\ 0 \end{bmatrix}.$$

Furthermore, A_{11}, $A_{1,2}$, F_{12} are $n \times n$ matrices, C is a $2 \times 2n$ matrix and B_1 is a $n \times 1$ matrix.

Or, we can write the nonlinear finite dimensional approximating system as

$$\dot{x} = Ax + F(x) + Bu, \quad y = Cx. \tag{2.31}$$

2.7.4. Implementation of Balanced Truncation Method. We compute the balanced truncated reduced order model using the "square root algorithm" described in [9]. The algorithm generates matrices $T_r \in R^{2n \times r}$ and $S_r \in R^{r \times 2n}$ such that $T_r = [\varphi_1, \varphi_{2, \cdots}, \varphi_r]$, where φ_j denote the jth column of T_r, and $S_r = [\psi_1, \psi_{2, \cdots}, \psi_r]^T$, where ψ_i denote the ith row of S_r. Further $S_r T_r = I_r$, where I_r is an identity matrix.

Approximate $x(t)$ in the nonlinear full order model (2.31) by $x(t) \approx T_r a(t)$, and multiply the full order model on the left by S_r to produce the reduced order model

$$\dot{a}(t) = A_r a(t) + B_r u(t) + S_r F(T_r a), \quad y_r(t) = C_r a(t).$$

The matrices A_r, B_r, and C_r in the reduced order model are given by $A_r = S_r A T_r$, $B_r = S_r B$ and $C_r = C T_r$. These are exactly the same matrices from the balanced truncated reduced order model in the linear case.

We want to rewrite the nonlinear term $S_r F(T_r a)$ in terms of a_j, φ_j, ψ_j so that we can compute the reduced order model using only low order operations. The $2n \times r$ matrix T_r has ij entries $\varphi_{j,i}$, where $\varphi_{j,i}$ denotes the ith entry of φ_j, for $i = 1 \ldots 2n$

and $j = 1 \ldots r$. Also, $a = [a_1, a_2, \ldots, a_r]^T$ is a $r \times 1$ dimension vector. Then $\sum_{j=1}^{r} \varphi_{j,i} a_j$ is the ith entry of the vector of $T_r a$ with $2n \times 1$ dimension where

$$T_r a = \left[\sum_{j=1}^{r} \varphi_{j,1} a_j, \ldots, \sum_{j=1}^{r} \varphi_{j,2n} a_j \right]^T . \qquad (2.32)$$

In our system we have only one nonlinear term that is in the right boundary condition. Let d_r be the vector consisting of the first n entries of $T_r a$. Using the definition of $F(x)$ from the previous section gives

$$F(T_r a) = \begin{bmatrix} 0 \\ F_0(d_r) \end{bmatrix} , \quad F_0(d_r) = [0, \ldots, 0, -m_l^{-1} k_3 (T_r a)_n^3]^T ,$$

where $(T_r a)_n$ denotes the nth entry of $T_r a$. Therefore, we do not need to compute the entire $2n \times 1$ vector $T_r a$ as in (2.32); we only need the nth entry. This gives

$$[F(T_r a)]_j = \begin{cases} 0 & j \neq 2n, \\ -m_l^{-1} k_3 \left(\sum_{j=1}^{r} \varphi_{j,n} a_j \right)^3 & j = 2n. \end{cases}$$

Therefore, the nonlinear term in the reduced order model can be computed using only low order operations by

$$[S_r F(T_r a)]_i = -m_l^{-1} k_3 \psi_{i,2n} \left(\sum_{j=1}^{r} \varphi_{j,n} a_j \right)^3 , \quad i = 1, 2, \ldots, r,$$

where $\psi_{i,2n}$ denotes the $2n$th entry of the vector ψ_i.

2.8. NUMERICAL RESULTS

In this section, we present the numerical results concerning the effectiveness of the balanced truncation MOR method applied to the finite difference approximation

Table 2.1. Fixed Simulation Parameters

l	m_0	m_l	k_3	β
1	1	1.5	1	1

of the cable-mass problem. For our experiments, we used 100 finite difference nodes and solved all ordinary differential equations with Matlab's `ode23s`. Increasing the number of nodes did not make any substantial change in the results. We fixed some of the basic problem parameters, as shown in Table 2.1, and tested variations of the remaining parameters to determine when the MOR approach is accurate.

In our model, there are two types of interior damping. One is Kelvin-Voigt damping and the other is viscous damping. The Kelvin-Voigt damping is proportional to the rate of change of strain. The viscous damping is proportional to velocity. The Kelvin-Voigt damping parameter is γ and the viscous damping parameters are $\alpha, \alpha_0, \alpha_l$ and those are interior and boundary damping parameters, respectively. Also there are three stiffness parameters: k_0, k_l, and k_3. Here k_3 is the stiffness parameter for the nonlinear term. We investigate the following examples:

- Example 1: Kelvin-Voigt damping in the interior ($\gamma > 0$) and damping in the in the right boundary ($\alpha_l > 0$). All other damping parameters are taken to be zero, i.e., $\alpha_0 = \alpha = 0$.

- Example 2: Viscous damping in the interior ($\alpha > 0$) and damping in both boundaries $\alpha_0, \alpha_l > 0$. The Kelvin-Voigt damping parameter γ is set to zero. Unlike Example 1, the C_0-semigroup generated by the linear problem is not analytic in this case and the PDE is hyperbolic.

- Example 3: Viscous damping in the interior ($\alpha > 0$) and Kelvin-Voigt damping in the interior ($\gamma > 0$). All other damping parameters are taken to be zero, i.e., $\alpha_0 = \alpha_l = 0$.

- Example 4: Viscous damping in the interior ($\alpha > 0$). All other damping parameters are taken to be zero, i.e., $\gamma = \alpha_0 = \alpha_l = 0$.

- Example 5: Kelvin-Voigt damping in the interior ($\gamma > 0$). All other damping parameters are taken to be zero, i.e., $\alpha = \alpha_0 = \alpha_l = 0$.

In Sections 2.5.2 and 2.6 we proved that the unforced linear and nonlinear systems are exponentially stable for Examples 1-3. Numerical results indicate that the linear problems are also exponentially stable for Examples 4-5. We do not investigate Examples 4-5 theoretically here.

2.8.1. Exponential Stability. Before we present the model reduction computational results, we briefly present numerical results concerning the linear and nonlinear exponential stability theory. For the linear problem, we test the exponential stability by analyzing the eigenvalues of the matrix A in the finite difference model (2.31). Figure 2.2(a) shows the eigenvalues of matrix A for $\gamma = \alpha_l = 0.1$, $k_0 = k_l = 1$, and $\alpha_0 = \alpha = 0$. This is a case of Example 1. The eigenvalues all have negative real parts. For the nonlinear problem, we consider the solution of the finite difference model (2.31), and compute an approximation to the (continuous) energy function in Theorem 2.8 by using trapezoidal rule quadrature on the integrals. Figure 2.2(b) shows the exponential decay of the energy with the same parameters and the initial data $e^x \sin(1 - x)$ for the position and $\cos(x)$ for the velocity.

We also approximated the eigenvalues and the energy for the nonlinear problem when $\gamma = 0$; see Figure 2.3. This is a case of Example 2. We see the exponential stability in both linear and nonlinear cases. The C_0-semigroup is not analytic in this case, and we see the imaginary part of the eigenvalues increase as is usual with hyperbolic problems. In the nonlinear case, if $\gamma = 0$ and all the other parameters are small, then the energy decays exponentially fast and also fluctuation takes place rapidly.

(a) Eigenvalues of the linear system

(b) Energy decay of the nonlinear system
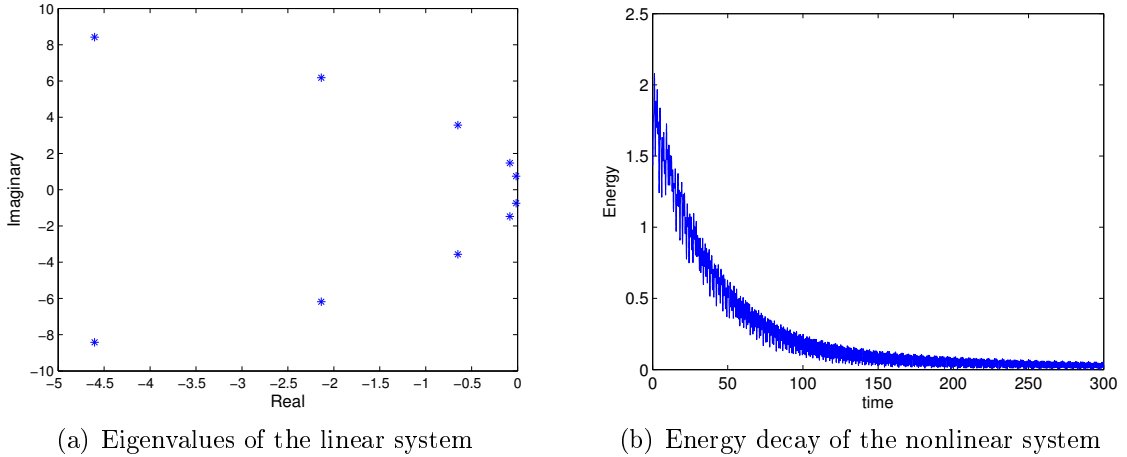
Figure 2.2. Eigenvalues and the energy decay for $\gamma = \alpha_l = 0.1$, $k_0 = k_l = 1$ and $\alpha_0 = \alpha = 0$

(a) Eigenvalues of the linear system

(b) Energy decay in nonlinear system
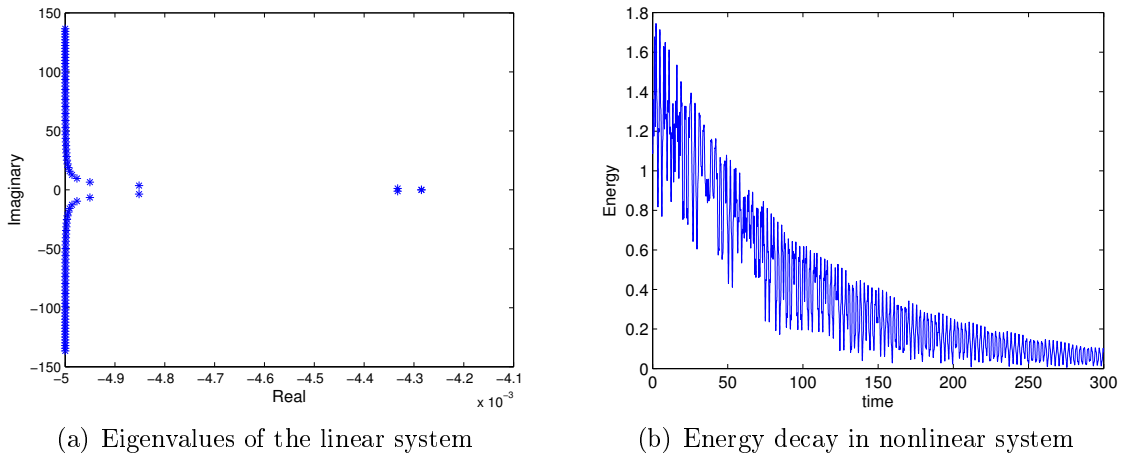
Figure 2.3. Eigenvalues and the energy decay for $\gamma = 0$ and $\alpha = \alpha_0 = \alpha_l = k_0 = k_l = 0.01$

Furthermore, we look at the behavior of the eigenvalue nearest the imaginary axis by increasing the number of spatial nodes. As we can see in Tables 2.2 and 2.3 the eigenvalue do not approach the imaginary axis when the number of spatial nodes is increased. This is the behavior we expect since the PDE system is exponentially stable.

Table 2.2. Eigenvalues of the linear system for number of spatial nodes with $\gamma = \alpha_l = 0.1$, $k_0 = k_l = 1$ and $\alpha = \alpha_0 = 0$

N	10	20	40	80	160
Re (λ)	-0.0160	-0.0160	-0.0160	-0.0160	-0.0160

Table 2.3. Eigenvalues of the linear system for number of spatial nodes with $\gamma = 0$ and $\alpha = \alpha_0 = \alpha_l = k_0 = k_l = 0.01$

N	10	20	40	80	160
Re (λ)	-0.0043	-0.0043	-0.0043	-0.0043	-0.0043

2.8.2. Model Reduction Results. Next, we begin the model reduction experiments. We study the effects of the various parameters on the accuracy of the model reduction. To do this, we consider the reduced order model (ROM) and full order model (FOM) with zero initial data and the same input $u(t)$ and compare the output of the FOM and ROM. Recall the output $y(t)$ of the cable-mass system is the position and velocity of the right mass.

Although we focus on the accuracy of the nonlinear ROM, we also present some results for the linear ROM for comparison. The output of the linear ROM is highly accurate in all cases considered, as expected by balanced truncation theory.

For our experiments, we investigate the behavior of the ROM and FOM for four different oscillating smooth or discontinuous input functions $u(t)$.

- Input 1: $u(t) = 0.1 \sin(0.2\pi t)$

- Input 2: $u(t) = 0.02 \cos(at) + 0.03 \cos(bt)$, where a, b are the two largest real parts of the eigenvalues of the matrix A

- Input 3: $u(t) = c_1 \sin(mt) + c_2 \cos(nt)$, where c_1, c_2, m, n are constants in the range of $c_1, c_2, < 0.1$ and $m, n < 0.2$

- Input 4: $u(t) = 0.1\text{square}(0.2\pi t)$, where the square wave function is defined by square$(\tau) = 1$ if $\sin(\tau) > 0$ and square$(\tau) = -1$ if $\sin(\tau) < 0$

Input 1 was originally considered for this problem in [19], where this cable-mass system was considered as a heuristic model for a wave tank with a wave energy converter. Input 2 was considered for a different cable-mass problem in [36]. We note that this input causes a type of resonance, i.e., the solution magnitude can initially grow in time before the damping causes the magnitude to return to a moderate level. We also considered Input 3 to test a variety of oscillating input behaviors. Finally, we considered Input 4 to see if a discontinuous input causes any change in the ROM output.

- Small damping parameters

Case 1a : Small damping parameters with smooth inputs

Here we investigate the behavior of the ROM for damping parameters that are small relative to the boundary stiffness parameters. We experiment for damping parameters α, α_0, α_l, γ in the range of 0.1 to 0.001, and fix $k_0 = k_l = 0.1$. In this case, for all smooth inputs (Inputs 1-3) the output of the nonlinear ROM is highly accurate compared to the FOM output. We present results for two specific scenarios. Figure 2.4 shows the output of the FOM and ROM for both the linear and nonlinear systems for Example 1, Input 2 with $\alpha_0 = \alpha = 0$, $\alpha_l = k_0 = k_l = 0.1$, and small Kelvin-Voigt parameter $\gamma = 0.001$. The agreement is excellent in both the linear and nonlinear cases.

Figure 2.5 shows the output of the FOM and ROM for both the linear and nonlinear systems for Example 2, Input 2 with $\gamma = 0$, $k_0 = k_l = 0.1$, $\alpha_0 = \alpha_l = 0.01$, and small interior viscous parameter $\alpha = 0.001$. The linear and nonlinear ROMs are highly accurate. Further, the output of the linear and nonlinear systems have similar patterns but the amplitudes are different in each graph.

(a) Linear system

(b) Nonlinear system
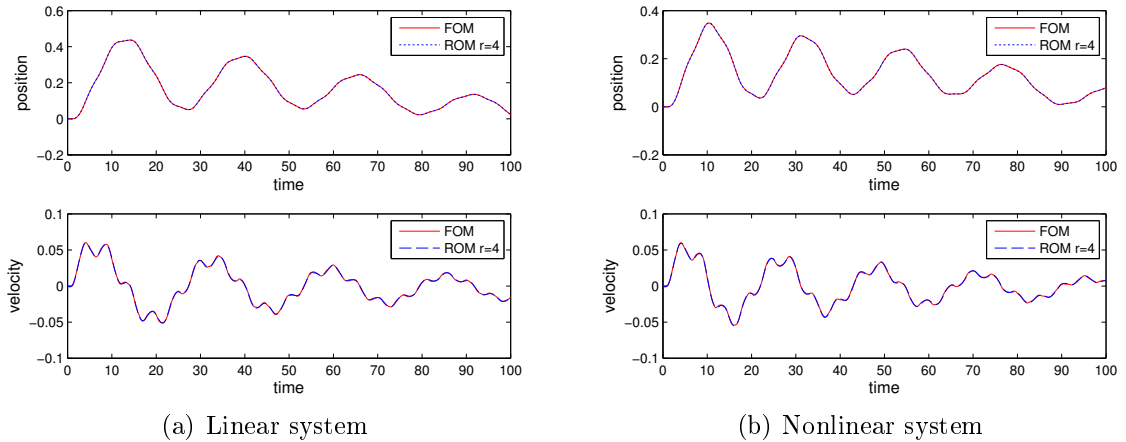
Figure 2.4. Example 1, Input 2: Output of the ROM and FOM for $\alpha_0 = \alpha = 0$, $\alpha_l = k_0 = k_l = 0.1$ and $\gamma = 0.001$

(a) Linear system

(b) Nonlinear system
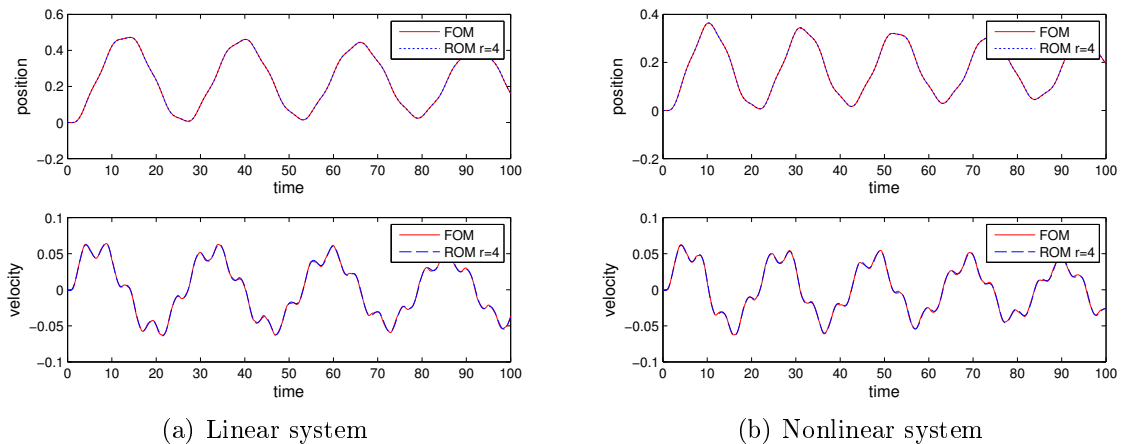
Figure 2.5. Example 2, Input 2: Output of the ROM and FOM for $\gamma = 0$, $k_0 = k_l = 0.1$, $\alpha_0 = \alpha_l = 0.01$, $\alpha = 0.001$

Case 1b : Small damping parameters with discontinuous input

Next we observe the behavior of the ROM and FOM for small damping with discontinuous input. Figure 2.6 shows the behavior of the linear and nonlinear FOM and ROM for Example 5, Input 4 (the square wave) with $\alpha = \alpha_0 = \alpha_l = 0$, $\gamma = 0.001$ and $k_0 = k_l = 0.1$. The linear and nonlinear FOM and ROM output are highly accurate even though the position and velocity outputs are very irregular.

(a) Linear system   (b) Nonlinear system
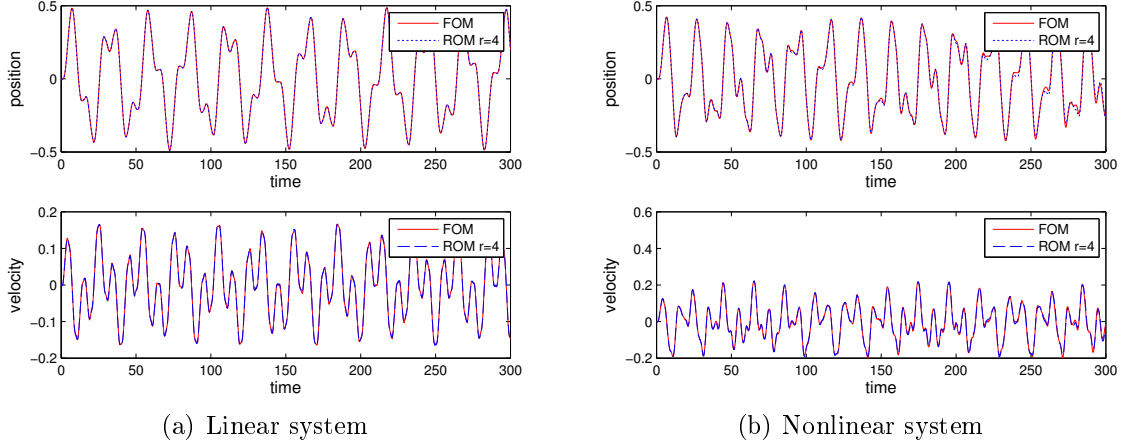
Figure 2.6. Example 5, Input 4: Output of the ROM and FOM for $\alpha = \alpha_0 = \alpha_l = 0$, $\gamma = 0.001$ and $k_0 = k_l = 0.1$

Overall, we can conclude that the linear and nonlinear ROM outputs are very accurate for a long time interval for all examples and all inputs when the damping parameters are small relative to the boundary stiffness parameters.

- Small stiffness parameters

Case 2a : Small stiffness parameters with smooth inputs

Next, we investigate the behavior of the FOM and ROM when the boundary stiffness parameters are small relative to the damping parameters. We fix the damping parameters as $\gamma = \alpha = \alpha_0 = \alpha_l = 0.1$. We observe that if one or both of the stiffness parameter are small (either k_0 or k_l in the range of 0.001 to 0.1), we get highly accurate ROM output for both linear and nonlinear systems with all smooth inputs. Two specific scenarios are presented below.

Figure 2.7 shows the behavior of the ROM and FOM of the linear and nonlinear systems for Example 1, Input 1 with $\alpha = \alpha_0 = 0$, $\gamma = \alpha_l = 0.1$, and $k_0 = k_l = 0.001$. Figure 2.8 shows the behavior of the ROM and FOM of the linear and nonlinear systems for Example 4, Input 3 with $\alpha = 0.1$, $\gamma = 0$, $\alpha_0 = \alpha_l = 0$, and $k_0 = 0.001$, $k_l = 0.01$.

(a) Linear system   (b) Nonlinear system
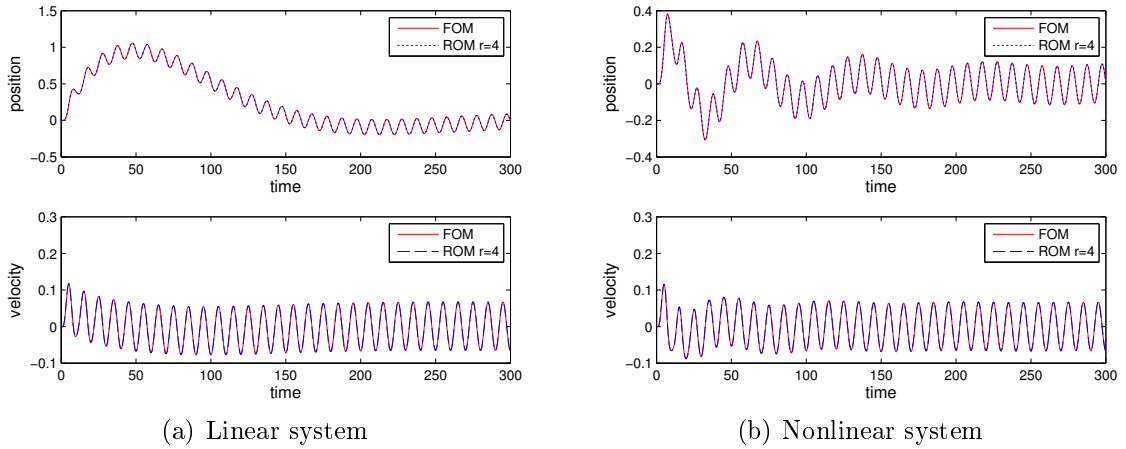
Figure 2.7. Example 1, Input 1: Output of the ROM and FOM for $k_0 = k_l = 0.001$, $\alpha = \alpha_0 = 0$, and $\gamma = \alpha_l = 0.1$

(a) Linear system   (b) Nonlinear system
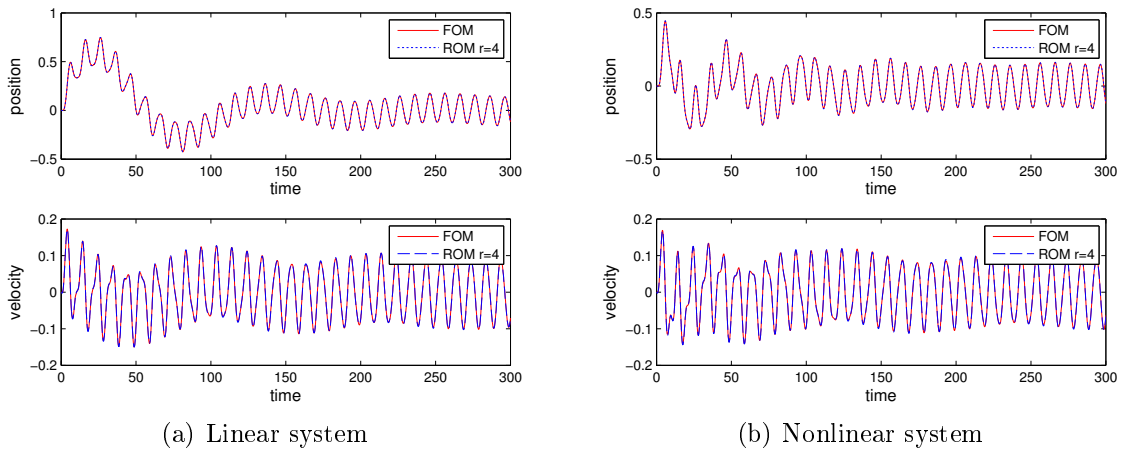
Figure 2.8. Example 4, Input 3: Output of the ROM and FOM for $\alpha = 0.1$, $\gamma = 0$, $\alpha_0 = \alpha_l = 0$ and $k_0 = 0.001$, $k_l = 0.01$

Overall, for all examples with all smooth inputs, the linear and nonlinear ROM are highly accurate over a long time interval.

Case 2b : Small stiffness parameters with discontinuous Input 4

Next, we explore the behavior of the ROM and FOM for smaller stiffness parameters with discontinuous input (square wave input). We present results of two specific

(a) Linear system (b) Nonlinear system
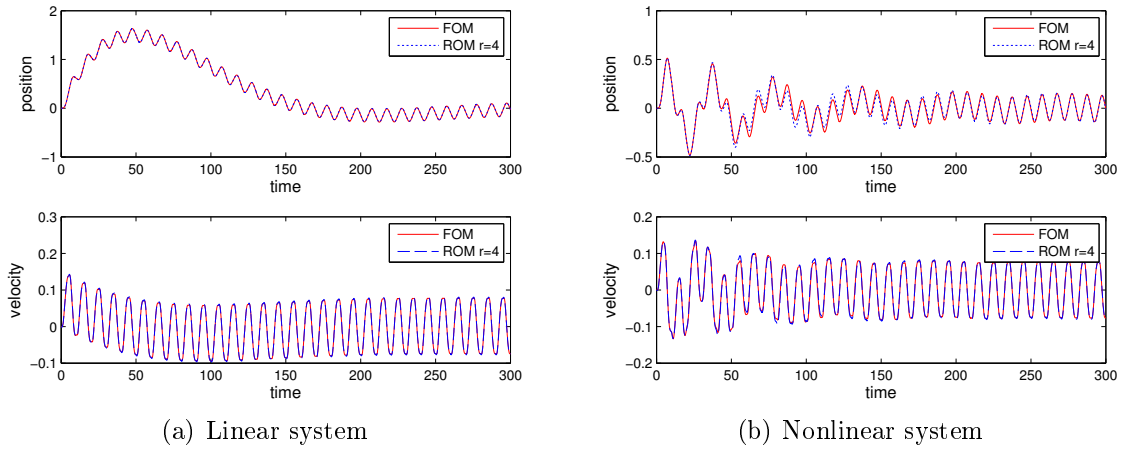
Figure 2.9. Example 1, Input 4: Output of the ROM and FOM for $\alpha = \alpha_0 = 0$, $\gamma = \alpha_l = 0.1$, and $k_0 = k_l = 0.001$

scenarios with small stiffness parameters. First, Figure 2.9 shows the behavior of the linear and nonlinear FOM and ROM output for Example 1 with $\alpha = \alpha_0 = 0$, $\gamma = \alpha_l = 0.1$, and small stiffness $k_0 = k_l = 0.001$. The nonlinear ROM for $r = 4$ is accurate over an initial time interval and thereafter loses some accuracy. Increasing r yields high accuracy for the entire time interval $0 \leq t \leq 300$. The linear ROM is highly accurate for a longer interval.

Figure 2.10 shows the FOM and ROM output over the longer interval $0 \leq t \leq 300$ for another scenario: Example 5, Input 4 with $\gamma = 0.1$, $\alpha = \alpha_0 = \alpha_l = 0$ and small stiffness $k_0 = k_l = 0.001$. The nonlinear ROM is highly accurate for an initial time period, but then suffers a loss of accuracy. Increasing r does not yield high accuracy.

Next, we explore the behavior of the nonlinear ROM depending on the right and left stiffness parameters. In Examples 1, 3, 4, 5 with Input 4, the left stiffness parameter affects the nonlinear ROM more than the right stiffness parameter. Figure 2.11(a) shows the behavior of the ROM of the nonlinear system for Example 3, Input 4 with $\alpha_0 = \alpha_l = 0$, $\alpha = \gamma = 0.1$ and $k_0 = 0.01$, $k_l = 0.001$, and in Figure 2.11(b) with

(a) Nonlinear system for $r = 4$ (b) Nonlinear system for $r = 8$
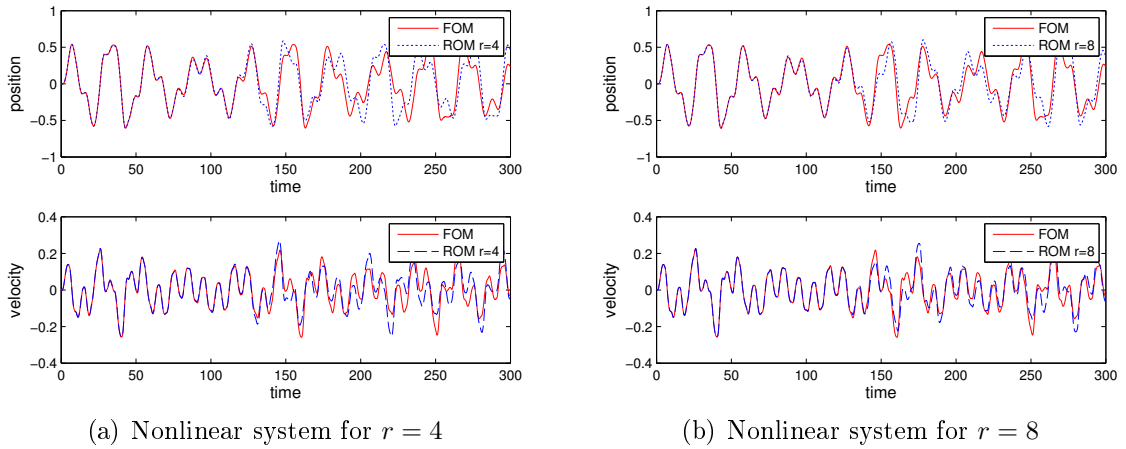
Figure 2.10. Example 5, Input 4: Output of the ROM and FOM for $\gamma = 0.1$, $\alpha = \alpha_0 = \alpha_l = 0$ and $k_0 = k_l = 0.001$

(a) $k_0 = 0.01$, $k_l = 0.001$.   (b) $k_0 = 0.001$, $k_l = 0.01$.
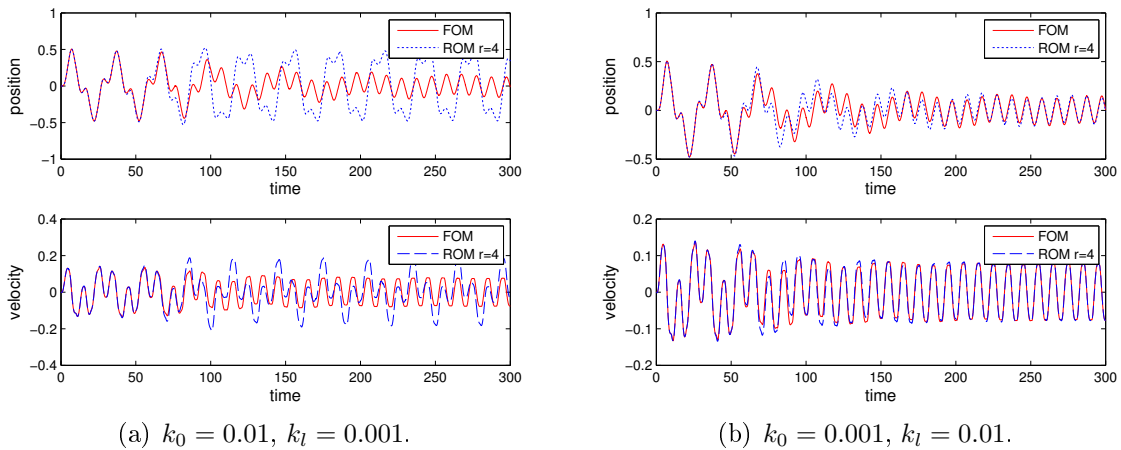
Figure 2.11. Example 3, Input 4: Output of the nonlinear ROM and FOM for $\alpha_0 = \alpha_l = 0$, $\alpha = \gamma = 0.1$

$\alpha_0 = \alpha_l = 0$, $\alpha = \gamma = 0.1$, and $k_0 = 0.001$, $k_l = 0.01$. The nonlinear ROM output belonging to the smaller right stiffness parameter is much less accurate compared to the ROM output belonging to the smaller left stiffness parameter. Increasing r improves the accuracy of the ROM in both cases over a long interval.

Succinctly, when the stiffness parameters are small relative to the damping parameters, the nonlinear ROM is highly accurate in all examples with smooth inputs.

However, for the discontinuous input, the nonlinear ROM is highly accurate over an initial interval and then accuracy is likely to be lost. Increasing the order r of the ROM may not improve the accuracy. Also, if the magnitude of the input is reduced, then the length of the highly accurate initial time interval does increase. Further, the nonlinear ROM is much less accurate when the right stiffness parameter is small when compared to the small left stiffness parameter.

- Small damping and stiffness parameters (All parameters are small)

Finally, we consider the behavior of the nonlinear ROM when the damping and stiffness parameters are small relative to the mass and nonlinear stiffness parameters ($m_0 = 1$, $m_l = 1.5$, and $k_3 = 1$).

Case 3a : Small damping and stiffness parameters with continuous Input 2

The nonlinear ROM is highly accurate in all examples with Input 2. Figure 2.12 shows the behavior of the ROM of the nonlinear system for Example 3 for $\alpha_0 = \alpha_l = 0$ and $\alpha = \gamma = k_0 = k_l = 0.001$ with input $u(t) = 0.02\cos(0.0001t) + 0.03\cos(0.0008t)$ and Example 5 for $\alpha = \alpha_0 = \alpha_l = 0$ and $\gamma = k_0 = k_l = 0.001$ with Input 2 $u(t) = 0.02\cos(0t) + 0.03\cos(0.0007t)$. Overall, we can conclude that the nonlinear ROM is very accurate in all examples with Input 2 when both damping and stiffness parameters are small.

Case 3b : Small damping and stiffness parameters with Input 3

The nonlinear ROM is highly accurate in Examples 1, 3, 4, 5 with Input 3 over a long interval. Only in Example 2 does the nonlinear ROM lose accuracy over a long time period, but increasing r improves the accuracy. Figure 2.13 shows the nonlinear ROM output for Example 2, Input 3 with $\gamma = 0$ and $\alpha = \alpha_0 = \alpha_l = k_0 = k_l = 0.001$ for $r = 4$ and $r = 6$. Overall, we can conclude that the nonlinear ROM is very accurate over a long interval in all examples except Example 2 with Input 3 when the damping and stiffness parameters are small. Increasing r improves the accuracy.

(a) Example 3, Input 2   (b) Example 5, Input: 2
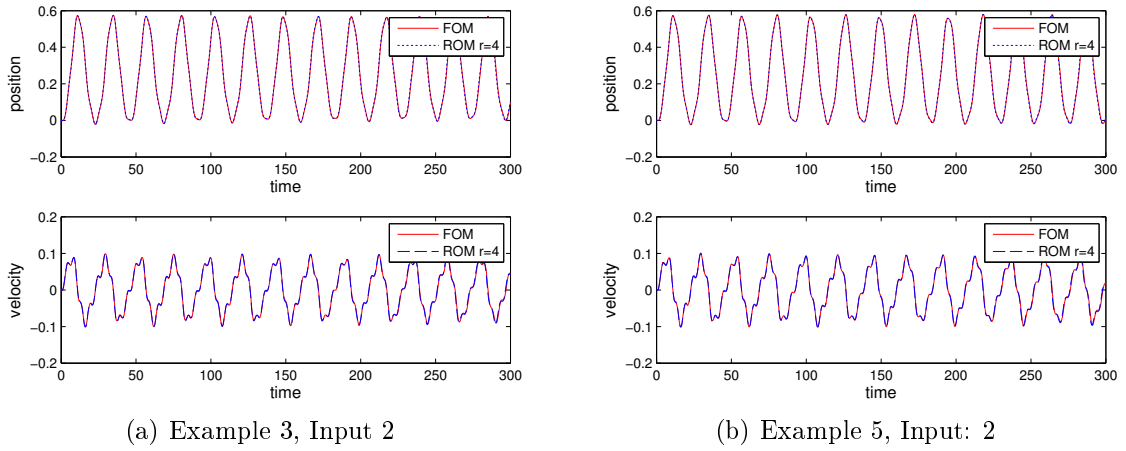
Figure 2.12. Output of the nonlinear ROM and FOM

(a) Nonlinear system for $r = 4$ (b) Nonlinear system for $r = 6$
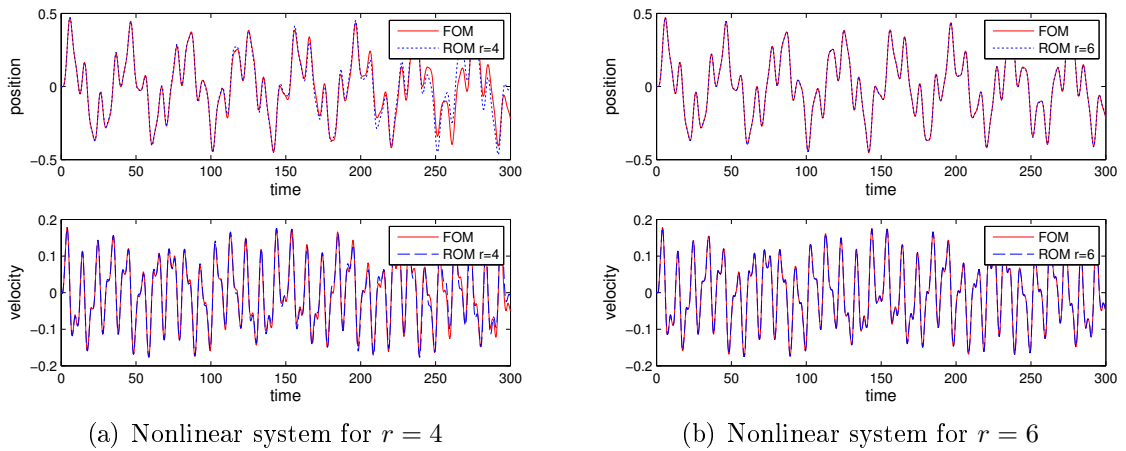
Figure 2.13. Example 2, Input 3: Output of the ROM and FOM for $\gamma = 0$, $\alpha = \alpha_0 = \alpha_l = k_0 = k_l = 0.001$

Case 3c : Small damping and stiffness parameters with Input 1

For all examples, the nonlinear ROM output is highly accurate for an initial time period, but then suffers loss of accuracy with Input 1. Increasing r improves the accuracy over a long interval.

Case 3d : Small damping and stiffness parameters with Input 4

(a) Nonlinear system for $r = 4$　　　　(b) Nonlinear system for $r = 10$
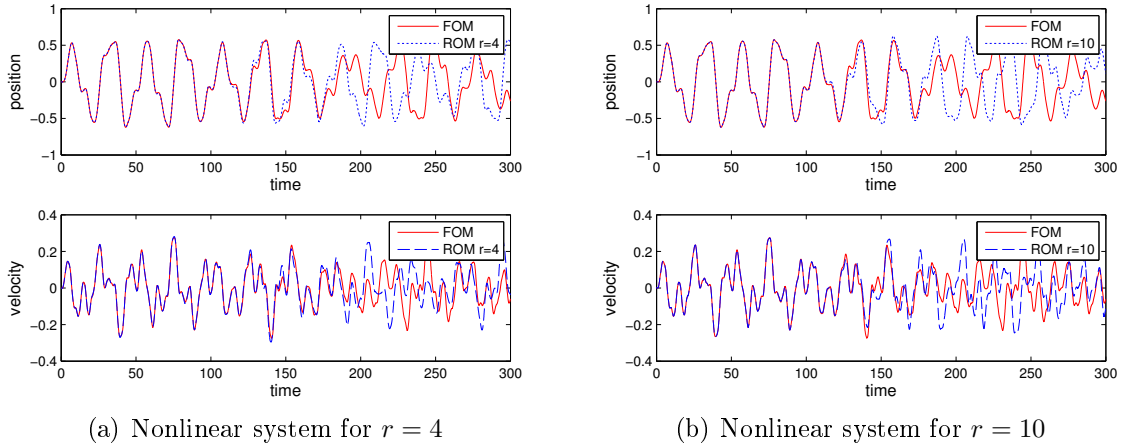
Figure 2.14. Example 1, Input 4: Output of the ROM and FOM for $\alpha = \alpha_0 = 0$, $\gamma = \alpha_l = k_0 = k_l = 0.001$

For all examples, the nonlinear ROM output is highly accurate only for an initial time period, but then suffers a great loss of accuracy. Increasing r does not improve the accuracy over a long time interval. Figure 2.14 shows the behavior of the nonlinear FOM and ROM for Example 1 with Input 4 with $\alpha = \alpha_0 = 0$ and $\gamma = \alpha_l = k_0 = k_l = 0.001$ for $r = 4$ and $r = 10$. Overall, when all parameters are small, all behaviors are possible. The nonlinear ROM may be highly accurate over a long time period, or it may lose high accuracy after an initial time period. Also, increasing r may or may not improve the accuracy over a long interval.

3. NONLINEAR CABLE-MASS PDE SYSTEM WITH UNBOUNDED INPUT OPERATOR

In this section, we study the performance of the balanced truncation model reduction when the operator $\mathcal{B}$ is unbounded. We do not attempt to prove the infinite dimensional balanced truncation theory for this problem. Instead, we investigate the model reduction numerically. As we mentioned in the introduction, several PDE examples have been investigated numerically in the literature to understand the behavior of ROMs (see e.g., [23, 24, 25, 26, 27, 28, 29, 30, 32, 33, 34, 35]). The unforced PDE system considered in this section differs from the cable-mass problem in Section 2. We prove the linear and nonlinear exponential stability for this model in this section.

3.1. THE MODEL

The flexible cable is driven by an external force $u(t)$ acting on the left end and is attached to a mass-spring system at the other end. The mass-spring system is connected to a rigid horizontal support, and we assume all motion takes place in the vertical direction. Let

- $w(t, x)$ denote the position of the cable at location x and time t, and

- $w_l(t)$ denote the position of the right mass above equilibrium at location $x = l$ and time t.

We assume there are no other external forces acting on the system.

We model the motion of the flexible cable with a damped 1D wave equation on $0 < x < l$. We include both Kelvin-Voigt and viscous damping in the model. We model the mass-spring system with a damped nonlinear second order oscillator. This

gives a wave equation with a dynamic boundary condition:

$$w_{tt}(t,x) + \alpha w_t(t,x) = \gamma w_{txx}(t,x) + \beta^2 w_{xx}(t,x), \tag{3.1}$$

$$\gamma w_{tx}(t,0) + \beta^2 w_x(t,0) = u(t), \tag{3.2}$$

$$m_l \ddot{w}_l(t) + \alpha_l \dot{w}_l(t) + k_l w_l(t) = -(\gamma w_{tx}(t,l) + \beta^2 w_x(t,l)) - k_3 \left[w_l(t) \right]^3. \tag{3.3}$$

The term in the parenthesis in the dynamic boundary condition is the force of the cable acting on the mass. The boundary condition (3.2) indicates the external force $u(t)$ is applied at the left end of the cable. Here, γ is the Kelvin-Voigt damping parameter, α and α_l are viscous damping parameters, m_l is the right mass, and k_l, k_3 are the stiffness parameters. The model damping parameters are nonnegative, and the wave equation parameter β as well as the mass and stiffness parameters are all positive. Finally, the position of the cable at the boundary must equal the position of the mass; therefore, we have the *displacement compatibility condition*

$$w(t,l) = w_l(t).$$

For the model reduction problem, we assume we have two system outputs as in Section 2: the position and the velocity of the right mass, i.e.,

$$y_1(t) = w_l(t), \quad y_2(t) = \dot{w}_l(t).$$

3.2. THE ENERGY FUNCTION

Next, we give a preliminary investigation of the change in energy of the unforced system, i.e., the system with $u(t) = 0$. This will help us to obtain the correct inner products for an abstract formulation of the system. We assume the solution for the above system is sufficiently smooth.

We define the total kinetic energy of the cable by

$$E_{T,K} = \frac{1}{2} \int_0^l w_t^2 \, dx.$$

Differentiate with respect to time and use the wave equation (3.1) to obtain

$$\frac{dE_{T,K}}{dt} = \frac{1}{2} \int_0^l 2w_t w_{tt} \, dx$$

$$= \frac{1}{2} \int_0^l 2w_t(t,x)(\gamma w_{txx}(t,x) + \beta^2 w_{xx}(t,x) - \alpha w_t(t,x)) \, dx.$$

Integrate by parts to obtain

$$\frac{dE_{T,K}}{dt} = -\gamma \int_0^l (w_{tx}(t,x))^2 \, dx - \beta^2 \int_0^l w_x(t,x) w_{tx}(t,x) dx - \alpha \int_0^l (w_t(t,x))^2 \, dx$$

$$+ w_t(t,l) \left[\gamma w_{tx}(t,l) + \beta^2 w_x(t,l) \right] - w_t(t,0) \left[\gamma w_{tx}(t,0) + \beta^2 w_x(t,0) \right].$$

Use the boundary conditions of our cable-mass model (3.2), (3.3) to obtain

$$\frac{dE_{T,K}}{dt} = -\gamma \int_0^l (w_{tx}(t,x))^2 \, dx - \beta^2 \int_0^l w_x(t,x) w_{tx}(t,x) dx - \alpha \int_0^l (w_t(t,x))^2 \, dx$$

$$- \dot{w}_l(t) \left[m_l \ddot{w}_l(t) + \alpha_l \dot{w}_l(t) + k_l w_l(t) + k_3 \left[w_l(t) \right]^3 \right].$$

This can be rewritten as

$$\frac{d}{dt} \left(\frac{1}{2} \int_0^l w_t^2 \, dx + \frac{m_l}{2} \left(\dot{w}_l(t) \right)^2 + \frac{\beta^2}{2} \int_0^l w_x^2 \, dx + \frac{k_l}{2} \left(w_l(t) \right)^2 + \frac{k_3}{4} \left(w_l(t) \right)^4 \right) =$$

$$-\gamma \int_0^l (w_{tx}(t,x))^2 \, dx - \alpha \int_0^l (w_t(t,x))^2 \, dx - \alpha_l \left(\dot{w}_l(t) \right)^2.$$

This suggests defining the system kinetic energy and potential energy as

$$E_K = \int_0^l \frac{1}{2} w_t^2 \, dx + \frac{m_l}{2} \left(\dot{w}_l(t) \right)^2,$$

$$E_P = \int_0^l \frac{\beta^2}{2} w_x^2 \, dx + \frac{k_l}{2} \left(w_l(t) \right)^2 + \frac{k_3}{4} \left(w_l(t) \right)^4.$$

This energy expression can also be obtained by considering the kinetic energy and potential energy of each component of the system. The above energy equation gives

$$\frac{d}{dt} E = \frac{d}{dt} \left(E_K + E_P \right)$$
$$= - \left[\gamma \int_0^l \left(w_{tx}(t,x) \right)^2 dx + \alpha \int_0^l \left(w_t(t,x) \right)^2 dx + \alpha_l \left(\dot{w}_l(t) \right)^2 \right],$$

and therefore $\dot{E}(t) \leq 0$. This result matches physical intuition and gives the correct energy inner products for the system. Later on, we prove the energy decays exponentially fast to zero.

3.3. VARIATIONAL FORM

In this section, we introduce the variational form (weak form) of the system. Later, we use this form to analyze the model. We assume the solution $[w, w_l]$ is smooth and satisfies the compatibility condition $w(t,l) = w_l(t)$. Multiply the wave equation (3.1) by a smooth test function $h = h(x)$, where $h(l) = h_l$ to obtain

$$\int_0^l w_{tt}(t,x) \, h \, dx + \alpha \int_0^l w_t(t,x) \, h \, dx - \gamma \int_0^l w_{txx}(t,x) \, h \, dx - \beta^2 \int_0^l w_{xx}(t,x) \, h \, dx = 0.$$

Now integrate by parts:

$$\int_0^l w_{tt}(t,x)\, h\, dx + \alpha \int_0^l w_t(t,x)\, h\, dx - h_l \left[\gamma w_{tx}(t,l) + \beta^2 w_x(t,l)\right]$$

$$+ h(0) \left[\gamma w_{tx}(t,0) + \beta^2 w_x(t,0)\right] + \gamma \int_0^l w_{tx}(t,x)\, h_x\, dx + \beta^2 \int_0^l w_x(t,x)\, h_x\, dx = 0.$$

As in the above energy argument, we use the boundary conditions to give the variational form

$$\int_0^l w_{tt}(t,x)\, h\, dx + m_l \ddot{w}_l(t) h_l + \beta^2 \int_0^l w_x(t,x)\, h_x\, dx + k_l w_l(t) h_l + k_3 \left[w_l(t)\right]^3$$

$$+ \alpha_l h_l \dot{w}_l(t) + \int_0^l \left[\alpha w_t(t,x)\, h + \gamma w_{tx}(t,x)\, h_x\right] dx = 0. \tag{3.4}$$

Now, we give details about the function spaces to make the weak formulation precise. Let H be the real Hilbert space $H = L^2(0,l) \times \mathbb{R}$ with the inner product of $z = [w,\, w_l] \in H$ and $\psi = [p,\, p_l] \in H$ defined by

$$(z,\psi)_H = \int_0^l wp\, dx + m_l w_l p_l. \tag{3.5}$$

Let $V \subset H$ be the set of elements $z = [w,\, w_l] \in H^1(0,l) \times \mathbb{R}$ satisfying the displacement compatibility condition $w(l) = w_l$. For $z \in V$ as above and $\psi = [p,\, p_l] \in V$ define the V inner product of z with ψ by

$$(z,\psi)_V = \int_0^l \beta^2 w_x p_x\, dx + k_l w_l p_l. \tag{3.6}$$

We also use the notation $\sigma_1(z,\psi) = (z,\psi)_V$.

The H and V inner products, (3.5) and (3.6), can be derived from the energy function; also, the H and V norms are directly related to the system kinetic and potential energies, respectively. Specifically,

$$E_K = \frac{1}{2}\,(z_t,\,z_t)_H = \frac{1}{2}\,\|z_t\|_H^2\,,\quad E_P = \frac{1}{2}\,(z,\,z)_V + \frac{k_3}{4}w_l^4 = \frac{1}{2}\,\|z\|_V^2 + \frac{k_3}{4}w_l^4.$$

Furthermore, both inner products appear in the variational form (3.4).

Also, we define the damping bilinear form $\sigma_2 : V \times V \to \mathbb{R}$

$$\sigma_2(z,\psi) = \int_0^l (\gamma w_x p_x + \alpha w p)\, dx + \alpha_l w_l p_l. \tag{3.7}$$

Note that this bilinear form occurs in the variational form (3.4) as a damping term with all first order time derivatives.

The spaces and inner products are motivated by the above variational form (3.4). Further we can rewrite the above variational form (3.4) as (2.9).

3.4. ABSTRACT FORM

Our original PDE model (3.1) with the boundary conditions (3.2), (3.3) can be written as a first order abstract form (2.10). Similar to Burns & King's work [36], the PDE system suggests that the operator $\mathcal{A}$ can be formally defined as

$$D(\mathcal{A}) = \left\{ x = [w, w_l, v, v_l]^T \in V \times H \ : \ w \in H^1(0,l),\ v \in H^1(0,l),\ w(l) = w_l, \right.$$

$$\left. v(l) = v_l,\ \left(\beta^2 \frac{d}{d\xi}v + \gamma\frac{d}{d\xi}w\right)(0) = 0 \right\}$$

and

$$
\mathcal{A}x = \begin{bmatrix} w \\ w_l \\ v \\ v_l \end{bmatrix} = \begin{bmatrix} v \\ v_l \\ \frac{d}{d\xi}\left[\beta^2 \frac{d}{d\xi}w + \gamma \frac{d}{d\xi}v\right] - \alpha v \\ -\delta_l\left[\frac{\beta^2}{m_l}\frac{d}{d\xi}w + \frac{\gamma}{m_l}\frac{d}{d\xi}v\right] - \frac{k_l}{m_l}w_l - \frac{\alpha_l}{m_l}v_l \end{bmatrix}, \tag{3.8}
$$

where δ_l denotes the evaluation operator as before. Because the left boundary condition does not contain any of $\dot{w}$, $\dot{w}_l$, $\dot{v}$, $\dot{v}_l$, therefore it is impossible to write $\dot{x} = \mathcal{A}x + \mathcal{B}u$ holding in $\mathcal{H} = V \times H$. Therefore the operator $\mathcal{B}$ is said to be unbounded. It is possible to use the variational form to define $\mathcal{B}$, but we do not consider this here.

Furthermore, define the operators C and $\mathcal{F}$ by

$$
C = \begin{bmatrix} 0 & 1 & 0 & 0 \\ 0 & 0 & 0 & 1 \end{bmatrix}, \quad \mathcal{F}(x) = \begin{bmatrix} 0 & 0 & 0 & m_l^{-1}k_3 w_l^3 \end{bmatrix}^T.
$$

As before, we do not use the formal definition of the operator $\mathcal{A}$ given above. Instead, we use theory from Banks [51] to rigorously define the operator $\mathcal{A}$ using the bilinear forms σ_1 and σ_2.

3.5. THE LINEAR PROBLEM

We prove the linear problem (2.12) is well-posed and also exponentially stable under certain assumptions on the damping parameters. The exponential stability is necessary for the application of the balanced truncation model reduction technique which is considered later.

3.5.1. Function Spaces. We first present basic results about the function spaces that we frequently use in this work.

Lemma 3.1. *The space V with the above inner product (3.6) is a real Hilbert space, and V is dense in H.*

Proof. First, if $(z, z)_V = 0$, where $z = [w, w_l]$, then $w(x)$ is a constant function and $w_l = 0$. The compatibility condition implies $w(x) = 0$ for all x, and so $z = 0$. It is straightforward to show that $(\cdot, \cdot)_V$ satisfies the remaining properties of an inner product.

Next, let $\{z^n\} \subset V$ be a Cauchy sequence, where $z^n = [w^n, w_l^n]$. Therefore, $[w_x^n, w_l^n]$ is a Cauchy sequence in $L^2(0, l) \times \mathbb{R}$, and so there exists $[q, w_l] \in L^2(0, l) \times \mathbb{R}$ such that

$$w_x^n \to q \text{ in } L^2(0, l), \quad w_l^n \to w_l.$$

Note:

$$w^n(x) = w^n(0) + \int_0^x w_x^n(\eta) d\eta$$

$$w^n(x) - w^n(0) = \int_0^x w_x^n(\eta) d\eta$$

$$w^n(l) - w^n(0) = \int_0^l w_x^n(\eta) d\eta$$

$$w^n(0) = w_l^n - \int_0^l w_x^n(\eta) d\eta.$$

We know $w_l^n \to w_l$ and $w_x^n \to q$ in $L^2(0, l)$. Therefore, $\lim_{n \to \infty} w^n(0)$ exists and

$$\lim_{n \to \infty} w^n(0) = w_l - \int_0^l q(\eta) d\eta = C \text{ (constant)}.$$

Define w by $w(x) = w_l - \int_x^l q(\eta) d\eta$. Then we can rewrite

$$w(x) = w_l - \int_0^l q(\eta) d\eta + \int_0^x q(\eta) d\eta,$$

$$w(x) = C + \int_0^x q(\eta) d\eta.$$

Then $w \in H^1(0, l)$, $w_x = q$, and $w(0) = C$. Also, $w(l) = w_l$ since

$$
\begin{aligned}
w(l) &= \lim_{n\to\infty} \left(C + \int_0^l w_x^n(\eta) d\eta \right) \\
&= \lim_{n\to\infty} \left(C + w^n(\eta) \big|_0^l \right) \\
&= \lim_{n\to\infty} \left(C + w^n(l) - w^n(0) \right) \\
&= \lim_{n\to\infty} w_l^n = w_l,
\end{aligned}
$$

where we used $w^n(l) = w_l^n$. Therefore $z = [w, w_l]$ satisfies the displacement compatibility condition and z^n converges in V to $z \in V$. This shows V is a Hilbert space.

To show V is dense in H, let $z = [w, w_l] \in H$ and define

$$
g(x) = C + l^{-1}(w_l - C)x,
$$

where C is defined above. Note that $g(0) = C$ and $g(l) = w_l$. Therefore, $w - g \in H^1(0, l)$. Since $H_0^1(0, l)$ is dense in $L^2(0, l)$, there exists a sequence $q_n \in H^1(0, l)$ such that $q_n \to w - g$ in $L^2(0, l)$. Define

$$
z_n = [q_n + g, \, w_l].
$$

Due to the properties of q_n and g, i.e., $q_n + g \in H^1(0, l)$, $(q_n + g)(0) = C$, and $(q_n + g)(l) = w_l$ we have $z_n \in V$ for all n. Also,

$$
\begin{aligned}
\lim_{n \to \infty} \|z_n - z\|_H^2 &= \lim_{n \to \infty} \|q_n + g - w\|_{L^2(0,l)}^2 + |w_l - w_l|^2 \\
&= \lim_{n \to \infty} \int_0^l (q_n + g - w)^2 dx \\
&= \lim_{n \to \infty} \int_0^l (q_n - (w - g))^2 dx \\
&= \lim_{n \to \infty} \|q_n - (w - g)\|_{L^2(0,l)}^2 \\
&= 0.
\end{aligned}
$$

This proves V is dense in H. $\qquad\square$

Lemma 3.2. *If $z = [w, w_l] \in V$, then*

$$
|w(x)|^2 \le 2|w_l|^2 + 2l \|w_x\|_{L^2(0,l)}^2, \tag{3.9}
$$

$$
\|w\|_{L^2(0,l)}^2 \le 2l \left[|w_l|^2 + l \|w_x\|_{L^2(0,l)}^2 \right], \tag{3.10}
$$

Proof. Since $w \in H^1(0, l)$ and $w(l) = w_l$,

$$
w(x) = w_l - \int_x^l w_\xi(\xi) \, d\xi.
$$

Take absolute values, and use the triangle inequality to obtain

$$
|w(x)| \le |w_l| + \int_x^l |w_\xi(\xi)| \, d\xi.
$$

Applying Hölder's inequality $(|w_\xi(\xi)| = 1.\, |w_\xi(\xi)|)$ gives

$$|w(x)| \le |w_l| + \left(\int\limits_0^l 1^2 d\xi\right)^{\frac{1}{2}} \cdot \left(\int\limits_0^l |w_x(x)|^2\, dx\right)^{\frac{1}{2}}$$

$$\le |w_l| + l^{\frac{1}{2}} \|w_x\|_{L^2(0,l)}.$$

Square this inequality and use Young's inequality to get (3.9), and integrate (3.9) from $x = 0$ to $x = l$ to obtain (3.10). $\qquad\square$

Lemma 3.3. *V is continuously embedded in H.*

Proof. Let $z = [w,\, w_l] \in V$. We use the H and V inner products and the inequality (3.10) from Lemma 3.2 to obtain

$$\|z\|_H^2 = \int_0^l w^2 dx + m_l w_l^2$$

$$= \|w\|_{L^2(0,l)}^2 + m_l w_l^2$$

$$\le 2l^2 \|w_x\|_{L^2(0,l)}^2 + 2l w_l^2 + m_l w_l^2$$

$$= 2l^2 \int\limits_0^l w_x^2\, dx + (m_l + 2l)w_l^2$$

$$= \left(\frac{2l^2}{\beta^2}\right) \int\limits_0^l \beta^2 w_x^2\, dx + \left(\frac{m_l + 2l}{k_l}\right) k_l w_l^2$$

$$\le C_1 \left[k_l w_l^2 + \beta^2 \int\limits_0^l w_x^2\, dx \right].$$

Therefore $C_1^{-1} \|z\|_H^2 \le \|z\|_V^2$ where $C_1 = \max\left\{ \frac{m_l + 2l}{k_l}, \frac{2l^2}{\beta^2} \right\}$. This proves the result. $\quad\square$

3.5.2. Well-Posedness and Exponential Stability. To show the linear problem is well-posed, we rewrite the problem as $\dot{x} = \mathcal{A}x$ as before and show $\mathcal{A}$ generates a C_0-semigroup on $\mathcal{H} = V \times H$.

As before, we restrict our analysis to the cases where the damping bilinear form σ_2 is H-elliptic or V-elliptic.

Example 1: $\gamma, \alpha_l > 0$ and $\alpha = 0$. We first consider the case of Kelvin-Voigt damping ($\gamma > 0$) and viscous damping in the right mass-spring system ($\alpha_l > 0$). We prove σ_2 is V-elliptic.

We rewrite the bilinear form σ_2 and the V inner product according to the above parameters:

$$\sigma_2(z, z) = \int_0^l \gamma w_x^2 \, dx + \alpha_l w_l^2,$$

$$\|z\|_V^2 = \int_0^l \beta^2 w_x^2 dx + k_l w_l^2.$$

Then

$$\|z\|_V^2 = \beta^2 \int_0^l w_x^2 dx + k_l w_l^2$$
$$= \left(\frac{\beta^2}{\gamma}\right) \int_0^l \gamma w_x^2 dx + \left(\frac{k_l}{\alpha_l}\right) \alpha_l w_l^2$$
$$\leq C_2 \left(\int_0^l \gamma w_x^2 dx + \alpha_l w_l^2\right)$$
$$\leq C_2 \sigma_2(z, z)$$

where $C_2 = \max\left\{\frac{\beta^2}{\gamma}, \frac{k_l}{\alpha_l}\right\}$. This proves that σ_2 is V-elliptic.

Example 2: $\alpha, \alpha_l > 0$ and $\gamma = 0$. Next, we consider the case of viscous damping in the wave equation and the right mass (α, $\alpha_l > 0$). We prove σ_2 is H-elliptic. Since

$$\sigma_2(z, z) = \int_0^l \alpha w^2 dx + \alpha_l w_l^2,$$

$$\|z\|_H^2 = \int_0^l w^2 dx + m_l w_l^2,$$

we have

$$\|z\|_H^2 = \int_0^l \left(\frac{1}{\alpha}\right) \alpha w^2 dx + \left(\frac{m_l}{\alpha_l}\right) \alpha_l w_l^2$$
$$\leq C_3 \left[\int_0^l \alpha w^2 dx + \alpha_l w_l^2\right].$$

Therefore, $C_3^{-1} \|z\|_H^2 \leq \sigma_2(z, z)$, where $C_3 = \max\left\{\frac{1}{\alpha}, \frac{m_l}{\alpha_l}\right\}$, and this proves σ_2 is H-elliptic.

Example 3: $\gamma, \alpha > 0$ and $\alpha_l = 0$. In this last case, we consider only Kelvin-Voigt damping ($\gamma > 0$) and interior viscous damping ($\alpha > 0$). We prove σ_2 is V-elliptic. We have

$$\sigma_2(z, \psi) = \int_0^l \left(\gamma w_x^2 + \alpha w^2\right) dx,$$
$$\|z\|_V^2 = \int_0^l \beta^2 w_x^2 dx + k_l w_l^2.$$

Since $L^\infty(0, l)$ is continuously embedded in $H^1(0, l)$, there exists a constant $C > 0$ such that

$$\|w\|_{L^\infty(0.l)}^2 \leq C \|w\|_{H^1(0,l)}^2 = C \int_0^l (w^2 + w_x^2) dx.$$

Therefore, since $w(l) = w_l$,

$$\|z\|_V^2 \leq \beta^2 \int_0^l w_x^2 \, dx + k_l \|w\|_{L^\infty(0.l)}^2$$
$$= \beta^2 \int_0^l w_x^2 \, dx + k_l C \int_0^l (w^2 + w_x^2) dx$$
$$\leq C_4 \, \sigma_2(z, z),$$

where $C_4 = \max\left\{\frac{\beta^2 + k_l C}{\gamma}, \frac{k_l C}{\alpha}\right\}$. This proves σ_2 is V-elliptic.

In Examples 1, 3 we proved σ_2 is V-elliptic and Theorem 8.1 in [51] gives us $\mathcal{A}$ is the infinitesimal generator of an analytic exponentially stable semigroup.

In Example 2 we proved σ_2 is H-elliptic and Theorem 8.3 in [51] gives us $\mathcal{A}$ generates an exponentially stable C_0-semigroup.

3.6. THE NONLINEAR PROBLEM

We write the nonlinear problem as

$$\dot{x}(t) = \mathcal{A}x(t) + \mathcal{F}(x(t)), \quad x(0) = x_0 \tag{3.11}$$

on $\mathcal{H} = V \times H$. Here the linear operator $\mathcal{A}$ is defined in Section 2.1 and the nonlinear operator $\mathcal{F} : \mathcal{H} \to \mathcal{H}$ is defined for $x = [\varphi, \psi] \in \mathcal{H}$ with $\varphi = [w, w_l] \in V$ by

$$\mathcal{F}(x) = \begin{bmatrix} 0 \\ F_0(\varphi) \end{bmatrix}, \quad F_0(\varphi) = \begin{bmatrix} 0 \\ m_l^{-1} k_3 w_l^3 \end{bmatrix}.$$

Theorem 3.4. *The nonlinear cable-mass system has a unique mild solution on some time interval $[0, t^*)$.*

Theorem 3.5. *If σ_2 is $H-$elliptic and the solution $x = [z, z_t]$, with $z = [w, w_l]$, of the unforced nonlinear cable-mass problem (3.11) is sufficiently smooth, then the energy $E(t) = \frac{1}{2} \|z_t\|_H^2 + \frac{1}{2} \|z\|_V^2 + \frac{k_3}{4} [w_l(t)]^4$ of the solution with the initial data $x(0) = x_0 \in \mathcal{H}$ decays exponentially fast as $t \to \infty$.*

Proofs of Theorems 3.4 and 3.5 are similar to Section 2.

3.7. BALANCED TRUNCATION MODEL REDUCTION

Since the input operator $\mathcal{B}$ is unbounded, it is more difficult to check the infinite dimensional balanced truncation theory [20, 21, 22]; we do not attempt to do this here. Therefore, we do not have the balanced truncation theory for the linear

PDE system. So, our main goal in this section is to analyze the performance of the model reduction numerically.

As before, we use a basic finite difference method to approximate the solution to our model problem with a dynamic boundary condition.

We place n equally spaced nodes $\{x_j\}_{j=1}^n$ in the interval $[0, l]$, where $x_j = jh$ and $h = 1/n$ so that $x_1 = h$ and $x_n = l$. In order to apply balanced truncation below, we also eliminate the second order time derivatives by introducing a velocity variable. Therefore, let d_i denote the finite difference approximation to the displacement $w(t, x_i)$, and let v_i denote the finite difference approximation to the velocity $w_t(t, x_i)$. We assume the solution is smooth so that the displacement and velocity compatibility conditions are satisfied; we obtain

$$w_l(t) = d_n(t),$$

$$\dot{w}_l(t) = v_n(t).$$

We use second order centered differences to form finite difference equations for (3.1)

$$v_i' = \frac{\gamma}{h^2}[v_{i+1} - 2v_i + v_{i-1}] + \frac{\beta^2}{h^2}[d_{i+1} - 2d_i + d_{i-1}] - \alpha v_i,$$

$$d_i' = v_i, \quad \text{for } i = 1, ..., n - 1. \tag{3.12}$$

To discretize our system we use (3.12) to obtain

$$v_i' = \left[-\alpha - \frac{2\gamma}{h^2}\right]v_i + \left[\frac{\gamma}{h^2}\right]v_{i-1} + \left[\frac{\gamma}{h^2}\right]v_{i+1} + \left[\frac{\beta^2}{h^2}\right]d_{i+1} - \left[\frac{2\beta^2}{h^2}\right]d_i + \left[\frac{\beta^2}{h^2}\right]d_{i-1},$$

$$d_i' = v_i, \quad \text{for } i = 1, ..., n - 1.$$

To discretize the boundary conditions we use second order accurate one side finite difference approximation to the first order spatial derivatives. After discretizing the left boundary condition we obtain

$$v_1' = - \left[\frac{2\beta^2}{3h^2}\right] d_1 + \left[\frac{2\beta^2}{3h^2}\right] d_2 + \left[-\frac{2\gamma}{3h^2} - \alpha\right] v_1 + \left[\frac{2\gamma}{3h^2}\right] v_2 - \frac{2u}{3h},$$
$$d_1' = v_1,$$

and for the right boundary condition we obtain

$$v_n' = \left[-\frac{k_l}{m_l} - \frac{3\beta^2}{2hm_l}\right] d_n + \left[\frac{4\beta^2}{2hm_l}\right] d_{n-1} - \left[\frac{\beta^2}{2hm_l}\right] d_{n-2}$$
$$+ \left[-\frac{\alpha_l}{m_l} - \frac{3\gamma}{2hm_l}\right] v_n + \left[\frac{4\gamma}{2hm_l}\right] v_{n-1} - \left[\frac{\gamma}{2hm_l}\right] v_{n-2} - \left[\frac{k_3}{m_l}\right] [d_n]^3,$$
$$d_n' = v_n,$$

where d_i, v_i and $u(t)$ represent displacement, velocity and input, respectively. The above system can be placed in the matrix form (2.29). First, the matrix A_{11} has nonzero (i, j) entries, where i, j represent the row and column respectively, as specified below. The nonzero first row entries of A_{11} in the $(1, 1)$ and $(1, 2)$, entries are $\left(-\frac{2\beta^2}{3h^2}\right)$, $\left(\frac{2\beta^2}{3h^2}\right)$, respectively. The nonzero last row entries of A_{11} in the $(n, n - 2)$, $(n, n - 1)$ and (n, n) entries are $\left(-\frac{\beta^2}{2hm_l}\right)$, $\left(\frac{4\beta^2}{2hm_l}\right)$, $\left(-\frac{k_l}{m_l} - \frac{3\beta^2}{2hm_l}\right)$, respectively. The middle part of the matrix $i = 2, 3, \ldots, n - 1$ is a tridiagonal matrix. The entries are

$$[A_{11}]_{i,j} = \begin{cases} \frac{\beta^2}{h^2}, & i = i - 1, \\ -\frac{2\beta^2}{h^2}, & i = i, \\ \frac{\beta^2}{h^2}, & i = i + 1. \end{cases}$$

Similarly, the nonzero first row entries of A_{12} in the $(1, 1)$ and $(1, 2)$ entries are $\left(-\alpha - \frac{2\gamma}{3h^2}\right)$, $\left(\frac{2\gamma}{3h^2}\right)$, respectively. The nonzero last row entries of A_{12} in the $(n, n-$

2), $(n, n-1)$ and (n, n) entries are $\left(-\frac{\gamma}{2hm_l}\right)$, $\left(\frac{4\gamma}{2hm_l}\right)$, $\left(-\frac{\alpha_l}{m_l} - \frac{3\gamma}{2hm_l}\right)$, respectively. The middle part of the matrix $i = 2, 3, \ldots, n-1$ is a tridiagonal matrix. The entries are

$$[A_{11}]_{i,j} = \begin{cases} \frac{\gamma}{h^2}, & i = i-1, \\[2mm] -\alpha - \frac{2\gamma}{h^2}, & i = i, \\[2mm] \frac{\gamma}{h^2}, & i = i+1. \end{cases}$$

Also,

$$F_{12} = \begin{bmatrix} 0 & \cdots & 0 \\ \vdots & \ddots & \vdots \\ 0 & \cdots & -\frac{k_3}{m_l} \end{bmatrix} \qquad C = \begin{bmatrix} 0 & \cdots & 1 & \cdots & 0 \\ 0 & \cdots & 0 & \cdots & 1 \end{bmatrix} \qquad B_1 = \begin{bmatrix} \frac{-2}{3h} \\ \vdots \\ 0 \end{bmatrix}.$$

Furthermore, A_{11}, $A_{1,2}$, F_{12} are $n \times n$ matrices, C is a $2 \times 2n$ matrix and B_1 is a $n \times 1$ matrix.

Or, we can write the nonlinear finite dimensional approximating system as

$$\dot{x} = Ax + F(x) + Bu, \quad y = Cx. \tag{3.13}$$

3.8. FORMULATING THE FINITE DIFFERENCE APPROXIMATION OF THE ENERGY FUNCTION

For the nonlinear problem, we consider the solution of the finite difference model and compute an approximation to the energy function in Theorem 3.5 using trapezoidal rule quadrature on the integrals.

The energy of the unforced system is $E = E_K + E_P$ where

$$E_K = \int_0^l \frac{1}{2} w_t^2 \, dx + \frac{m_l}{2} \left(\dot{w}_l(t)\right)^2,$$

$$E_P = \int_0^l \frac{\beta^2}{2} w_x^2 \, dx + \frac{k_l}{2} \left(w_l(t)\right)^2 + \frac{k_3}{4} \left(w_l(t)\right)^4.$$

Recall trapezoidal rule quadrature for an integral:

$$\int_a^b F(x)dx \approx \frac{h}{2}\left[F(a) + F(b)\right] + \sum_{i=2}^{n-1} hF(x_i).$$

Applying the trapezoidal rule to each integral term in the energy gives

$$\int_0^l \frac{1}{2}w_t^2\, dx \approx \frac{1}{2}\left[\frac{h}{2}\left(v_1(t)\right)^2 + \frac{h}{2}\left(v_M(t)\right)^2\right] + \frac{1}{2}\sum_{i=2}^{n-1} h\left(v_i(t)\right)^2,$$

and

$$\int_0^l \frac{\beta^2}{2}w_x^2\, dx \approx \frac{\beta^2}{2}\left[\frac{h}{2}\left(w_x(t,\,x_1)\right)^2 + \frac{h}{2}\left(w_x(t,\,x_n)\right)^2\right] + \frac{\beta^2}{2}\sum_{i=2}^{n-1} h\left(w_x(t,x_i)\right)^2.$$

Use one-sided and centered difference formulas to get

$$\int_0^l \frac{\beta^2}{2}w_x^2\, dx \approx \frac{\beta^2}{2}\left[\frac{h}{2}\left(\frac{-3w_1 + 4w_2 - w_3}{2h}\right)^2 + \frac{h}{2}\left(\frac{3w_n - 4w_{n-1} + w_{n-2}}{2h}\right)^2\right]$$
$$+ \frac{\beta^2 h}{2}\sum_{i=2}^{n-1}\left(\frac{w_{i+1} - w_{i-1}}{2h}\right)^2.$$

Then the energy of the system is approximated as follows:

$$E(t) \approx \frac{h}{4}v_1^2 + \left[\frac{h}{4} + \frac{m_l}{2}\right]v_n^2 + \frac{h}{2}\sum_{i=2}^{n-1}\left(v_i(t)\right)^2 + \frac{\beta^2}{16h}\left[-3w_1 + 4w_2 - w_3\right]^2$$
$$+ \frac{\beta^2}{16h}\left[3w_n - 4w_{n-1} + w_{n-2}\right]^2 + \frac{\beta^2}{8h}\sum_{i=2}^{n-1}\left[w_{i+1} - w_{i-1}\right]^2$$
$$+ \frac{k_l}{2}\left(w_n\right)^2 + \frac{k_3}{4}\left(w_n\right)^4.$$

Table 3.1. Fixed Simulation Parameters

l	m_l	k_3	β
1	1.5	1	1

3.9. NUMERICAL RESULTS

In this section, we examine the performance of ROM when the input operator is unbounded. For our experiments, we used 100 finite difference nodes and solved all ordinary differential equations the Matlab's `ode23s`. We fixed some of the basic problem parameters, as shown in Table 3.1, and tested variations of the remaining parameters to determine when the MOR approach is accurate.

We investigate the following examples:

- Example 1: Kelvin-Voigt damping in the interior ($\gamma > 0$) and damping in the right boundary ($\alpha_l > 0$). The interior viscous damping parameter is taken to be zero, i.e., $\alpha = 0$.

- Example 2: Viscous damping in the interior ($\alpha > 0$) and damping in right boundary $\alpha_l > 0$. The Kelvin-Voigt damping parameter γ is set to zero. Unlike Example 1, the C_0-semigroup generated by the linear problem is not analytic in this case and the PDE is hyperbolic.

- Example 3: Viscous damping in the interior ($\alpha > 0$) and Kelvin-Voigt damping in the interior ($\gamma > 0$). The boundary damping parameter is taken to be zero, i.e., $\alpha_l = 0$.

- Example 4: Kelvin-Voigt damping in the interior ($\gamma > 0$). All other damping parameters are taken to be zero, i.e., $\alpha = \alpha_l = 0$.

- Example 5: Viscous damping in the interior ($\alpha > 0$). All other damping parameters are taken to be zero, i.e., $\gamma = \alpha_l = 0$.

(a) Eigenvalues of the linear system

(b) Energy decay of the nonlinear system
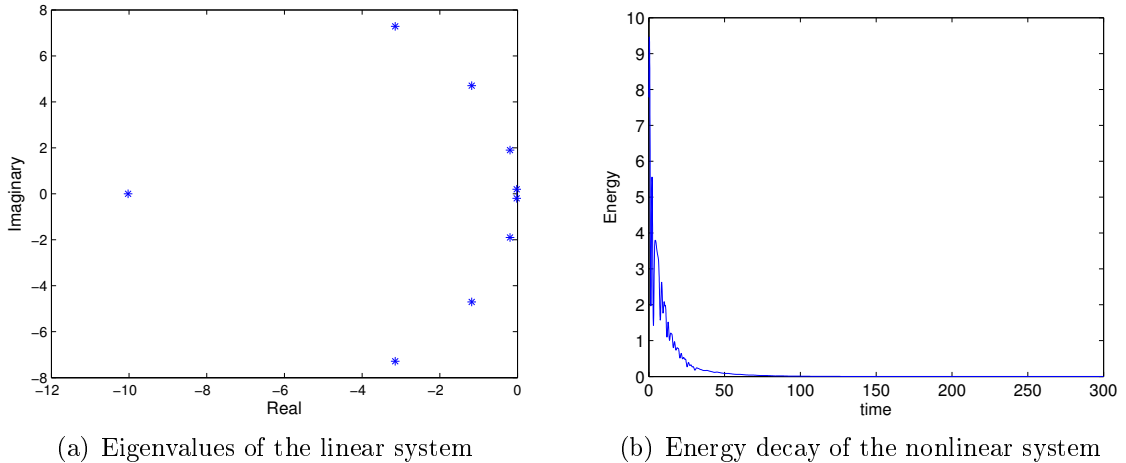
Figure 3.1. Eigenvalues and energy decay for $\gamma = \alpha_l = 0.1$, $k_l = 0.1$ and $\alpha = 0$

In Sections 3.5.2 and 3.6 we proved that the unforced linear and nonlinear systems are exponentially stable for Examples 1-3. Numerical results indicate that the linear problems are also exponentially stable for Examples 4-5.

3.9.1. Exponential Stability. Before we present the model reduction computational results, we briefly present numerical results concerning the linear and nonlinear exponential stability theory. For the linear problem, we test the exponential stability by analyzing the eigenvalues of the matrix A in the finite difference model (3.13). Figure 3.1(a) shows the eigenvalues of matrix A for $\gamma = \alpha_l = 0.1$, $k_l = 0.1$, and $\alpha = 0$. This is a case of Example 1. The eigenvalues all have negative real parts. For the nonlinear problem, we consider the solution of the finite difference model (3.13), and compute an approximation to the (continuous) energy function in Theorem 3.5 by using trapezoidal rule quadrature on the integrals in Section 3.8. Figure 3.1(b) shows the exponential decay of the energy with same parameters and the initial data $xe^x \sin(x)$ for the position and $\cos(x)$ for the velocity. We choose the initial condition to match the boundary condition at $x = 0$ to produce a smooth solution. So the initial condition for the position $w_0(x)$ satisfies $w_0'(0) = 0$, and the initial condition for the velocity $v_0(x)$ satisfies $v_0'(0) = 0$.

(a) Eigenvalues of the linear system

(b) Energy decay in nonlinear system
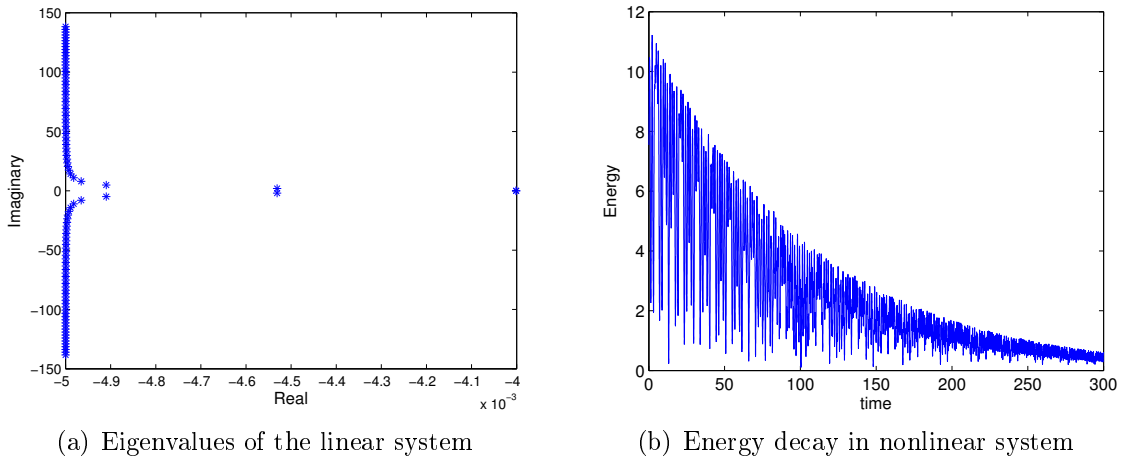
Figure 3.2. Eigenvalues and energy decay for $\gamma = 0$ and $\alpha = \alpha_l = k_l = 0.01$

Table 3.2. Eigenvalue with largest $Re(\lambda)$ for the linear system with N spatial nodes, $\gamma = \alpha_l = 0.1$, $k_l = 0.1$ and $\alpha = 0$

N	10	20	40	80	160
Re (λ)	-0.0189	-0.0194	-0.0196	-0.0197	-0.0197

We also approximated the eigenvalues and the energy for the nonlinear problem when $\gamma = 0$ (this is a case of Example 2); see Figure 3.2. We see the exponential stability in both linear and nonlinear cases. In the nonlinear case, if $\gamma = 0$ and all the other parameters are small, then the energy decay becomes exponentially stable and also fluctuation takes place rapidly.

Furthermore, we look at the behavior of the eigenvalue nearest the imaginary axis by increasing the number of spatial nodes. As we can see in Tables 3.2 and 3.3 the eigenvalue do not approach the imaginary axis when the number of spatial nodes is increased. This is the behavior we expect since the PDE system is exponentially stable.

3.9.2. Model Reduction Results. Next, we begin the model reduction experiments. We study the effects of the various parameters on the accuracy of the

Table 3.3. Eigenvalue with largest $Re(\lambda)$ for the linear system with N spatial nodes, $\gamma = 0$, and $\alpha = \alpha_l = k_l = 0.1$

N	10	20	40	80	160
Re (λ)	-0.0040	-0.0040	-0.0040	-0.0040	-0.0040

model reduction. To do this, we consider the reduced order model (ROM) and full order model (FOM) with zero initial data and the same input $u(t)$ and compare the output of the FOM and ROM. Recall the output $y(t)$ of the cable-mass system is the position and velocity of the right mass.

We focus on the accuracy of the linear and nonlinear ROM and present some results to show the performance of the ROM in both systems.

For our experiments we investigate the behavior of the ROM and FOM in the four different input functions from Section 2:

- Input 1: $u(t) = 0.1 \sin(0.2\pi t)$

- Input 2: $u(t) = 0.02 \cos(at) + 0.03 \cos(bt)$, where a, b are the two largest real parts of the eigenvalues of the matrix A

- Input 3: $u(t) = c_1 \sin(mt) + c_2 \cos(nt)$, where c_1, c_2, m, n are constants in the range of $c_1, c_2, < 0.1$ and $m, n < 0.2$

- Input 4: $u(t) = 0.1 \text{square}(0.2\pi t)$

We consider the same parameter scenarios as in Section 2.

- Small interior damping parameters

Here we investigate the behavior of the ROM for interior damping parameters that are small relative to the boundary stiffness parameter. We experiment for damping parameters α and γ in the range of 0.1 to 0.001 and fix $k_l = 0.1$ and $\alpha_l = 0.1$.

Case 1a : Small interior damping parameters with smooth Inputs 1, 2

(a) Linear system   (b) Nonlinear system
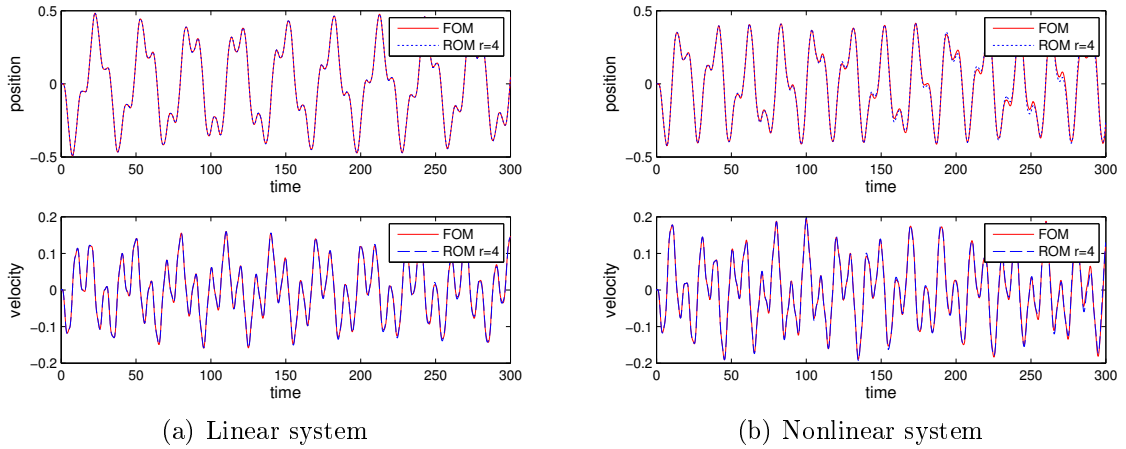
Figure 3.3. Example 3, Input 1: Output of the ROM and FOM for $\gamma = \alpha = 0.001$, $k_l = 0.1$ and $\alpha_l = 0$

In this case, in all examples for smooth Inputs 1, 2 the output of the linear and nonlinear ROM is highly accurate compared to the FOM output. We present results for two specific scenarios. Figure 3.3 shows the output of the FOM and ROM for both the linear and nonlinear systems for Example 3, Input 1 with $\alpha_l = 0$, $\gamma = \alpha = 0.001$. The agreement is excellent in both the linear and nonlinear cases.

Figure 3.4 shows the output of the FOM and ROM for both the linear and nonlinear systems for Example 4, Input 2 with $k_l = 0.1$, $\alpha = \alpha_l = 0$ and small Kelvin-Voigt parameter $\gamma = 0.001$. The linear and nonlinear ROM outputs are highly accurate.

Overall, for all examples with smooth Inputs 1, 2 the linear and nonlinear ROM outputs are highly accurate over a long interval.

Case 1b : Small interior damping parameters with smooth Input 3 and discontinuous Input 4

Next, we observe the behavior of the ROM and FOM for small interior damping with Inputs 3 and 4. In this case all behaviors are possible. We show different behaviors for three specific scenarios below. Figure 3.5 shows the behavior of the

(a) Linear system

(b) Nonlinear system
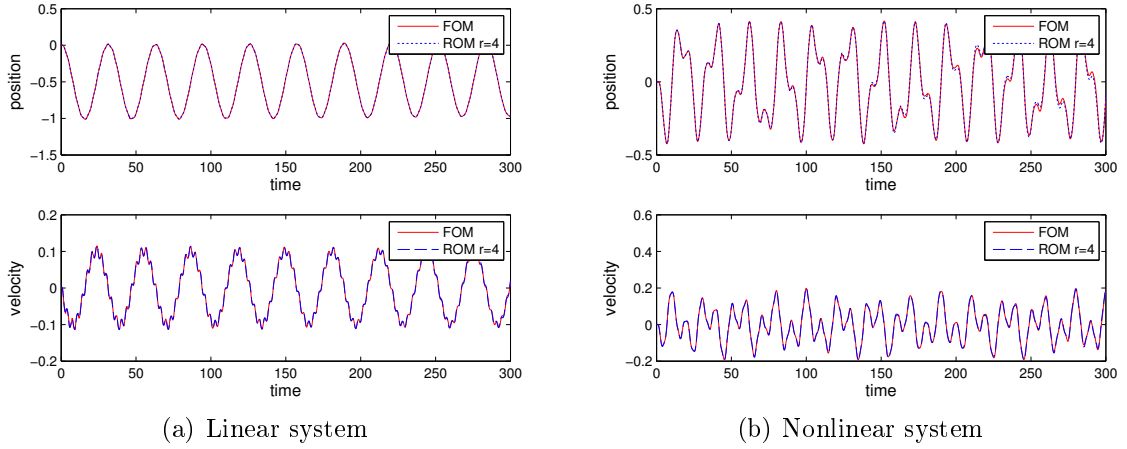
Figure 3.4. Example 4, Input 2: Output of the ROM and FOM for $\gamma = 0.001$, $k_l = 0.1$, $\alpha_l = \alpha = 0$

(a) Linear system

(b) Nonlinear system
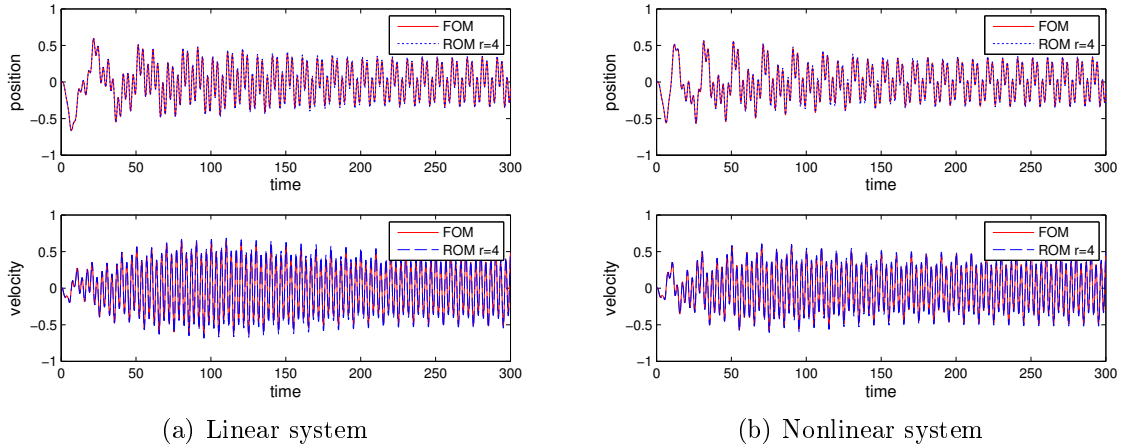
Figure 3.5. Example 1, Input 4: Output of the ROM and FOM for $\alpha = 0$, $\gamma = 0.001$ and $\alpha_l = k_l = 0.1$.

linear and nonlinear FOM and ROM for Example 1, Input 4 with $\alpha = 0$, $\gamma = 0.001$ and $\alpha_l = k_l = 0.1$. The linear and nonlinear ROM outputs are highly accurate.

Next, we present a case where the output of the nonlinear ROM is highly accurate over a short time period and increasing r improves the accuracy over a long time interval. Figure 3.6 shows the behavior of the nonlinear FOM and ROM for

(a) Nonlinear system for $r = 4$ (b) Nonlinear system for $r = 8$
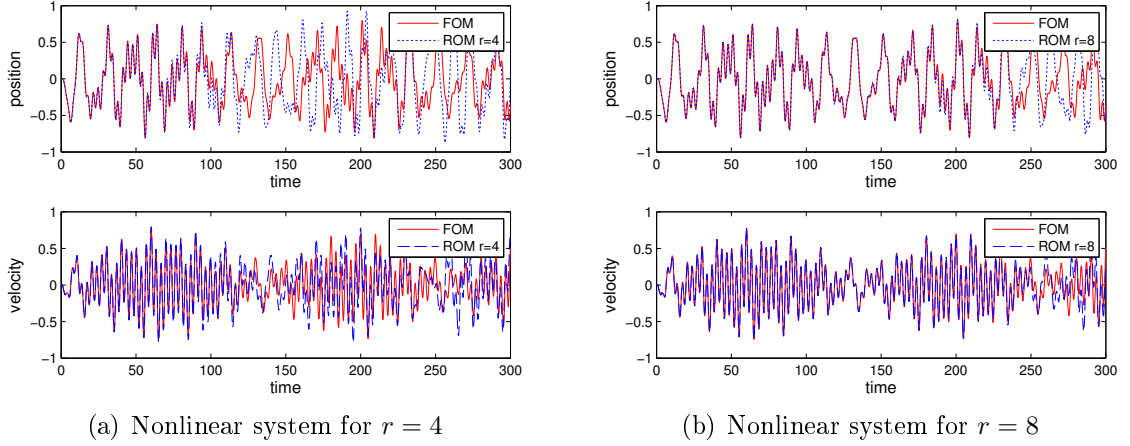
Figure 3.6. Example 4, Input 4: Output of the ROM and FOM for $\alpha = \alpha_l = 0$, $\gamma = 0.001$ and $k_l = 0.1$.

Example 4, Input 4 with $\alpha_l = 0$, $\alpha = \gamma = 0.001$ and $k_l = 0.1$ for $r = 4$ and $r = 8$. We note the linear ROM is highly accurate over a long time interval with Inputs 3, 4.

Now, we present a case where the output of the nonlinear ROM is highly accurate over a short interval and increasing r does not greatly improve the accuracy. Figure 3.7 shows the behavior of the nonlinear FOM and ROM for Example 5, Input 3 with $\gamma = \alpha_l = 0$, $\alpha = 0.001$ and $k_l = 0.1$ for $r = 4$ and $r = 8$.

Overall, all behaviors are possible with Inputs 3 and 4 for nonlinear ROM. The linear ROM is highly accurate over a long time interval. In Example 1, the nonlinear ROM may be highly accurate over a longer time interval and in Examples 3, 4, 5 the nonlinear ROM may lose high accuracy after an initial time period. Also, increasing r may or may not greatly improve the accuracy over a long period of time.

- Small boundary damping parameter

Here we investigate the behavior of the ROM for a boundary damping parameter that is small relative to the interior damping parameters and boundary stiffness parameter. We experiment for boundary damping parameter α_l in the range of 0.1 to 0.001 and

(a) Nonlinear system for $r = 4$ (b) Nonlinear system for $r = 8$
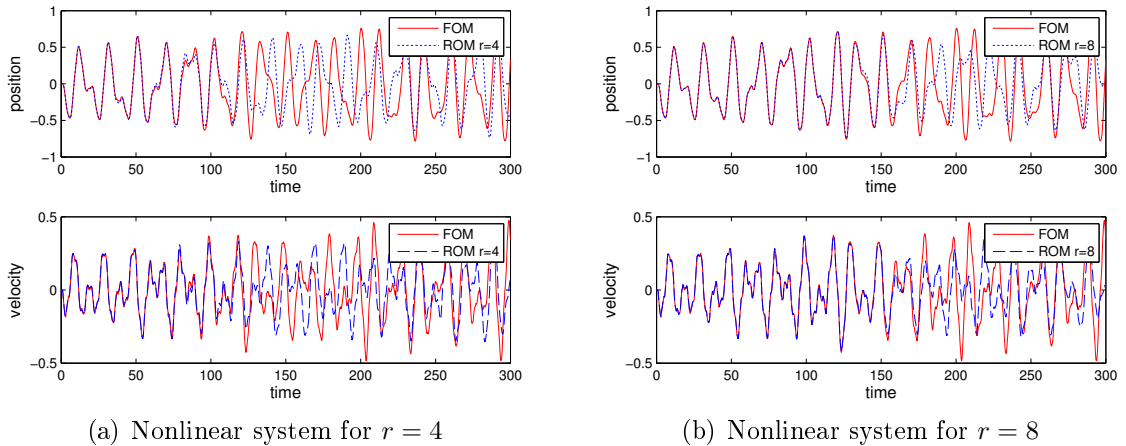
Figure 3.7. Example 5, Input 3: Output of the ROM and FOM for $\gamma = \alpha_l = 0$, $\alpha = 0.001$ and $k_l = 0.1$

fix $k_l = \gamma = \alpha = 0.1$. Note only Examples 1 and 2 are applicable here since Examples 3-5 have $\alpha_l = 0$.

Case 2a : Small boundary damping parameter with smooth Inputs 1, 2

In this case, in Examples 1 and 2 with smooth Inputs 1 and 2, the output of the nonlinear ROM is highly accurate. We present results only for one specific scenario. Figure 3.8 shows the behavior of the ROM and FOM of the linear and nonlinear systems for Example 1, Input 1 with $\alpha = 0$, $\gamma = k_l = 0.1$ and small boundary damping $\alpha_l = 0.001$.

Overall the performance of both linear and nonlinear ROM outputs are excellent.

Case 2b : Small boundary damping parameter with smooth Input 3 and discontinuous Input 4

Here, for Example 2 with Inputs 3, 4 the output of the linear and nonlinear ROM is highly accurate. For Example 1 with Inputs 3, 4 the nonlinear ROM is accurate for an initial time interval. Increasing r improves the length of the accurate time

(a) Linear system   (b) Nonlinear system
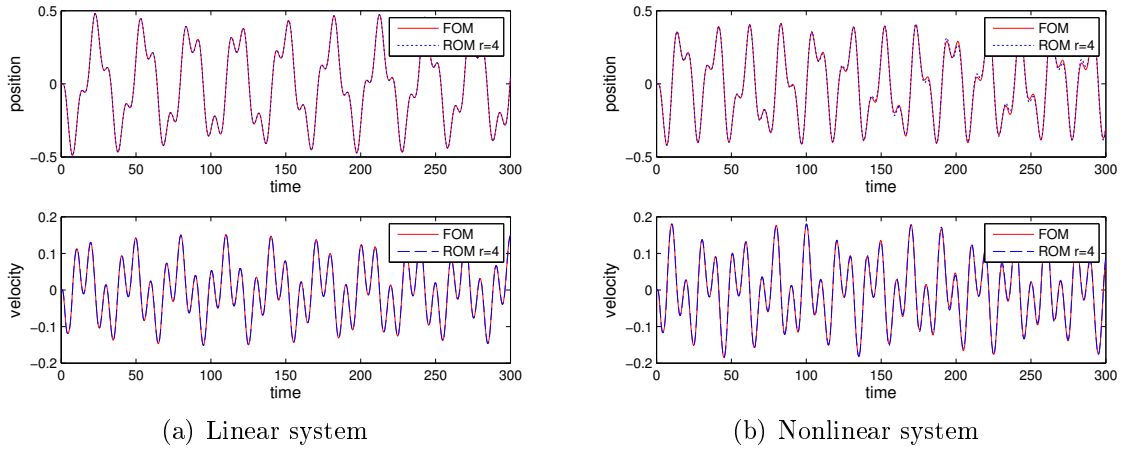
Figure 3.8. Example 1, Input 1: Output of the ROM and FOM for $\alpha = 0$, $\gamma = k_l = 0.1$ and $\alpha_l = 0.001$

(a) Nonlinear system for $r = 4$ (b) Nonlinear system for $r = 8$
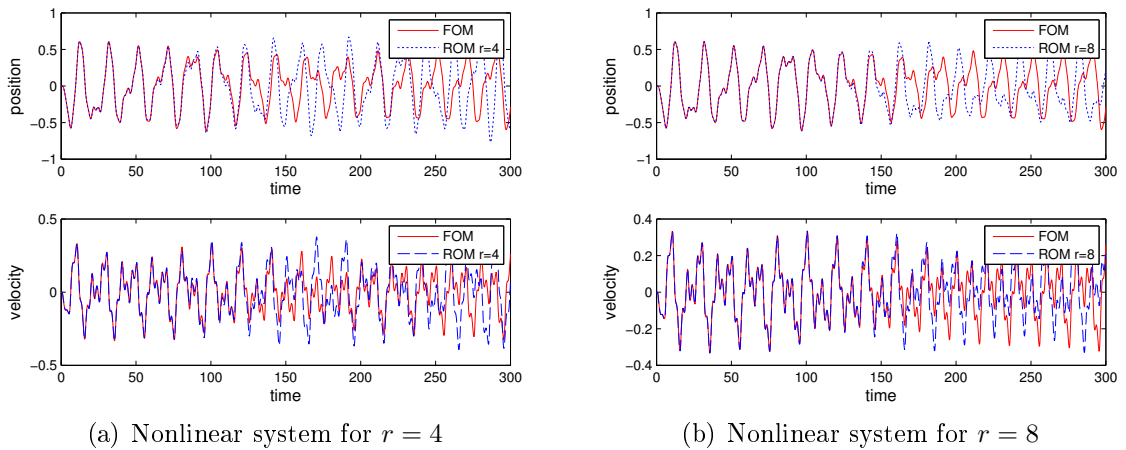
Figure 3.9. Example 1, Input 4: Output of the ROM and FOM for $\alpha = 0$, $\gamma = k_l = 0.1$ and $\alpha_l = 0.001$

interval but does not yield accuracy over a long time interval. Figure 3.9 shows the behavior of the nonlinear ROM and FOM of the nonlinear systems for Example 1, Input 4 with $\alpha = 0$, $\gamma = k_l = 0.1$ and small boundary damping $\alpha_l = 0.001$ for $r = 4$ and $r = 8$.

Succinctly, the linear ROM is highly accurate when the boundary damping parameter is small. The nonlinear ROM may be highly accurate over a longer time

(a) Linear system   (b) Nonlinear system
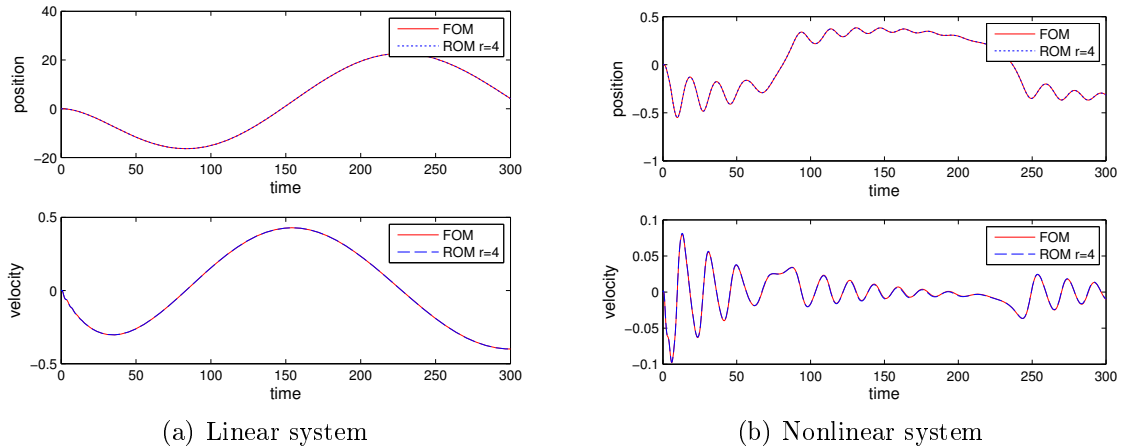
Figure 3.10. Example 3, Input 2: Output of the ROM and FOM for $\alpha_l = 0$, $\alpha = \gamma = 0.1$ and $k_l = 0.001$

interval or highly accurate only for an initial period of time and increasing r can improve the accuracy.

- Small boundary stiffness parameter

Next, we investigate the behavior of the FOM and ROM when the boundary stiffness parameter is small relative to the damping parameters. We experiment for stiffness parameter k_l in the range of 0.1 to 0.001 and fix the damping parameters $\gamma = \alpha = \alpha_l = 0.1$.

Case 3a : Small stiffness parameter with smooth Input 2

In all examples for smooth Input 2, the output of the nonlinear and linear ROM is highly accurate compared to the FOM output.

In Figure 3.10 shows the behavior of the ROM and FOM of the linear and nonlinear systems for Example 3, Input 2 with $\alpha_l = 0$, $\alpha = \gamma = 0.1$ and $k_l = 0.001$.

Overall, in all examples with smooth Input 2, the linear and nonlinear ROM are highly accurate for a longer time period.

Case 3b : Small stiffness parameter with smooth Inputs 1, 3 and discontinuous Input 4.
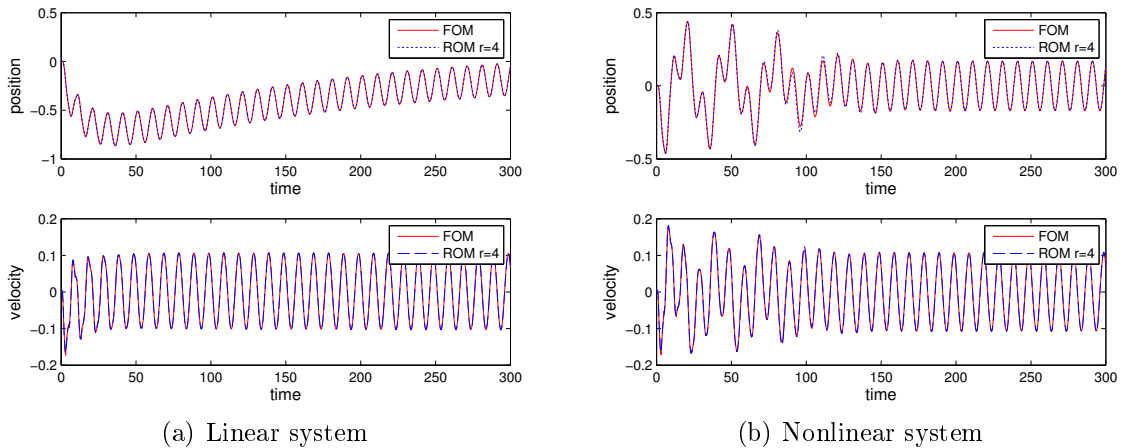
Figure 3.11. Example 2, Input 3: Output of the ROM and FOM for $\gamma = 0$, $\alpha = \alpha_l = 0.1$ and $k_l = 0.001$

Next, we explore the behavior of the ROM and FOM for smaller boundary stiffness parameter with smooth Inputs 1, 3 and discontinuous Input 4 . For Examples 1, 2, 3, 5 with Inputs 1, 3, 4 the nonlinear ROM is highly accurate over a long time period. Only Example 4 behaves differently. For Example 4 with Inputs 1, 3, and 4 the nonlinear ROM is highly accurate over an initial time interval, and then it loses accuracy. We present results for two specific scenarios. First, Figure 3.11 shows the behavior of the linear and nonlinear FOM and ROM output for Example 2, Input 3 with $\gamma = 0$, $\alpha = \alpha_l = 0.1$ and small boundary stiffness $k_l = 0.001$. In this case both the linear and nonlinear outputs of ROM are highly accurate over a long period of time.

Figure 3.12 shows another scenario for the nonlinear output over a long time interval: Example 4, Input 4 with $\gamma = 0.1$, $\alpha = \alpha_l = 0$ and small stiffness $k_l = 0.001$. The nonlinear ROM is highly accurate over an initial time period, but then suffers a loss of accuracy. Increasing r does not yield high accuracy.

Succinctly, when the boundary stiffness parameter is small relative to the damping parameters, the accuracy of the nonlinear ROM can vary with different

(a) Nonlinear system for $r = 4$ (b) Nonlinear system for $r = 8$
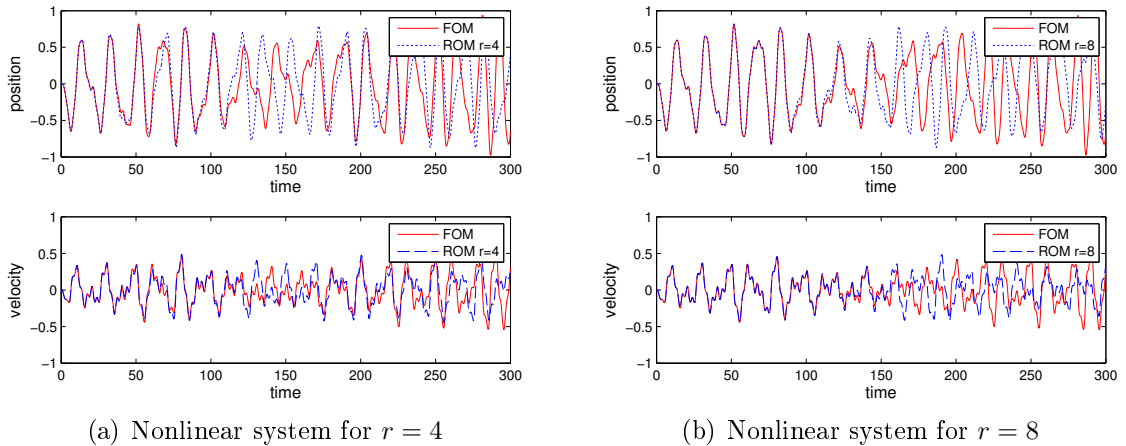
Figure 3.12. Example 4, Input 4: Output of the ROM and FOM for $\gamma = 0.1$, $\alpha = \alpha_l = 0$ and $k_l = 0.001$

examples and inputs. The linear ROM is highly accurate in all examples with all inputs.

- Small damping and stiffness parameters (all parameters are small)

Finally, we consider the behavior of the nonlinear ROM when the damping and boundary stiffness parameter are small relatively to the mass and nonlinear stiffness parameters ($m_0 = 1$, $m_l = 1.5$, and $k_3 = 1$). We experiment for damping parameters α, α_l, γ and stiffness parameter k_l in the range of 0.1 to 0.001.

Case 4a : Small damping and stiffness parameters with continuous Input 2

The nonlinear ROM is highly accurate in all examples with Input 2. We present results for two specific scenarios. In Figure 3.13 shows the behavior of the ROM of the nonlinear system for Example 3 with Input 2 and Example 4 with Input 2.

Overall, the linear and nonlinear ROM outputs are very accurate in all examples with Input 2 when the damping and stiffness parameters are small.

Case 4b : Small damping and stiffness parameters with Inputs 1, 3 and 4

(a) Example 3, Input 2 $\alpha_l = 0$ and $\gamma = \alpha = k_l = 0.001$

(b) Example 5, Input: 2 $\alpha = \alpha_l = 0$ and $\gamma = k_l = 0.001$
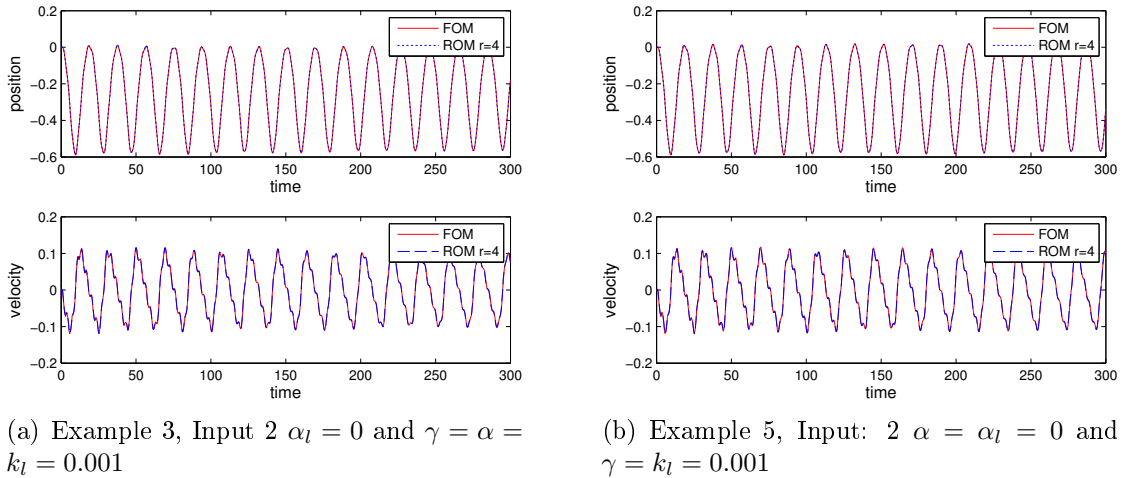
Figure 3.13. Output of the nonlinear ROM and FOM

In all examples, the nonlinear ROM output is highly accurate over an initial time period, but then suffers a large loss of accuracy with Inputs 1, 3 and 4. Increasing r does improve the length of the accurate time interval but may not yield high accuracy for a long time interval. We present results for two specific scenarios. Figure 3.14 shows the behavior of the ROM of the nonlinear system for Example 3 with Input 3 with $\alpha_l = 0$ and $\gamma = \alpha = k_l = 0.001$ for $r = 4$ and $r = 10$. Increasing r greatly improves the length of the accurate time interval.

Figure 3.15 shows the behavior of the ROM of the nonlinear system for Example 1, Input 4 with $\alpha = 0$ and $\gamma = \alpha_l = k_l = 0.001$ for $r = 4$ and $r = 10$. Increasing r greatly improves the accuracy, but we do not get accuracy for a long time interval.

Overall, when all parameters are small all behaviors are possible. The nonlinear ROM may be highly accurate over a long period of time, or it may lose high accuracy after an initial time period. Also, increasing r may or may not give accuracy over a long time interval. The linear ROM is highly accurate in all cases.
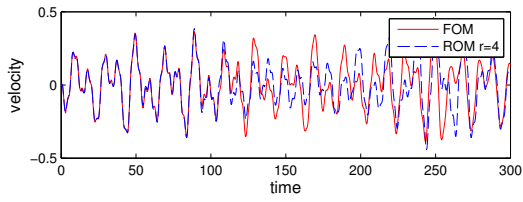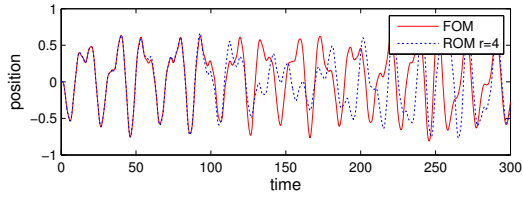
(a) Nonlinear system for $r = 4$
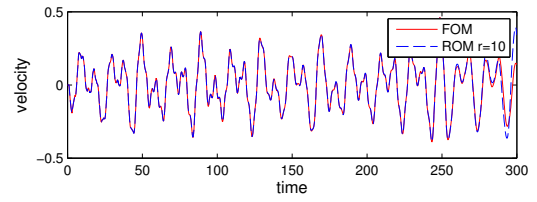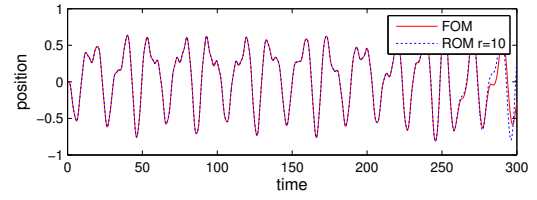
(b) Nonlinear system for $r = 10$

Figure 3.14. Example 3, Input 3: Output of the ROM and FOM for $\alpha_l = 0$, $\gamma = \alpha = k_l = 0.001$
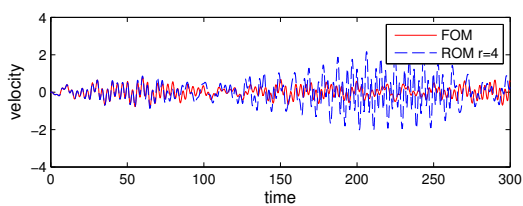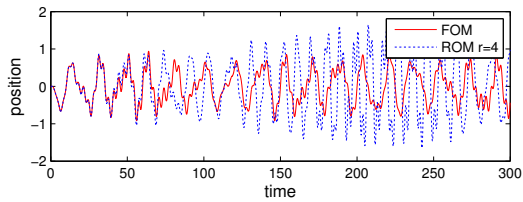
(a) Nonlinear system for $r = 4$
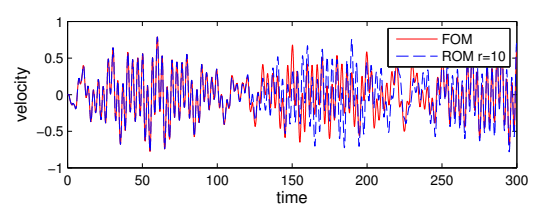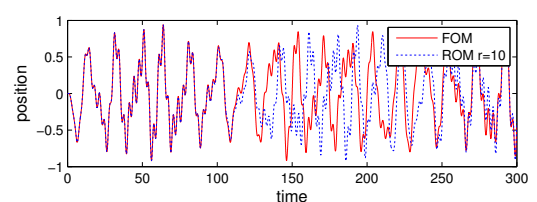
(b) Nonlinear system for $r = 10$

Figure 3.15. Example 1, Input 4: Output of the ROM and FOM for $\alpha = 0$, $\gamma = \alpha_l = k_l = 0.001$

4. NONLINEAR CABLE-MASS PDE SYSTEM WITH UNBOUNDED OUTPUT OPERATOR

In this section, we study the effect of an unbounded output operator to the model reduction. Here, we use the same wave equation and boundary conditions as described in Section 2 with a different output. We do not attempt to prove the PDE balanced truncation theory for this problem. Instead, we examine the performance of the model order reduction numerically.

4.1. THE MODEL

As we explained in Section 2, the model is the same and we investigate the model reduction with different outputs. Recall the wave equation with dynamic boundary conditions is given by

$$w_{tt}(t,x) + \alpha w_t(t,x) = \gamma w_{txx}(t,x) + \beta^2 w_{xx}(t,x), \tag{4.1}$$

$$m_0 \ddot{w}_0(t) + \alpha_0 \dot{w}_0(t) + k_0 w_0(t) = (\gamma w_{tx}(t,0) + \beta^2 w_x(t,0)) + u(t), \tag{4.2}$$

$$m_l \ddot{w}_l(t) + \alpha_l \dot{w}_l(t) + k_l w_l(t) = (-\gamma w_{tx}(t,l) - \beta^2 w_x(t,l)) - k_3 \left[w_l(t)\right]^3. \tag{4.3}$$

We assume we have one system output: the force of the cable acting on the right mass, i.e.,

$$y(t) = \gamma w_{tx}(t,l) + \beta^2 w_x(t,l).$$

4.2. ABSTRACT FORM

Our original PDE model (4.1) with the boundary conditions (4.2), (4.3) can be written in the first order abstract form (2.10). The operators $\mathcal{A}$ and $\mathcal{B}$ are given in Section 2. We define the output operator $\mathcal{C}$, which is unbounded in this case. Define

Table 4.1. Fixed Simulation Parameters

l	m_0	m_l	k_3	β
1	1	1.5	1	1

the operator $\mathcal{C}$, where $\mathcal{C} : \mathcal{D}(\mathcal{A}) \to \mathbb{R}$, by $\mathcal{C}x = \delta_l \left(\beta^2 \frac{d}{d\xi} w + \gamma \frac{d}{d\xi} v \right)$. Since $\mathcal{C}$ maps the domain of $\mathcal{A}$ to $\mathbb{R}$, and $\mathcal{C}x$ is not well-defined in general for $x \in \mathcal{H} = V \times H$, $\mathcal{C}$ is called an unbounded operator.

4.3. NUMERICAL EXPERIMENTS

In this section, we examine the performance of ROM when the output operator is unbounded. For our experiments, we used 100 finite difference nodes and solved all ordinary differential equations the Matlab's `ode23s`. We fixed some of the basic problem parameters, as shown in Table 4.1, and tested variations of the remaining parameters to determine when the MOR approach is accurate.

We investigated the following examples. Here we only consider the examples when the Kelvin-Voigt parameter is positive.

- Example 1: Kelvin-Voigt damping in the interior ($\gamma > 0$) and damping in the in the right boundary ($\alpha_l > 0$). All other damping parameters are taken to be zero, i.e., $\alpha_0 = \alpha = 0$.

- Example 3: Viscous damping in the interior ($\alpha > 0$) and Kelvin-Voigt damping in the interior ($\gamma > 0$). All other damping parameters are taken to be zero, i.e., $\alpha_0 = \alpha_l = 0$.

- Example 5: Kelvin-Voigt damping in the interior ($\gamma > 0$). All other damping parameters are taken to be zero, i.e., $\alpha = \alpha_0 = \alpha_l = 0$

4.3.1. Formulating the Finite Difference Approximation. The matrices A, B, and F are given in Section 2. We define the matrix C, which is $1 \times 2n$, by

$$C = \begin{bmatrix} 0 & \cdots & 0 & \frac{\gamma}{2h} & -\frac{4\gamma}{2h} & \frac{3\gamma}{2h} & 0 & \cdots & 0 & \frac{\beta^2}{2h} & -\frac{4\beta^2}{2h} & \frac{3\beta^2}{2h} \end{bmatrix}.$$

This gives the nonlinear finite dimensional approximating system:

$$\dot{x} = Ax + F(x) + Bu, \quad y = Cx. \tag{4.4}$$

4.3.2. Model Reduction Results. Next, we begin the model reduction experiments. We study the effects of the various parameters on the accuracy of the model reduction. To do this, we consider the reduced order model (ROM) and full order model (FOM) with zero initial data and the same input $u(t)$ and compare the output of the FOM and ROM. Recall the output $y(t)$ of the cable-mass system is the force of the cable on the right mass.

We focus on the accuracy of the linear and nonlinear ROM and present some results to analyze the performance of the ROM.

For our experiments, we investigate the behavior of the ROM and FOM for four different input functions as before.

- Input 1: $u(t) = 0.1\sin(0.2\pi t)$

- Input 2: $u(t) = 0.02\cos(at) + 0.03\cos(bt)$, where a, b are the two largest real parts of the eigenvalues of the matrix A

- Input 3: $u(t) = c_1 \sin(mt) + c_2 \cos(nt)$, where c_1, c_2, m, n are constants in the range of c_1, $c_2, < 0.1$ and m, $n < 0.2$.

- Input 4: $u(t) = 0.1\text{square}(0.2\pi t)$

The inputs are the same as previously described in Section 2.

(a) Linear system   (b) Nonlinear system
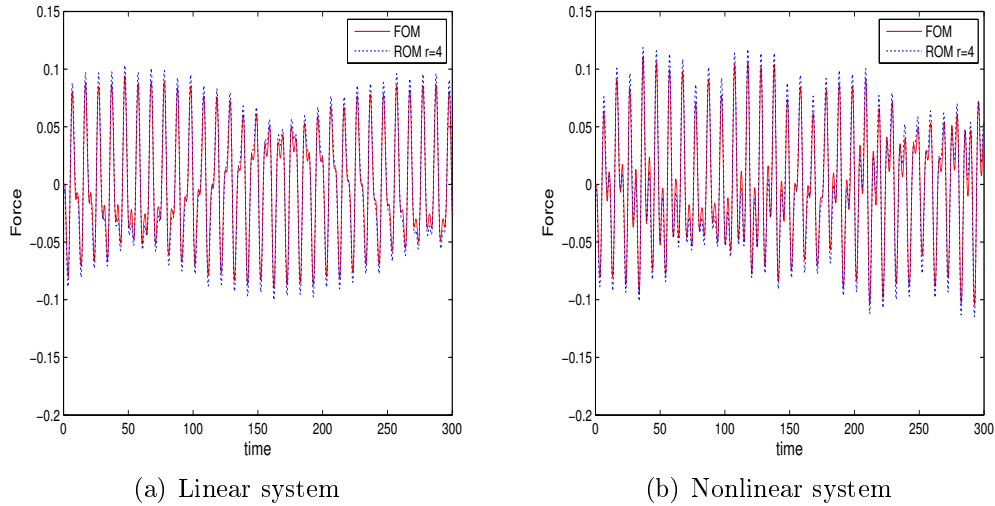
Figure 4.1. Example 5, Input 1: Output of the ROM and FOM for $\gamma = 0.001$, $k_0 = k_l = 0.1$, $\alpha = \alpha_0 = \alpha_l = 0$ when $r = 4$

- Small interior damping parameters

We first investigate the behavior of the ROM for interior damping parameters which are small relative to the boundary stiffness parameter and boundary damping parameters. We experiment for damping parameters α and γ in the range of 0.1 to 0.001, and fix $k_0 = k_l = 0.1$ and $\alpha_l = 0.1$.

Case 1a : Small interior damping parameters with all inputs

In this case, for Examples 3 and 5 with all inputs, the output of linear and nonlinear ROM is accurate for $r = 4$ but the amplitude of the ROM is slightly different compared to the FOM. Increasing r does give high accuracy. Figure 4.1 shows the output of the FOM and ROM for both linear and nonlinear systems for Example 5, Input 1 with $\alpha = \alpha_0 = \alpha_l = 0$, $k_0 = k_l = 0.1$, and small Kelvin-Voigt parameter $\gamma = 0.001$.

The behavior of Example 1 is different from the other two examples. We present results for two specific scenarios. For Example 1 with smooth Input 1 the output of linear and nonlinear ROM is highly accurate. Figure 4.2 shows the behavior

(a) Linear system   (b) Nonlinear system
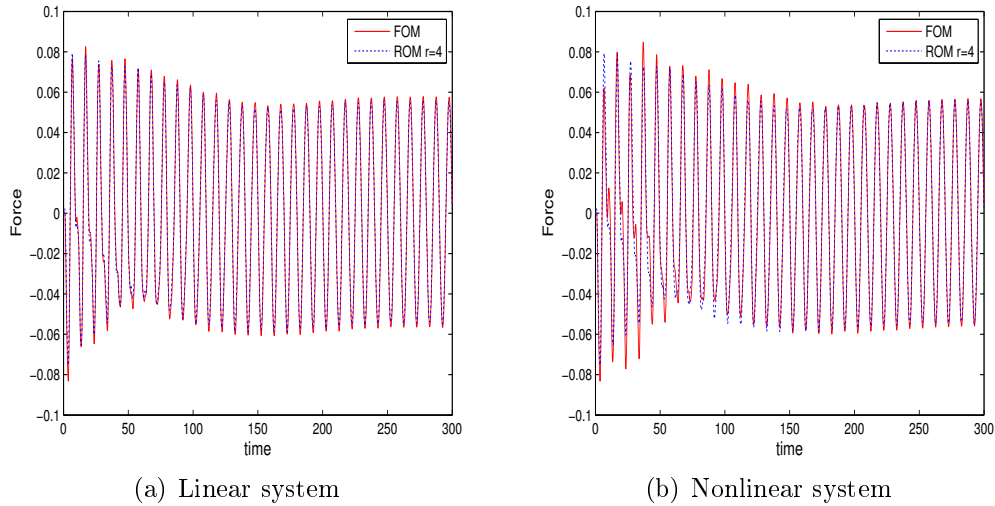
Figure 4.2. Example 1, Input 1: Output of the ROM and FOM for $\alpha_0 = \alpha = 0$, $\alpha_l = k_0 = k_l = 0.1$ and $\gamma = 0.001$ when $r = 4$

of the linear and nonlinear FOM and ROM for Example 1, Input 1 with $\alpha_0 = \alpha = 0$, $\alpha_l = k_0 = k_l = 0.1$ and $\gamma = 0.001$ when $r = 4$.

Next, Example 1 with Inputs 2, 3 and 4 the nonlinear ROM is moderately accurate and increasing r does not yield high accuracy. The linear ROM for Example 1 with Inputs 2, 3 and 4 is accurate but the amplitude of the ROM is slightly different from the FOM and increasing r does give high accuracy. Figures 4.3 and 4.4 show the behavior of the linear and nonlinear FOM and ROM for Example 1, Input 4 with $\alpha_0 = \alpha = 0$, $\alpha_l = k_0 = k_l = 0.1$ and $\gamma = 0.001$ when $r = 4$ and $r = 10$.

Overall, when interior damping parameters are small, for Examples 3 and 5 with all inputs, the outputs of linear and nonlinear ROM are accurate with little amplitude difference compared to the FOM and increasing r gives high accuracy. In Example 1 high accuracy may be lost after an initial time period. Increasing r may or may not improve the accuracy.

• Small boundary damping parameter

(a) Linear system (b) Nonlinear system
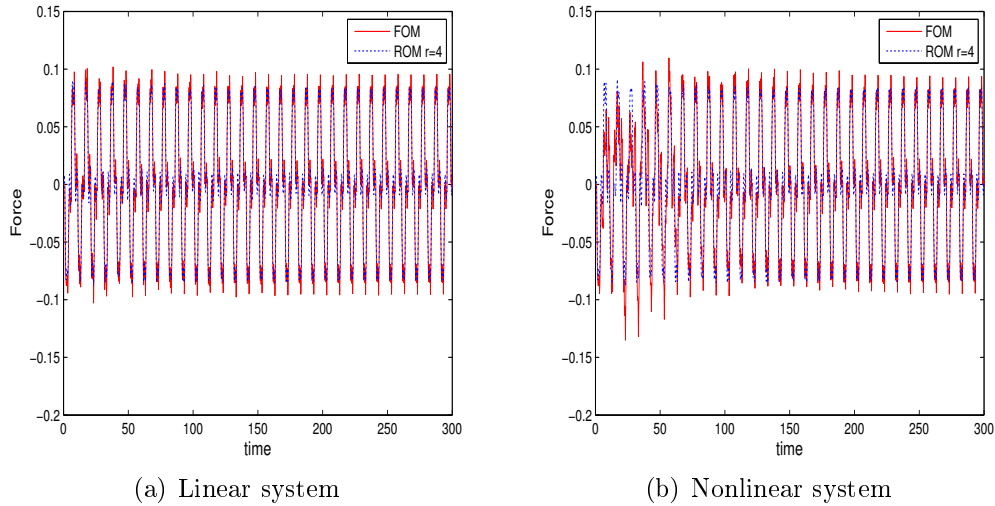
Figure 4.3. Example 1, Input 4: Output of the ROM and FOM for $\alpha_0 = \alpha = 0$, $\alpha_l = k_0 = k_l = 0.1$ and $\gamma = 0.001$ when $r = 4$

Here we investigate the behavior of the ROM for boundary damping parameters that are small relative to the interior damping parameters and boundary stiffness parameters. We experiment for boundary damping parameters α_l and α_0 in the range of 0.1 to 0.001 and fix $k_0 = k_l = \gamma = \alpha = 0.1$. Note only Example 1 is applicable here since Examples 3, 5 have $\alpha_l = 0$.

Case 2a : Small boundary damping parameter with all inputs

For Example 1 with all inputs, the linear and nonlinear ROMs are accurate only for an initial time interval. Increasing r yield highly accurate ROMs.

- Small damping parameters

Here we investigate the behavior of the ROM for boundary and interior damping parameters which are small relative to the boundary stiffness parameter. We experiment for damping parameters α, γ, α_l, α_0 in the range of 0.1 to 0.001 and fix $k_0 = k_l = 0.1$.

Case 3a : Small damping parameters with all inputs

(a) Linear system   (b) Nonlinear system
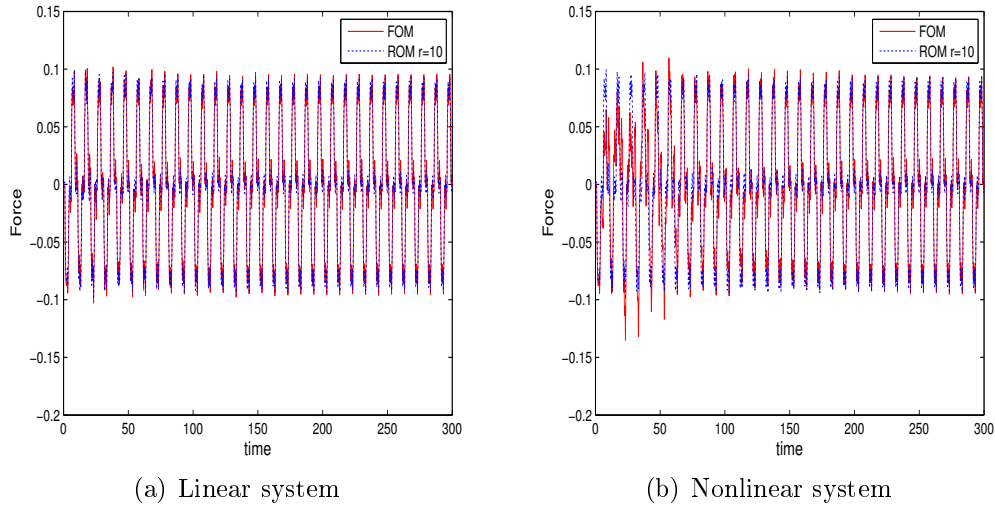
Figure 4.4. Example 1, Input 4: Output of the ROM and FOM for $\alpha_0 = \alpha = 0$, $\alpha_l = k_0 = k_l = 0.1$ and $\gamma = 0.001$ when $r = 10$

In this case all linear and nonlinear ROMs are accurate with little amplitude difference compared to the FOM and increasing r does give high accuracy. Figures 4.5 and 4.6 show the output of the FOM and ROM for the linear and nonlinear systems for Example 3, Input 3 with $\alpha_0 = \alpha_l = 0$, $k_0 = k_l = 0.1$ and $\alpha = \gamma = 0.001$ when $r = 4$ and $r = 6$.

- Small stiffness parameters

Next, we investigate the behavior of the FOM and ROM when the boundary stiffness parameters are small relative to the damping parameters. We experiment for stiffness parameters k_0 and k_l in the range of 0.1 to 0.001 and fix damping parameters as $\gamma = \alpha = \alpha_0 = \alpha_l = 0.1$.

Case 4a : Small stiffness parameters with all inputs

We test when one of k_0 or k_l is small, and also when both are small. In this case, for all examples with all inputs both the nonlinear and linear output of the ROM are moderately accurate and increasing r does yield high accuracy.

(a) Linear system   (b) Nonlinear system
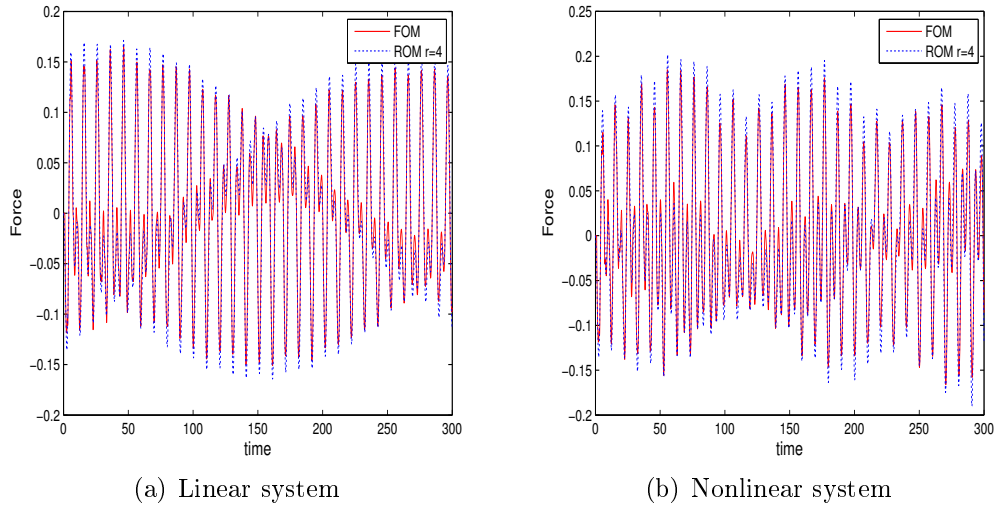
Figure 4.5. Example 3, Input 3: Output of the ROM and FOM for $\alpha_0 = \alpha_l = 0$, $k_0 = k_l = 0.1$ and $\alpha = \gamma = 0.001$ when $r = 4$

- All parameters are small

Finally, we observe the behavior of the nonlinear and linear ROM when the damping and stiffness parameters are small relative to the mass and nonlinear stiffness parameters ($m_0 = 1$, $m_l = 1.5$, and $k_3 = 1$). We experiment for damping parameters α, α_l, γ and the stiffness parameter k_0, k_l in the range of 0.1 to 0.001.

Case 5a : All parameters are small with all inputs for Examples 1 and 3

Here, for Examples 1, 3 with Inputs 1, 3 the output of the linear ROM is highly accurate and the output of nonlinear ROM is moderately accurate. Figure 4.7 shows the output of the FOM and ROM for the linear and nonlinear systems for Example 3, Input 3 with $\alpha_0 = \alpha_l = 0$ and $k_0 = k_l = \alpha = \gamma = 0.001$ when $r = 4$.

In Examples 1, 3 with Input 2, the output of linear and nonlinear ROM is moderately accurate. Increasing r does not give high accuracy. Figure 4.8 shows the output of the FOM and ROM for the linear and nonlinear systems for Example 1, Input 2 with $\alpha_0 = \alpha = 0$ and $k_0 = k_l = \alpha_l = \gamma = 0.001$ when $r = 4$.

(a) Linear system   (b) Nonlinear system
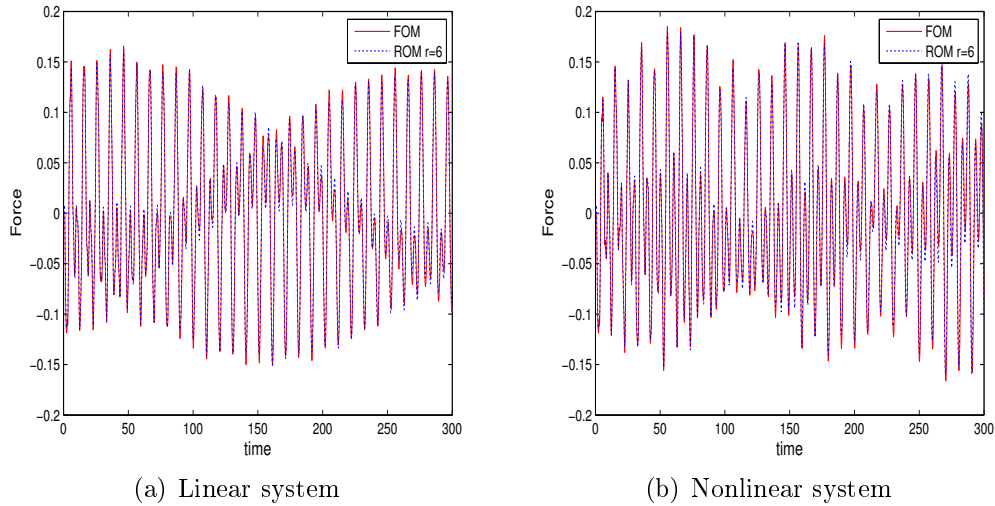
Figure 4.6. Example 3, Input3: Output of the ROM and FOM for $\alpha_0 = \alpha_l = 0$, $k_0 = k_l = 0.1$ and $\alpha = \gamma = 0.001$ when $r = 6$

Next, for Examples 1, 3 with Input 4 the nonlinear ROM is moderately accurate. The linear ROM is accurate with little amplitude difference compared to the FOM and increasing r does produce high accuracy.

Overall, the linear ROM is highly accurate or moderately accurate when r is small with all inputs and increasing r does yield high accuracy except Input 2. The nonlinear ROM is moderately accurate and increasing r may or may not yield high accuracy.

Case 5b : All parameters are small with all inputs for Example 5.

In Example 5, the linear and nonlinear ROM is highly accurate for an initial time interval and then accuracy may be lost. Increasing r for both the linear and nonlinear ROM yields high accuracy.

(a) Linear system   (b) Nonlinear system
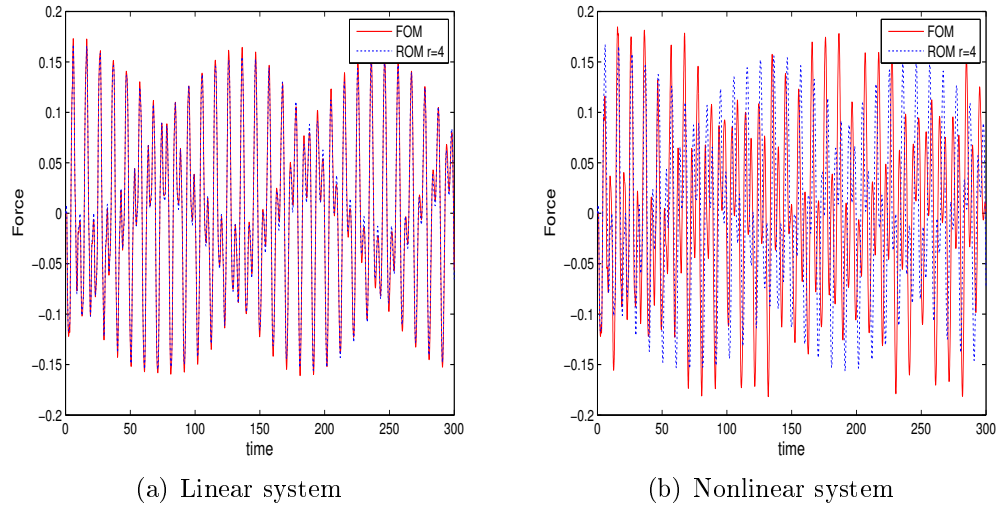
Figure 4.7. Example 3, Input 3: Output of the ROM and FOM for $\alpha_0 = \alpha_l = 0$ and $\alpha = \gamma = k_0 = k_l = 0.001$ when $r = 4$

(a) Linear system   (b) Nonlinear system
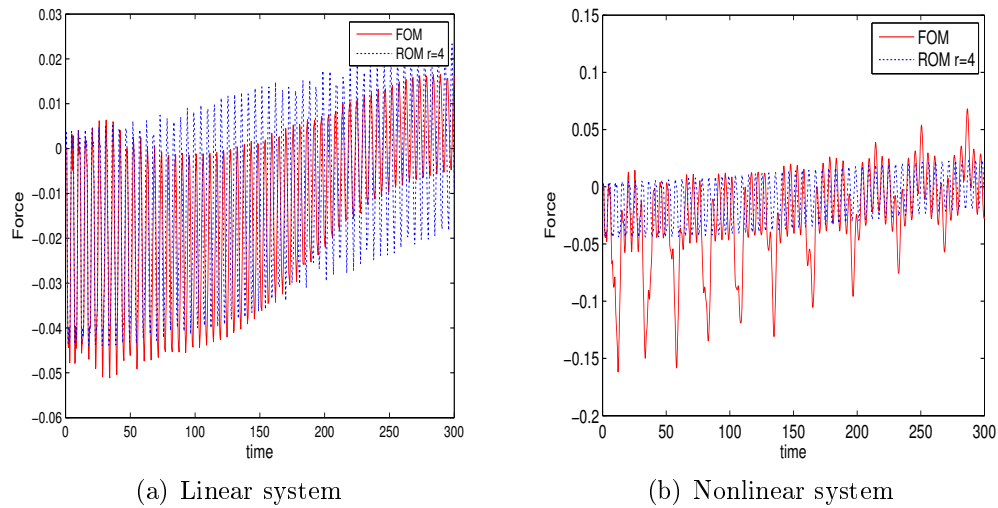
Figure 4.8. Example 1, Input 2: Output of the ROM and FOM for $\alpha_0 = \alpha = 0$ and $k_0 = k_l = \alpha_l = \gamma = 0.001$ when $r = 4$.

5. NONLINEAR EXPONENTIAL STABILITY OF ANOTHER NONLINEAR CABLE-MASS PDE SYSTEM

Next, we consider a cable-mass model similar to Section 2, but with different boundary condition at the left end. This problem was originally studied theoretically by Burns and King in [36], but our model includes one additional damping term. In [36], Burns and King proved the solution of the unforced nonlinear system decays to zero exponentially fast if the initial condition is small enough. The primary goal of this section is to prove the nonlinear exponential stability for large initial conditions. Further, we demonstrate the exponential stability of the linear and nonlinear systems numerically. We do not consider model reduction for this system.

5.1. THE MODEL

We consider a flexible cable which is fixed at one end and attached to mass-spring at the other end. Let

- $w(t, x)$ denote the position of the cable at location x and time t, and

- $w_l(t)$ denote the position of the right mass above equilibrium at location $x = l$ and time t.

The left side is fixed and the right mass is located at $x = l$. We assume there are no external forces. The right mass-spring system includes a nonlinear stiffening force, as before. This gives a wave equation with a dynamic boundary condition:

$$w_{tt}(t, x) + \alpha w_t(t, x) = \gamma w_{txx}(t, x) + \beta^2 w_{xx}(t, x), \tag{5.1}$$

$$w(t, 0) = 0, \tag{5.2}$$

$$m_l \ddot{w}_l(t) + \alpha_l \dot{w}_l(t) + k_l w_l(t) = -(\gamma w_{tx}(t, l) + \beta^2 w_x(t, l)) - k_3 \left[w_l(t) \right]^3. \tag{5.3}$$

Finally, the position of the cable at each boundary must equal the position of the mass; therefore, we have the *displacement compatibility condition*

$$w(t,0) = 0, \quad w(t,l) = w_l(t).$$

5.2. THE ENERGY FUNCTION

Next, we give a preliminary investigation of the change in energy of system. The only difference with the model considered in [36] is the addition of the viscous damping term αw_t in the wave equation. As before, we assume all damping parameters are nonnegative, and the remaining parameters are positive. This will help us to obtain the correct inner products for an abstract formulation of the system. We assume the solution for the above system is sufficiently smooth. We define the total kinetic energy of the cable by

$$E_{T,K} = \frac{1}{2} \int\limits_0^l w_t^2 \, dx.$$

Differentiating with respect to time and using the wave equation (5.1) gives

$$\frac{dE_{T,K}}{dt} = \frac{1}{2} \int\limits_0^l 2w_t w_{tt} \, dx$$

$$= \frac{1}{2} \int\limits_0^l 2w_t(t,x)(\gamma w_{txx}(t,x) + \beta^2 w_{xx}(t,x) - \alpha w_t(t,x)) \, dx.$$

Integrate by parts to obtain

$$\frac{dE_{T,K}}{dt} = -\gamma \int_0^l \left(w_{tx}(t,x)\right)^2 dx - \beta^2 \int_0^l w_x(t,x)w_{tx}(t,x) dx - \alpha \int_0^l \left(w_t(t,x)\right)^2 dx$$
$$+ w_t(t,l)\left[\gamma w_{tx}(t,l) + \beta^2 w_x(t,l)\right] - w_t(t,0)\left[\gamma w_{tx}(t,0) + \beta^2 w_x(t,0)\right].$$

Use the boundary conditions of our cable-mass model (5.2), (5.3), which gives $w(t, 0) = 0$ and since the solution is smooth this implies $w_t(t, 0) = 0$, to obtain

$$\frac{dE_{T,K}}{dt} = -\gamma \int_0^l (w_{tx}(t, x))^2 \, dx - \beta^2 \int_0^l w_x(t, x) w_{tx}(t, x) dx - \alpha \int_0^l (w_t(t, x))^2 \, dx$$
$$- \dot{w}_l(t) \left[m_l \ddot{w}_l(t) + \alpha_l \dot{w}_l(t) + k_l w_l(t) + k_3 \left[w_l(t) \right]^3 \right].$$

This can be rewritten as

$$\frac{d}{dt} \left(\frac{1}{2} \int_0^l w_t^2 \, dx + \frac{m_l}{2} (\dot{w}_l(t))^2 + \frac{\beta^2}{2} \int_0^l w_x^2 \, dx + \frac{k_l}{2} (w_l(t))^2 + \frac{k_3}{4} (w_l(t))^4 \right) =$$
$$- \gamma \int_0^l (w_{tx}(t, x))^2 \, dx - \alpha \int_0^l (w_t(t, x))^2 \, dx - \alpha_l (\dot{w}_l(t))^2.$$

This suggests defining the system kinetic energy and potential energy as

$$E_K = \int_0^l \frac{1}{2} w_t^2 \, dx + \frac{m_l}{2} (\dot{w}_l(t))^2,$$

$$E_P = \int_0^l \frac{\beta^2}{2} w_x^2 \, dx + \frac{k_l}{2} (w_l(t))^2 + \frac{k_3}{4} (w_l(t))^4.$$

This energy expression may be obtained by considering the kinetic energy and potential energy of each component of the system. The above energy equation gives

$$\frac{d}{dt} E = \frac{d}{dt} (E_K + E_P)$$
$$= - \left[\gamma \int_0^l (w_{tx}(t, x))^2 \, dx + \alpha \int_0^l (w_t(t, x))^2 \, dx + \alpha_l (\dot{w}_l(t))^2 \right],$$

and therefore $\dot{E}(t) \leq 0$.

5.3. VARIATIONAL FORM

In this section, we introduce the variational form (weak form) of the system. We assume the solution $[w, w_l]$ is smooth and satisfies the compatibility condition $w(t, l) = w_l(t)$. Multiply the wave equation (5.1) by a smooth test function $h = h(x)$ satisfying $h(0) = 0$ and $h(l) = h_l$ and integrate by parts to obtain

$$\int_0^l w_{tt}(t, x)\, h\, dx + \alpha \int_0^l w_t(t, x)\, h\, dx - \gamma \int_0^l w_{txx}(t, x)\, h\, dx - \beta^2 \int_0^l w_{xx}(t, x)\, h\, dx = 0.$$

$$\int_0^l w_{tt}(t, x)\, h\, dx + \alpha \int_0^l w_t(t, x)\, h\, dx - h_l \left[\gamma w_{tx}(t, l) + \beta^2 w_x(t, l) \right]$$

$$+ h(0) \left[\gamma w_{tx}(0) + \beta^2 w_x(0) \right] + \gamma \int_0^l w_{tx}(t, x)\, h_x\, dx + \beta^2 \int_0^l w_x(t, x)\, h_x\, dx = 0.$$

The boundary conditions give

$$\int_0^l w_{tt}(t, x)\, h\, dx + h_l \left[m_l \ddot{w}_l(t) + \alpha_l \dot{w}_l(t) + k_l w_l(t) + k_3 \left[w_l(t) \right]^3 \right]$$

$$+ \alpha \int_0^l w_t(t, x)\, h\, dx + \gamma \int_0^l w_{tx}(t, x)\, h_x\, dx + \beta^2 \int_0^l w_x(t, x)\, h_x\, dx = 0.$$

$$\int_0^l w_{tt}(t, x)\, h\, dx + m_l \ddot{w}_l(t) h_l + \int_0^l \left[\alpha w_t(t, x)\, h + \gamma w_{tx}(t, x)\, h_x \right] dx$$

$$+ \beta^2 \int_0^l w_x(t, x)\, h_x\, dx + k_l w_l(t) h_l + \alpha_l h_l \dot{w}_l(t) + k_3 \left[w_l(t) \right]^3 = 0. \tag{5.4}$$

Let H be the real Hilbert space $H = L^2(0, l) \times \mathbb{R}$ with the inner product of $z = [w, w_l] \in H$ and $\psi = [p, p_l] \in H$ defined by

$$(z, \psi)_H = \int_0^l wp\, dx + m_l w_l p_l. \tag{5.5}$$

Let $V \subset H$ be the set of elements $z = [w, w_l] \in H^1(0, l) \times \mathbb{R} = V$ satisfying the boundary condition $w(0) = 0$ and the displacement compatibility condition $w(l) = w_l$. For $z \in V$ as above and $\psi = [p, p_l] \in V$, define the V inner product of z with ψ by

$$(z, \psi)_V = \int_0^l \beta^2 w_x p_x dx + k_l w_l p_l. \tag{5.6}$$

We also use the notation $\sigma_1(z, \psi) = (z, \psi)_V$.

As before the, H and V norms are directly related to the system kinetic and potential energies, respectively. Specifically,

$$E_K = \frac{1}{2}(z_t,\, z_t)_H = \frac{1}{2}\|z_t\|_H^2, \quad E_P = \frac{1}{2}(z,\, z)_V + \frac{k_3}{4}w_l^4 = \frac{1}{2}\|z\|_V^2 + \frac{k_3}{4}w_l^4.$$

Also, we define the damping bilinear form $\sigma_2 : V \times V \to \mathbb{R}$,

$$\sigma_2(z, \psi) = \int_0^l (\gamma w_x p_x + \alpha w p)\, dx + \alpha_l w_l p_l. \tag{5.7}$$

5.4. ABSTRACT FORM

Our original PDE model (5.1) with the boundary conditions (5.2), (5.3) can be written in the first order abstract form (2.10). Similar to [36], the PDE system suggests the operator $\mathcal{A}$ may be formally defined as

$$D(\mathcal{A}) = \left\{ x = [w, w_l, v, v_l]^T \in \mathcal{H} = V \times H \; : \; w \in H^1(0, l),\, v \in H^1(0, l), \right.$$
$$\left. w(0) = 0,\, w(l) = w_l,\, v(0) = 0,\, v(l) = v_l \right\},$$

$$\mathcal{A}x = \mathcal{A}\begin{bmatrix} w \\ w_l \\ v \\ v_l \end{bmatrix} = \begin{bmatrix} v \\ v_l \\ \frac{d}{d\xi}\left[\beta^2 \frac{d}{d\xi}w + \gamma \frac{d}{d\xi}v\right] - \alpha v \\ -\delta_l\left[\frac{\beta^2}{m_l}\frac{d}{d\xi}w + \frac{\gamma}{m_l}\frac{d}{d\xi}v\right] - \frac{k_l}{m_l}w_l - \frac{\alpha_l}{m_l}v_l \end{bmatrix}. \tag{5.8}$$

As before, we do not use the formal definition of the operator $\mathcal{A}$ given above. Instead, we use theory from Banks [51] to rigorously define the operator $\mathcal{A}$ using the bilinear forms σ_1 and σ_2.

5.5. THE LINEAR PROBLEM

We prove the linear problem (2.12) is well-posed and also exponentially stable under certain assumptions on the damping parameters.

5.5.1. Function Spaces.

Lemma 5.1. *The space V with the above inner product (5.6) is a real Hilbert space and V is dense in H.*

Proof. First, if $(z, z)_V = 0$, where $z = [w, w_l]$, then $w(x)$ is a constant function and $w_l = 0$. The compatibility condition implies $w(x) = 0$ for all x, and so $z = 0$. It is clear that $(\cdot, \cdot)_V$ satisfies the remaining properties of an inner product.

Next, let $\{z^n\} \subset V$ be a Cauchy sequence, where $z^n = [w^n, w_l^n]$. Therefore, $[w_x^n, w_l^n]$ is a Cauchy sequence in $L^2(0, l) \times \mathbb{R}$, and so there exists $[q, w_l] \in L^2(0, l) \times \mathbb{R}$ such that

$$w_x^n \to q \text{ in } L^2(0, l), \quad w^n(0) = 0, \quad w_l^n \to w_l.$$

Define w by $w(x) = \int_0^x q(\eta)d\eta$. Then $w \in H^1(0,l)$, $w_x = q$, and $w(0) = 0$. Also, $w(l) = w_l$ since

$$
\begin{aligned}
w(l) &= \lim_{n\to\infty} \int_0^l w_x^n(\eta)d\eta \\
&= \lim_{n\to\infty} w^n(\eta)\,|_0^l \\
&= \lim_{n\to\infty} \left(w^n(l) - w^n(0) \right) \\
&= \lim_{n\to\infty} w_l^n \\
&= w_l.
\end{aligned}
$$

Therefore $z = [w, w_l]$ satisfies the displacement compatibility condition and z^n converges in V to $z \in V$. This shows V is a Hilbert space.

To show V is dense in H, let $z = [w, w_l] \in H$ and define

$$
g(x) = l^{-1}w_l x.
$$

Note that $g(0) = 0$ and $g(l) = w_l$, Since $H_0^1(0,l)$ is dense in $L^2(0,l)$, there exists a sequence $q_n \in H_0^1(0,l)$ such that $q_n \to w - g$ in $L^2(0,l)$. Define

$$
z_n = [q_n + g,\, w_l].
$$

Due to the properties of q_n and g, i.e., $q_n + g \in H^1$, $(q_n + g)(0) = 0$, and $(q_n + g)(l) = w_l$, we have $z_n \in V$ for all n. Also,

$$
\begin{aligned}
\lim_{n \to \infty} \|z_n - z\|_H^2 &= \lim_{n \to \infty} \|q_n + g - w\|_{L^2(0,l)}^2 + \|w_l - w_l\|^2 \\
&= \lim_{n \to \infty} \int_0^l (q_n + g - w)^2 dx \\
&= \lim_{n \to \infty} \int_0^l (q_n - (w - g))^2 dx \\
&= \lim_{n \to \infty} \|q_n - (w - g)\|_{L^2(0,l)}^2 \\
&= 0.
\end{aligned}
$$

This proves V is dense in H. $\qquad\square$

Lemma 5.2. *If $z = [w, w_l] \in V$, then*

$$
|w(x)|^2 \le l \, \|w_x\|_{L^2(0,l)}^2 , \tag{5.9}
$$

$$
\|w\|_{L^2(0,l)}^2 \le l^2 \, \|w_x\|_{L^2(0,l)}^2 , \tag{5.10}
$$

$$
w_l^2 \le l \, \|w_x\|_{L^2(0,l)}^2 . \tag{5.11}
$$

Proof. Since $w \in H^1(0, l)$ and $w(0) = 0$, we have

$$
w(x) = \int_0^x w_\xi(\xi) \, d\xi.
$$

Taking absolute values and using the triangle inequality gives

$$
|w(x)| \le \int_0^x |w_\xi(\xi)| \, d\xi.
$$

Applying Hölder's inequality gives

$$|w(x)| \leq \left(\int_0^l 1^2 d\xi \right)^{\frac{1}{2}} \cdot \left(\int_0^l |w_x(x)|^2 \, dx \right)^{\frac{1}{2}}$$

$$\leq l^{\frac{1}{2}} \|w_x\|_{L^2(0,l)} \, .$$

Squaring this inequality and using Young's inequality gives (5.9); integrating from $x = 0$ to $x = l$ gives us (5.10); and evaluating equation (5.9) at $x = l$ yields (5.11). $\square$

Lemma 5.3. *V is continuously embedded in H.*

Proof. Let $z = [w, w_l] \in V$. We use the H and V inner products and the inequality (5.10) from Lemma (5.2) to obtain

$$\|z\|_H^2 = \int_0^l w^2 dx + m_l w_l^2$$

$$= \|w\|_{L^2(0,l)}^2 + m_l w_l^2$$

$$\leq l^2 \|w_x\|_{L^2(0,l)}^2 + m_l w_l^2$$

$$= l^2 \int_0^l w_x^2 \, dx + m_l w_l^2$$

$$= \left(\frac{l^2}{\beta^2} \right) \int_0^l \beta^2 w_x^2 \, dx + \left(\frac{m_l}{k_l} \right) k_l w_l^2$$

$$\leq C_1 \left[k_l w_l^2 + \beta^2 \int_0^l w_x^2 \, dx \right],$$

where $C_1 = \max\left\{ \frac{l^2}{\beta^2}, \frac{m_l}{k_l} \right\}$. This gives $C_1^{-1} \|z\|_H^2 \leq \|z\|_V^2$, therefore V is continuously embedded in H. $\square$

5.5.2. Well-Posedness and Exponential Stability. To show the linear problem is well-posed, we rewrite the problem as $\dot{x} = \mathcal{A}x$ as before and show $\mathcal{A}$ generates a C_0-semigroup on $\mathcal{H} = V \times H$.

As before, we restrict our analysis to the cases where the damping bilinear form σ_2 is H-elliptic or V-elliptic.

Example 1: $\gamma, \alpha_l > 0$ and $\alpha = 0$. We first consider the case of Kelvin-Voigt damping ($\gamma > 0$) and viscous damping in the right mass-spring system ($\alpha_l > 0$). We prove σ_2 is V-elliptic. We rewrite the bilinear form of σ_2 and the V inner products according to the above parameters:

$$\sigma_2(z, z) = \int_0^l \gamma w_x^2 \, dx + \alpha_l w_l^2,$$

$$\|z\|_V^2 = \int_0^l \beta^2 w_x^2 dx + k_l w_l^2.$$

Then

$$\|z\|_V^2 = \beta^2 \int_0^l w_x^2 dx + k_l w_l^2$$

$$= \left(\frac{\beta^2}{\gamma}\right) \int_0^l \gamma w_x^2 dx + \left(\frac{k_l}{\alpha_l}\right) \alpha_l w_l^2$$

$$\leq C_2 \left(\int_0^l \gamma w_x^2 dx + \alpha_l w_l^2\right)$$

$$\leq C_2 \sigma_2(z, z)$$

where $C_2 = \max\left\{\frac{\beta^2}{\gamma}, \frac{k_l}{\alpha_l}\right\}$, This proves that σ_2 is $V - $elliptic.

Example 2: $\alpha, \alpha_l > 0$ and $\gamma = 0$. Next, we consider the case of viscous damping in the wave equation and the right mass ($\alpha, \alpha_l > 0$). We prove σ_2 is H-elliptic. Since

$$\sigma_2(z, z) = \int_0^l \alpha w^2 dx + \alpha_l w_l^2,$$

$$\|z\|_H^2 = \int_0^l w^2 dx + m_l w_l^2,$$

we have

$$\|z\|_H^2 = \int_0^l \left(\frac{1}{\alpha}\right) \alpha w^2 dx + \left(\frac{m_l}{\alpha_l}\right) \alpha_l w_l^2$$
$$\leq C_3 \left[\int_0^l \alpha w^2 dx + \alpha_l w_l^2\right],$$

where $C_3 = \max\left\{\frac{1}{\alpha}, \frac{m_l}{\alpha_l}\right\}$, and this proves σ_2 is H-elliptic.

Example 3: $\gamma > 0$ and $\alpha = \alpha_l = 0$. In this last case, we consider only Kelvin-Voigt damping ($\gamma > 0$) and no other viscous damping. We prove σ_2 is $V - $ elliptic. Since

$$\sigma_2(z, \psi) = \int_0^l \gamma w_x^2 dx,$$
$$\|z\|_V^2 = \int_0^l \beta^2 w_x^2 dx + k_l w_l^2,$$

use (5.11) to obtain

$$\|z\|_V^2 \leq \beta^2 \int_0^l w_x^2 \, dx + k_l l \int_0^l w_x^2 \, dx$$
$$= \left(\frac{\beta^2 + k_l l}{\gamma}\right) \gamma \int_0^l w_x^2 \, dx.$$

Therefore $C_4^{-1} \|z\|_H^2 \leq \sigma_2(z, z)$, where $C_4 = \frac{\beta^2 + k_l l}{\gamma}$, and this proves σ_2 is H-elliptic.

In Examples 1, 3 we proved σ_2 is V-elliptic and Theorem 8.1 in [51] gives us $\mathcal{A}$ is the infinitesimal generator of an analytic exponentially stable semigroup.

In Example 2 we proved σ_2 is H-elliptic and Theorem 8.3 in [51] gives us $\mathcal{A}$ generates an exponentially stable C_0-semigroup.

5.6. THE NONLINEAR PROBLEM

We write the nonlinear problem as

$$\dot{x}(t) = \mathcal{A}x(t) + \mathcal{F}(x(t)), \;\; x(0) = x_0 \tag{5.12}$$

on $\mathcal{H} = V \times H$. Here the linear operator $\mathcal{A}$ is defined in Section 2.1 and the nonlinear operator $\mathcal{F} : \mathcal{H} \to \mathcal{H}$ is defined for $x = [\varphi, \psi] \in \mathcal{H}$ with $\varphi = [w, w_l] \in V$ by

$$\mathcal{F}(x) = \begin{bmatrix} 0 \\ F_0(\varphi) \end{bmatrix}, \;\; F_0(\varphi) = \begin{bmatrix} 0 \\ m_l^{-1} k_3 w_l^3 \end{bmatrix}.$$

Theorem 5.4. *The nonlinear cable-mass system has a unique mild solution on some time interval $[0, t^*)$.*

Theorem 5.5. *If σ_2 is H-elliptic and the solution $x = [z, z_t]$, with $z = [w, w_l]$, of the unforced nonlinear cable-mass problem (5.12) is sufficiently smooth, then the energy $E(t) = \frac{1}{2} \|z_t\|_H^2 + \frac{1}{2} \|z\|_V^2 + \frac{k_3}{4} [w_l(t)]^4$ of the solution with the initial data $x(0) = x_0 \in \mathcal{H}$ decays exponentially fast as $t \to \infty$.*

Proofs of Theorems 5.4 and 5.5 are similar to Section 2.

5.6.1. Formulating the Finite Difference Approximation. In this section, we present numerical results concerning the linear and nonlinear exponential stability theory. For the linear problem, we test the exponential stability by analyzing the eigenvalues of the matrix A in the finite difference model (5.12).

We place n equally spaced nodes $\{x_j\}_{j=1}^{n}$ in the interval $[0, l]$, where $x_j = jh$ and $h = l/n$ so that $x_1 = h$ and $x_n = l$. In order to apply balanced truncation below, we also eliminate the second order time derivatives by introducing a velocity variable. Therefore, let d_i denote the finite difference approximation to the displacement $w(t, x_i)$, and let v_i denote the finite difference approximation to the velocity $w_t(t, x_i)$.

We assume the solution is smooth so that the displacement and velocity satisfy the zero Dirichlet boundary condition at $x = 0$ and the compatibility condition; we obtain

$$w_0(t) = 0, \quad w_l(t) = d_n(t),$$
$$\dot{w}_0(t) = 0, \quad \dot{w}_l(t) = v_n(t).$$

We use second order centered differences to form finite difference equations for the wave equation (5.1):

$$v_i' = \frac{\gamma}{h^2}[v_{i+1} - 2v_i + v_{i-1}] + \frac{\beta^2}{h^2}[d_{i+1} - 2d_i + d_{i-1}] - \alpha v_i,$$
$$d_i' = v_i, \quad \text{for } i = 2, ..., n - 1. \tag{5.13}$$

To discretize our system we use (5.13) to obtain

$$v_i' = \left[-\alpha - \frac{2\gamma}{h^2}\right]v_i + \left[\frac{\gamma}{h^2}\right]v_{i-1} + \left[\frac{\gamma}{h^2}\right]v_{i+1} + \left[\frac{\beta^2}{h^2}\right]d_{i+1} - \left[\frac{2\beta^2}{h^2}\right]d_i + \left[\frac{\beta^2}{h^2}\right]d_{i-1},$$
$$d_i' = v_i, \quad \text{for } i = 1, ..., n - 1.$$

After discretizing the left boundary condition using one-sided finite difference approximations and substituting the result in the above equation with $i = 1$, we obtain

$$v_1' = -\left[\frac{2\beta^2}{h^2}\right]d_1 + \left[\frac{\beta^2}{h^2}\right]d_2 + \left[-\frac{2\gamma}{h^2} - \alpha\right]v_1 + \left[\frac{\gamma}{h^2}\right]v_2,$$
$$d_1' = v_1.$$

For the dynamic right boundary condition we obtain

$$v_n' = \left[-\frac{k_l}{m_l} - \frac{3\beta^2}{2hm_l}\right]d_n + \left[\frac{4\beta^2}{2hm_l}\right]d_{n-1} - \left[\frac{\beta^2}{2hm_l}\right]d_{n-2}$$
$$+ \left[-\frac{\alpha_l}{m_l} - \frac{3\gamma}{2hm_l}\right]v_n + \left[\frac{4\gamma}{2hm_l}\right]v_{n-1} - \left[\frac{\gamma}{2hm_l}\right]v_{n-2} - \left[\frac{k_3}{m_l}\right][d_n]^3 ,$$

$$d'_n = v_n.$$

where d_i, v_i and $u(t)$ represent displacement, velocity and input respectively. The above system can be placed in the matrix form (2.29). First, the matrix A_{11} has nonzero (i, j) entries, where i, j represent the row and column, respectively, as specified below. The nonzero first row entries of A_{11} in the $(1, 1)$ and $(1, 2)$ entries are $\left(-\frac{2\beta^2}{h^2}\right)$, $\left(\frac{\beta^2}{h^2}\right)$, respectively. The nonzero last row entries of A_{11} in the $(n, n-2)$, $(n, n-1)$ and (n, n) entries are $\left(-\frac{\beta^2}{2hm_l}\right)$, $\left(\frac{4\beta^2}{2hm_l}\right)$, $\left(-\frac{k_l}{m_l} - \frac{3\beta^2}{2hm_l}\right)$, respectively. The middle part of the matrix $i = 2, 3, \dots, n-1$ is a tridiagonal matrix. The entries are

$$[A_{11}]_{i,j} = \begin{cases} \frac{\beta^2}{h^2}, & i = i - 1, \\ -\frac{2\beta^2}{h^2}, & i = i, \\ \frac{\beta^2}{h^2}, & i = i + 1. \end{cases}$$

Similarly, the nonzero first row entries of A_{12} in the $(1, 1)$ and $(1, 2)$ entries are $\left(-\alpha - \frac{2\gamma}{h^2}\right)$, $\left(\frac{\gamma}{h^2}\right)$, respectively. The nonzero last row entries of A_{12} in the $(n, n-2)$, $(n, n-1)$ and (n, n) are $\left(-\frac{\gamma}{2hm_l}\right)$, $\left(\frac{4\gamma}{2hm_l}\right)$, $\left(-\frac{\alpha_l}{m_l} - \frac{3\gamma}{2hm_l}\right)$, respectively. The middle part of the matrix $i = 2, 3, \dots, n-1$ is a tridiagonal matrix. The entries are

$$[A_{11}]_{i,j} = \begin{cases} \frac{\gamma}{h^2}, & i = i - 1, \\ -\alpha - \frac{2\gamma}{h^2}, & i = 1, \\ \frac{\gamma}{h^2}, & i = i + 1. \end{cases}$$

Also, the matrix F_{12} in the nonlinear term is defined similarly to earlier sections. Furthermore A_{11}, $A_{1,2}$, F_{12} are $n \times n$ matrices.

We can write the nonlinear finite dimensional approximating system as

$$\dot{x} = Ax + F(x). \tag{5.14}$$

5.6.2. Formulating the Finite Difference Approximation of the Energy Function. For the nonlinear problem, we consider the solution of the finite

difference model and compute an approximation to the energy function in Theorem 5.5 using trapezoidal rule quadrature on the integrals.

The energy of the unforced system is $E = E_K + E_P$ where

$$E_K = \int_0^l \frac{1}{2} w_t^2 \, dx + \frac{m_l}{2} \left(\dot{w}_l(t) \right)^2,$$

$$E_P = \int_0^l \frac{\beta^2}{2} w_x^2 \, dx + \frac{k_l}{2} \left(w_l(t) \right)^2 + \frac{k_3}{4} \left(w_l(t) \right)^4.$$

Recall trapezoidal rule quadrature for an integral:

$$\int_a^b F(x) dx \approx \frac{h}{2} \left[F(a) + F(b) \right] + \sum_{i=2}^{n-1} h F(x_i)$$

Applying the trapezoidal rule to each term in the energy function gives

$$\int_0^l \frac{1}{2} w_t^2 \, dx \approx \frac{1}{2} \left[\frac{h}{2} \left(v_1(t) \right)^2 + \frac{h}{2} \left(v_n(t) \right)^2 \right] + \frac{1}{2} \sum_{i=2}^{n-1} h \left(v_i(t) \right)^2$$

and

$$\int_0^l \frac{\beta^2}{2} w_x^2 \, dx \approx \frac{\beta^2}{2} \left[\frac{h}{2} \left(w_x(t, \, x_1) \right)^2 + \frac{h}{2} \left(w_x(t, \, x_n) \right)^2 \right] + \frac{\beta^2}{2} \sum_{i=2}^{n-1} h \left(w_x(t, x_i) \right)^2.$$

Use one-sided and centered difference formulas to get

$$\int_0^l \frac{\beta^2}{2} w_x^2 \, dx \approx \frac{\beta^2}{2} \left[\frac{h}{2} \left(\frac{-3w_1 + 4w_2 - w_3}{2h} \right)^2 + \frac{h}{2} \left(\frac{3w_n - 4w_{n-1} + w_{n-2}}{2h} \right)^2 \right]$$

$$+ \frac{\beta^2 h}{2} \sum_{i=2}^{n-1} \left(\frac{w_{i+1} - w_{i-1}}{2h} \right)^2.$$

Table 5.1. Eigenvalues of the linear system for number of spatial nodes with $\gamma = \alpha_l = 0.01$, $k_l = 0.01$ and $\alpha = 0$

N	10	20	40	80	160
Re (λ)	-0.0050	-0.0052	-0.0053	-0.0053	-0.0054

Then the energy of the system is approximated as follows:

$$E(t) \approx \frac{h}{4}v_1^2(t) + \left[\frac{h}{4} + \frac{m_l}{2}\right]v_n^2 + \frac{h}{2}\sum_{i=2}^{n-1}(v_i)^2 + \frac{\beta^2}{16h}\left[-3w_1 + 4w_2 - w_3\right]^2$$

$$+ \frac{\beta^2}{16h}\left[3w_n - 4w_{n-1} + w_{n-2}\right]^2 + \frac{\beta^2}{8h}\sum_{i=2}^{n-1}\left[w_{i+1} - w_{i-1}\right]^2$$

$$+ \frac{k_l}{2}(w_n)^2 + \frac{k_3}{4}(w_n)^4$$

5.6.3. Numerical Results. Figure 5.1(a) shows the eigenvalues of the matrix A for $\gamma = \alpha_l = 0.01$, $k_l = 0.01$, and $\alpha = 0$ (this is a case of Example 1), and Figure 5.2(a) shows the eigenvalues of the matrix A for $\alpha = \alpha_l = 0.01$, $k_l = 0.01$, and $\gamma = 0$ (this is a case of Example 2). All eigenvalues have negative real parts. Similarly, the eigenvalues of Example 3 have negative real parts. We do not give figures for this case.

Figure 5.1(b) and 5.2(b) shows the exponential decay of the energy with the same parameters with the initial data $e^x \sin(x)$ for the position and $\cos(x)$ for the velocity. We choose the initial condition to match the boundary condition at $x = 0$ to produce a smooth solution.

First, we look at the behavior of the eigenvalue nearest the imaginary axis by increasing the number of spatial nodes. As we can see in Tables 5.1 and 5.2 the eigenvalue do not approach the imaginary axis when the number of spatial nodes is increased. This is the behavior we expect since the PDE system is exponentially stable.

Table 5.2. Eigenvalues of the linear system for number of spatial nodes with $\alpha = \alpha_l = 0.01$, $k_l = 0.01$ and $\gamma = 0$

N	10	20	40	80	160
Re (λ)	-0.0037	-0.0037	-0.0037	-0.0037	-0.0037

(a) Linear system
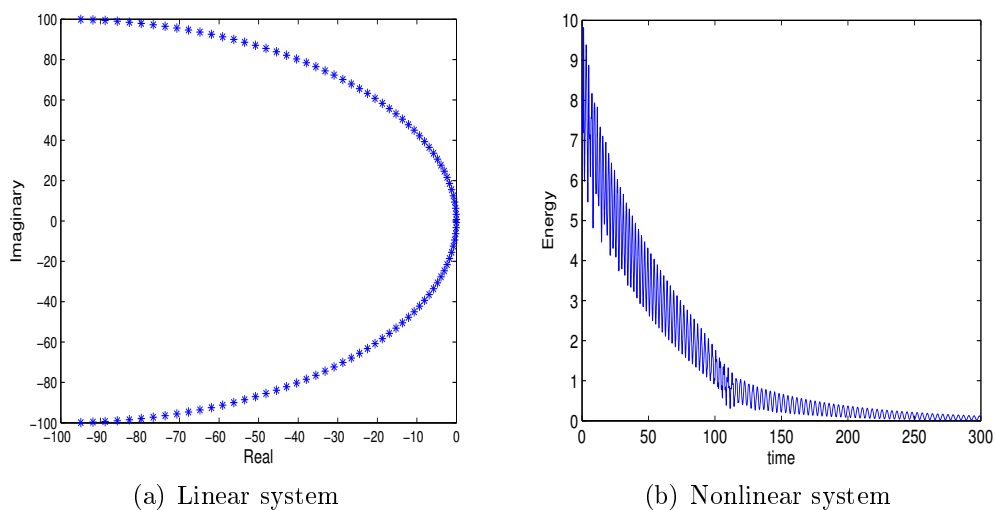
(b) Nonlinear system

Figure 5.1. Eigenvalues of the linear system and energy decay of the nonlinear system with $\gamma = \alpha_l = 0.01$, $k_l = 0.01$ and $\alpha = 0$

Next, Figures 5.1 and 5.2 show the exponential stability for examples of both the linear and nonlinear cases. In the nonlinear case, if $\gamma = 0$ and all the other parameters are small then the energy decays exponentially fast and fluctuates rapidly.

(a) Linear system   (b) Nonlinear system
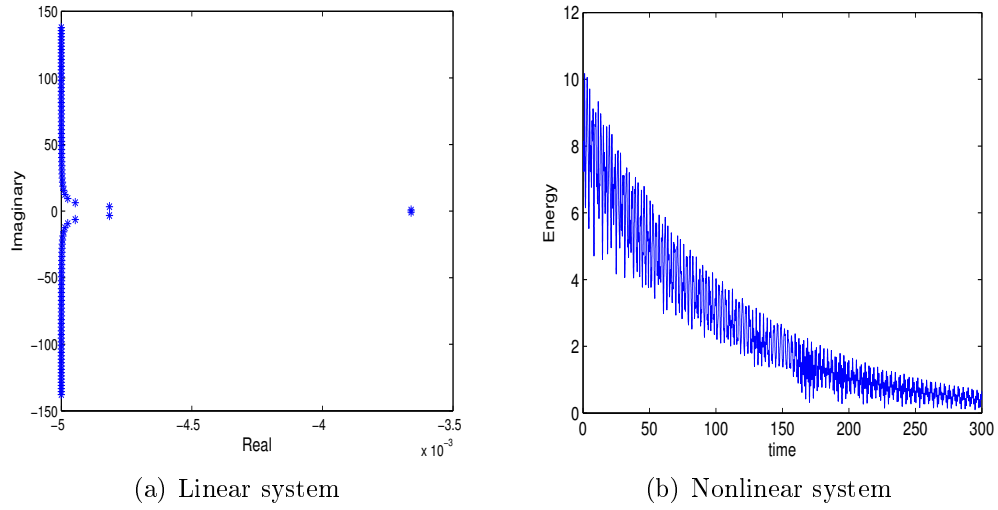
Figure 5.2. Eigenvalues of the linear system and energy decay of the nonlinear system
with $\alpha = \alpha_l = 0.01$, $k_l = 0.01$ and $\gamma = 0$

6. CONCLUSION

We considered a cable-mass system originally motivated by an application to wave energy that is modeled by a 1D wave equation with linear and nonlinear second order oscillator dynamic boundary conditions. In this work, we discussed four different cable-mass models, and we proved the well-posedness of the unforced linear and nonlinear problems. Under certain assumptions on the damping parameters, we proved the linear problems are exponentially stable and the energy decays exponentially fast for the nonlinear problems.

For the forced input-output nonlinear cable-mass system, we described and numerically investigated a model order reduction (MOR) approach based on balanced truncation. Overall, we analyzed the performance of the ROM under three cases: the damping parameters are small, the stiffness parameters are small, and both the damping and stiffness parameters are small (i.e., all parameters are small).

When both input/output operators are bounded as in Section 2, we proved the PDE balanced truncation theory holds. No theory currently exists for this nonlinear balanced truncation approach.

In Section 2, the output of the linear ROM is highly accurate in all cases considered, as expected in balanced truncation theory. The nonlinear ROM is highly accurate in most cases. The other cases the nonlinear ROM is always highly accurate over an initial time interval and increasing r may or may not improve the accuracy.

In Section 3 the input operator and in Section 4 the output operator are unbounded. We did not attempt to prove the PDE balanced truncation theory holds.

In Section 3 the linear ROM is highly accurate in all cases. The nonlinear ROM is highly accurate for all cases with smooth input 2. In other cases the nonlinear

ROM is highly accurate over initial period of interval and increasing r may or may not greatly improve the accuracy.

In Section 4 the performance of ROM is not accurate as Sections 2 and 3. The linear ROM is not always highly accurate for a longer time period but increasing r improves the accuracy. The nonlinear ROM does show high accuracy for few cases. When either damping parameters are small or stiffness parameters are small the nonlinear ROM is moderately accurate and increasing r improves the accuracy. When all parameters are small, both the linear and nonlinear ROM are moderately accurate. Increasing r gives high accuracy for the linear ROM but for the nonlinear ROM increasing r may or may not improve the accuracy.

To summarize, the linear ROM is always highly accurate when both the input and output operators are bounded or the output operator is bounded. If the output operator is unbounded the linear ROM is highly accurate over a long time period or loses accuracy after an initial time interval and increasing r does improve the accuracy. The accuracy of the nonlinear ROM can vary when the input and output operators are bounded or the output operator is bounded or the input operator is bounded. Increasing r may or may not improve the accuracy.

If the magnitude of the input is decreased, then the length of the accurate time interval for the nonlinear ROM increases. The output of the linear and nonlinear ROM is always accurate for an initial time interval and increasing r does improve the accuracy.

The results in this work suggest some beginning theoretical results that could be investigated. Specifically, our numerical results suggest it may be possible to prove that the error in the output for the nonlinear ROM is small over an initial time period, and that the length of this interval increases as the magnitude of the input decreases or r increases.

For our linear and nonlinear exponential stability results, we required the damping bilinear form to be H-elliptic. For each cable-mass system, we proved this H-elliptic condition assuming various conditions on the damping parameters. For Example 4 and 5 the damping bilinear form is not H-elliptic, and so the exponential stability theory in our work does not apply. Investigating these examples theoretically is a topic for future research. Furthermore, it would be interesting to investigate the exponential stability and MOR of a cable-mass system with only with boundary damping terms.

BIBLIOGRAPHY

[1] Peter Benner, Ekkehard Sachs, and Stefan Volkwein. Model order reduction for PDE constrained optimization. In *Trends in PDE constrained optimization*, volume 165 of *Internat. Ser. Numer. Math.*, pages 303–326. Birkhäuser/Springer, Cham, 2014.

[2] Tan Bui-Thanh, Karen Willcox, and Omar Ghattas. Parametric reduced-order models for probabilistic analysis of unsteady aerodynamic applications. *AIAA Journal*, 46(10):2520–2529, 2008.

[3] D. N. Daescu and I. M. Navon. Efficiency of a POD-based reduced second-order adjoint model in 4D-var data assimilation. *Internat. J. Numer. Methods Fluids*, 53(6):985–1004, 2007.

[4] F Fang, T Zhang, D Pavlidis, CC Pain, AG Buchan, and IM Navon. Reduced order modelling of an unstructured mesh air pollution model and application in 2d/3d urban street canyons. *Atmospheric Environment*, 96:96–106, 2014.

[5] Max Gunzburger and Hyung-Chun Lee. Reduced-order modeling of Navier-Stokes equations via centroidal Voronoi tessellation. In *Recent advances in adaptive computation*, volume 383 of *Contemp. Math.*, pages 213–224. Amer. Math. Soc., Providence, RI, 2005.

[6] Max Gunzburger, Nan Jiang, and Michael Schneier. An ensemble-proper orthogonal decomposition method for the nonstationary Navier-Stokes equations. *SIAM J. Numer. Anal.*, 55(1):286–304, 2017.

[7] Amit Varshney, Sivakumar Pitchaiah, and Antonios Armaou. Feedback control of dissipative pde systems using adaptive model reduction. *AIChE journal*, 55(4):906–918, 2009.

[8] Bruce C. Moore. Principal component analysis in linear systems: controllability, observability, and model reduction. *IEEE Trans. Automat. Control*, 26(1):17–32, 1981.

[9] Athanasios C. Antoulas. *Approximation of large-scale dynamical systems*, volume 6 of *Advances in Design and Control*. Society for Industrial and Applied Mathematics (SIAM), Philadelphia, PA, 2005. With a foreword by Jan C. Willems.

[10] K. Zhou, J. C. Doyle, and K. Glover. *Robust and Optimal Control*. Prentice-Hall, 1996.

[11] J. M. A. Scherpen. Balancing for nonlinear systems. *Systems Control Lett.*, 21(2):143–153, 1993.

[12] Sanjay Lall, Jerrold E. Marsden, and Sonja Glavaški. A subspace approach to balanced truncation for model reduction of nonlinear control systems. *Internat. J. Robust Nonlinear Control*, 12(6):519–535, 2002.

[13] C. W. Rowley. Model reduction for fluids, using balanced proper orthogonal decomposition. *Internat. J. Bifur. Chaos Appl. Sci. Engrg.*, 15(3):997–1013, 2005.

[14] Juan Carlos De Los Reyes and Tatjana Stykel. A balanced truncation-based strategy for optimal control of evolution problems. *Optim. Methods Softw.*, 26(4-5):671–692, 2011.

[15] Karen Willcox and Jaime Peraire. Balanced model reduction via the proper orthogonal decomposition. *AIAA journal*, 40(11):2323–2330, 2002.

[16] W Steven Gray and Joseph Mesko. General input balancing and model reduction for linear and nonlinear systems. In *Control Conference (ECC), 1997 European*, pages 2862–2867. IEEE, 1997.

[17] Marissa Condon and Rossen Ivanov. Nonlinear systems–algebraic gramians and model reduction. *COMPEL-The international journal for computation and mathematics in electrical and electronic engineering*, 24(1):202–219, 2005.

[18] Miloš. Ilak, Shervin Bagheri, Luca Brandt, Clarence W. Rowley, and Dan S. Henningson. Model reduction of the nonlinear complex Ginzburg-Landau equation. *SIAM J. Appl. Dyn. Syst.*, 9(4):1284–1302, 2010.

[19] Hesam E. Shoori J. An approach to reduced-order modeling and feedback control for wave energy converters. Master's thesis, Oregon State University, 2014.

[20] R. F. Curtain and A. J. Sasane. Compactness and nuclearity of the Hankel operator and internal stability of infinite-dimensional state linear systems. *Internat. J. Control*, 74(12):1260–1270, 2001.

[21] Mark R. Opmeer. Nuclearity of Hankel operators for ultradifferentiable control systems. *Systems Control Lett.*, 57(11):913–918, 2008.

[22] Chris Guiver and Mark R. Opmeer. Model reduction by balanced truncation for systems with nuclear Hankel operators. *SIAM J. Control Optim.*, 52(2):1366–1401, 2014.

[23] Alessandro Alla and Stefan Volkwein. Asymptotic stability of POD based model predictive control for a semilinear parabolic PDE. *Adv. Comput. Math.*, 41(5):1073–1102, 2015.

[24] Patricia Astrid, Leo Huisman, Siep Weiland, and ACPM Backx. Reduction and predictive control design for a computational fluid dynamics model. In *Decision and Control, 2002, Proceedings of the 41st IEEE Conference on*, volume 3, pages 3378–3383. IEEE, 2002.

[25] Peter Benner and Tobias Breiten. Two-sided projection methods for nonlinear model order reduction. *SIAM J. Sci. Comput.*, 37(2):B239–B260, 2015.

[26] Saifon Chaturantabut and Danny C. Sorensen. Nonlinear model reduction via discrete empirical interpolation. *SIAM J. Sci. Comput.*, 32(5):2737–2764, 2010.

[27] Traian Iliescu and Zhu Wang. Are the snapshot difference quotients needed in the proper orthogonal decomposition? *SIAM J. Sci. Comput.*, 36(3):A1221–A1250, 2014.

[28] Geoffrey M. Oxberry, Tanya Kostova-Vassilevska, William Arrighi, and Kyle Chand. Limited-memory adaptive snapshot selection for proper orthogonal decomposition. *Internat. J. Numer. Methods Engrg.*, 109(2):198–217, 2017.

[29] Liqian Peng and Kamran Mohseni. Symplectic model reduction of Hamiltonian systems. *SIAM J. Sci. Comput.*, 38(1):A1–A27, 2016.

[30] Miguel Fosas de Pando, Peter J. Schmid, and Denis Sipp. Nonlinear model-order reduction for compressible flow solvers using the discrete empirical interpolation method. *J. Comput. Phys.*, 324:194–209, 2016.

[31] Reinout Romijn, Leyla Özkan, Siep Weiland, Jobert Ludlage, and Wolfgang Marquardt. A grey-box modeling approach for the reduction of nonlinear systems. *Journal of Process Control*, 18(9):906–914, 2008.

[32] Jonathan H. Tu and Clarence W. Rowley. An improved algorithm for balanced POD through an analytic treatment of impulse response tails. *J. Comput. Phys.*, 231(16):5317–5333, 2012.

[33] Matthew O. Williams, Peter J. Schmid, and J. Nathan Kutz. Erratum: Hybrid reduced-order integration with proper orthogonal decomposition and dynamic mode decomposition. *Multiscale Model. Simul.*, 11(4):1311, 2013.

[34] D. Wirtz, D. C. Sorensen, and B. Haasdonk. A posteriori error estimation for DEIM reduced nonlinear dynamical systems. *SIAM J. Sci. Comput.*, 36(2):A311–A338, 2014.

[35] Zhu Wang. Nonlinear model reduction based on the finite element method with interpolated coefficients: semilinear parabolic equations. *Numer. Methods Partial Differential Equations*, 31(6):1713–1741, 2015.

[36] John A. Burns and Belinda B. King. A reduced basis approach to the design of low-order feedback controllers for nonlinear continuous systems. *J. Vib. Control*, 4(3):297–323, 1998.

[37] Francis Conrad and Abdelkrim Mifdal. Uniform stabilization of a hybrid system with a class of nonlinear feedback laws. *Adv. Math. Sci. Appl.*, 11(2):549–569, 2001.

[38] Nicolas Fourrier and Irena Lasiecka. Regularity and stability of a wave equation with a strong damping and dynamic boundary conditions. *Evol. Equ. Control Theory*, 2(4):631–667, 2013.

[39] Ömer Morgül. Stabilization and disturbance rejection for the wave equation. *IEEE Trans. Automat. Control*, 43(1):89–95, 1998.

[40] Zhifei Zhang. Stabilization of the wave equation with variable coefficients and a dynamical boundary control. *Electronic Journal of Differential Equations*, 2016(27):1–10, 2016.

[41] D. Amsallem and U. Hetmaniuk. Error estimates for Galerkin reduced-order models of the semi-discrete wave equation. *ESAIM Math. Model. Numer. Anal.*, 48(1):135–163, 2014.

[42] Belinda A. Batten and Katie A. Evans. Reduced-order compensators via balancing and central control design for a structural control problem. *Internat. J. Control*, 83(3):563–574, 2010.

[43] Yuezheng Gong, Qi Wang, and Zhu Wang. Structure-preserving Galerkin POD reduced-order modeling of Hamiltonian systems. *Comput. Methods Appl. Mech. Engrg.*, 315:780–798, 2017.

[44] Sabrina Herkt, Michael Hinze, and Rene Pinnau. Convergence analysis of Galerkin POD for linear second order evolution equations. *Electron. Trans. Numer. Anal.*, 40:321–337, 2013.

[45] D. B. Phuong Huynh, David J. Knezevic, and Anthony T. Patera. A Laplace transform certified reduced basis method; application to the heat equation and wave equation. *C. R. Math. Acad. Sci. Paris*, 349(7-8):401–405, 2011.

[46] Victor Pereyra. Model order reduction with oblique projections for large scale wave propagation. *J. Comput. Appl. Math.*, 295:103–114, 2016.

[47] John A Burns and Eugene M Cliff. Control of hyperbolic pde systems with actuator dynamics. In *Decision and Control (CDC), 2014 IEEE 53rd Annual Conference on*, pages 2864–2869. IEEE, 2014.

[48] John A Burns and Lizette Zietsman. Control of a thermal fluid heat exchanger with actuator dynamics. In *Decision and Control (CDC), 2016 IEEE 55th Conference on*, pages 3131–3136. IEEE, 2016.

[49] John A Burns and Lizette Zietsman. On the inclusion of actuator dynamics in boundary control of distributed parameter systems. *IFAC Proceedings Volumes*, 45(19):138–142, 2012.

[50] KA Morris. H1-control of acoustic noise in a duct with a feedforward configuration. In *15th International Symposium on Mathematical Theory of Networks and Systems, South Bend, IN, August*, pages 12–16, 2002.

[51] H Thomas Banks. *A Functional Analysis Framework for Modeling, Estimation and Control in Science and Engineering*. CRC Press, 2012.

[52] A. Pazy. *Semigroups of linear operators and applications to partial differential equations*, volume 44 of *Applied Mathematical Sciences*. Springer-Verlag, New York, 1983.

[53] V. Komornik. *Exact controllability and stabilization*. RAM: Research in Applied Mathematics. Masson, Paris; John Wiley & Sons, Ltd., Chichester, 1994.

[54] Keith Glover, Ruth F. Curtain, and Jonathan R. Partington. Realisation and approximation of linear infinite-dimensional systems with error bounds. *SIAM J. Control Optim.*, 26(4):863–898, 1988.

VITA

Madhuka Hareena Lochana Weerasinghe was born in Colombo, Sri Lanka on October 13, 1981. After completing her schoolwork at Nalanda Balika Vidyalaya in Minuwangoda, Sri Lanka in 2000, Madhuka entered to the University of Kelaniya, Sri Lanka for her bachelors degree in 2003. She has earned her Bachelor of Science degree majoring Mathematics in 2007. After receiving the bachelors degree she was employed as a tutor at University of Kelaniya and University of Colombo in 2007 and 2008 respectively. In 2009, she joined Sri Lanka Institute of Information Technology as an Assistant Lecturer in Mathematics. In August 2011, she started graduate studies at Missouri University of Science and Technology in Missouri. Madhuka received her Master of Science in Mathematics in May 2014, and her PhD in Mathematics in July 2017 from Missouri University of Science and Technology.